THE AGEING BEHAVIOUR OF CERTAIN NICKEL ALLOYS CONTAINING ALUMINIUM AND TITANIUM.

A thesis presented for the Degree of

Doctor of Philosophy

of London University

by

Brendon Aston Parker, B.Sc.(Eng.)

Department of Metallurgy,
Imperial College of Science and Technology,
London, S.W.7.

November 1967.

Abstract:

Ageing processes in two nickel-rich alloys of the nickel-aluminium-titanium system of different γ/γ' mismatch have been studied over the temperature range 400 - 800°C by means of electron microscopy, and Curie temperature and elastic modulus measurements. The results allow an interpretation of the early stages of decomposition of the supersaturated solid solution formed on quenching. The microstructural observations in the later stages of ageing are in general agreement with those of other recent work on binary nickel alloys.

Particle coarsening measurements made concurrently with measurements of the solute content of the matrix have allowed independent determinations of the precipitate/matrix interfacial energies and the diffusion coefficients of solute in the alloys. An increased coarsening rate has been observed for the high misfit alloy.

Measurements of the mechanical properties after different ageing treatments have been interpreted in terms of recent theoretical treatments and the results related to the observed microstructures. An increase in strength due to the misfit at the particle/matrix interface is shown.

CONTENTS.

1. INTRODUCTION.

Complex nickel based alloys now play a very important part in many high temperature applications. The excellent properties of these materials are known to be largely based on the coherent precipitation of the γ' phase from supersaturated solid solution. The fundamental phenomena governing the precipitation processes have however yet to be understood completely; furthermore, the various features associated with precipitation in the various alloys have not been fully correlated with the mechanical properties of the alloys.

It was with the object of extending the knowledge of the precipitation processes and of relating the structures to the mechanical properties that the research to be described was undertaken.

It was decided that alloys should be chosen that would give a very good picture of the processes taking place and yet be sufficiently simple to allow the application of existing results and theoretical knowledge in the interpretation of the results obtained.

The majority of the commercial alloys have a nickel-chromium or nickel-chromium-cobalt solid solution matrix in which a precipitate of the intermetallic compound Ni_3Al,Ti is dispersed. A number of other alloying elements are present for various reasons but do not affect the general behaviour of these alloys. Chromium is present because of its beneficial effect on the corrosion resistance and because

of its combination with carbon to form carbides which have an important role in inhibiting grain boundary sliding under high temperature creep conditions.

It was considered that as the precipitation of the δ' was the object of this research, then chromium and cobalt could be left out of the alloys to be investigated, thus reducing the problem to one of precipitation in a three component system. This is an approachable problem in view of the existing knowledge on the behaviour of the binary nickel-aluminium and nickel-titanium systems. An interesting result of the removal of chromium, together with a reduction in the aluminium and titanium contents (resulting in a lowering of the equilibrium precipitate volume), is that the alloys have Curie temperatures close to room temperature, thus enabling interesting and informative magnetic measurements to be made.

It was noted during a survey of the literature that little was known of the effects of precipitation on the elastic properties of materials and therefore an apparatus was constructed to allow the measurement of the elastic properties after the ageing treatments.

Recently, a number of theoretical papers have been published on the effect of coherent precipitation on mechanical properties and the results obtained in this work will be discussed in the light of these papers.

This report commences with a brief description of the nickel-aluminium-titanium

system and of the previous structural work on this and the binary systems, sufficient to provide a basis for understanding the work that follows. The remainder of the relevant literature is considered under the headings to which it refers in the discussion of the results at the end of the thesis.

2.1. The Nickel Aluminium Titanium system.

The nickel-aluminium-titanium phase diagram was established by Taylor and Floyd[1]; their published 750°C isothermal section is shown in figure (2.1.1.). The alloys used in this investigation and in other investigations referred to in this thesis are indicated in the figure.

All the alloys referred to show the common features of being single phase γ solid solutions at high temperature and are in the $\gamma + \gamma'$ two phase region in the range of ageing temperatures used. Some of the high titanium alloys have the η phase in equilibrium with the γ or $\gamma + \gamma'$ but the evidence is that this phase only develops after very long ageing times in alloys containing significant amounts of aluminium.

Figure2.2. shows part of the vertical sections of the diagram corresponding to the alloys investigated. The sections are extended to lower temperatures using the Curie temperature results as outlined later in the thesis. The directions of the sections in the ternary system were taken to correspond to the tie lines shown by Taylor and Floyd.

The diagrams are considered to be sufficiently accurate to allow them to be used for quantitative measurements.

2.2. Structural studies by other workers.

The precipitation sequences in simple nickel based alloys were first examined in detail by Manenc [2] and Williams [3]. Manenc showed

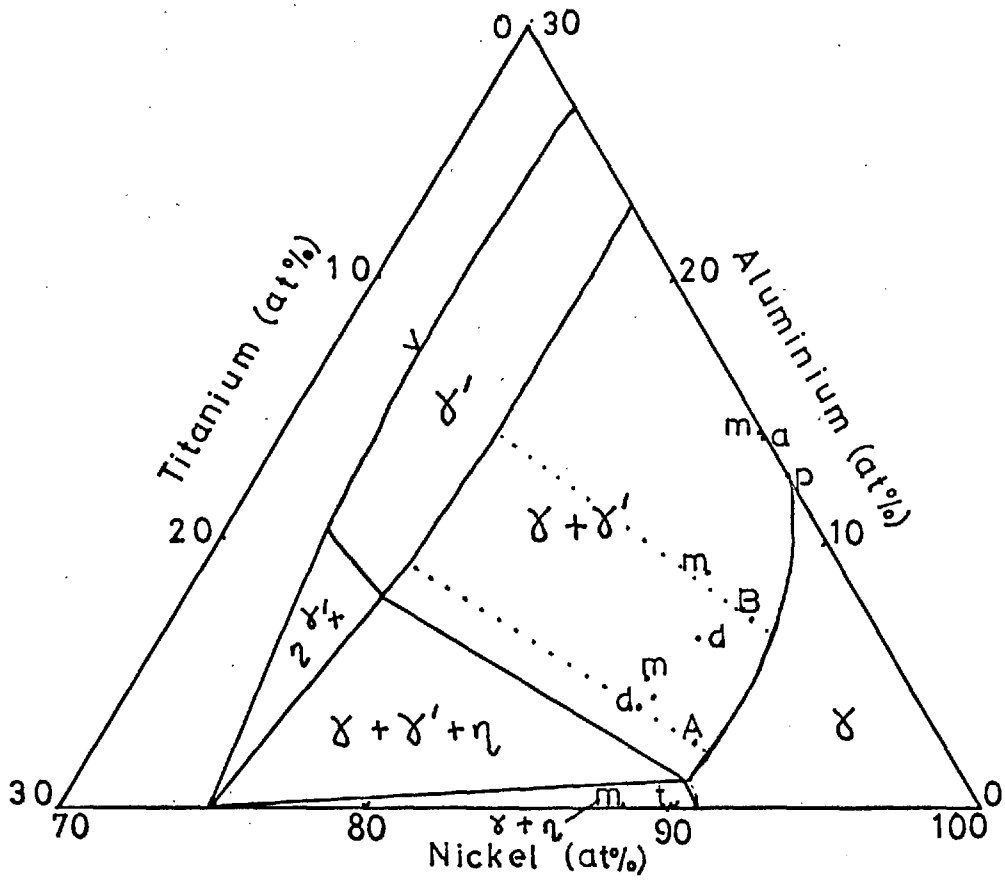

Fig.2.1.1. 750°C. Isothermal: From the work of Taylor And Floyd.

Alloys studied by previous workers shown as follows:

a Ardell and Nicholson.

p Phillips.

d Detert and Pohl.

m Mihalisin and Decker.

t Fine et Al.

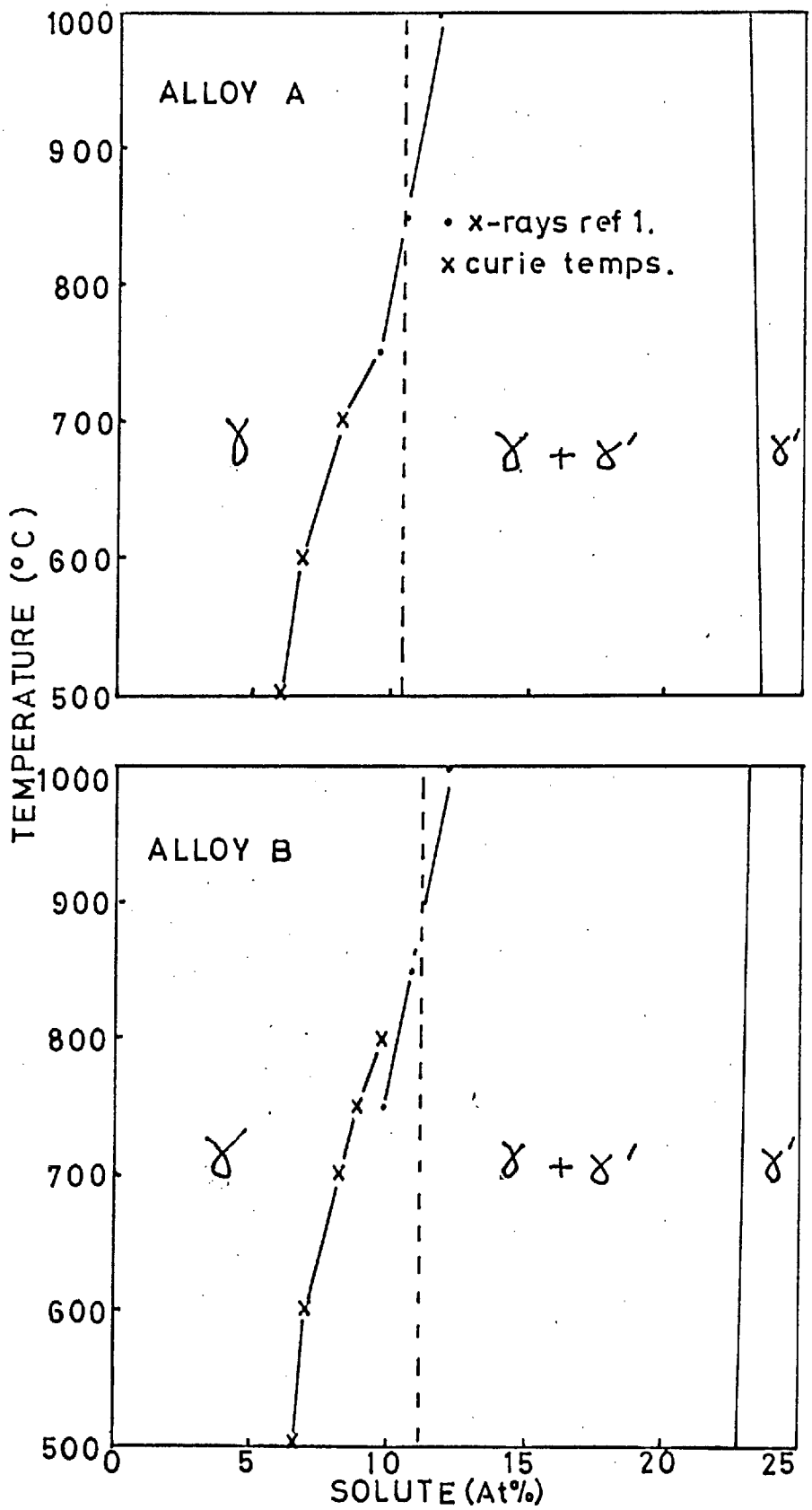

Fig.2.4.2. Vertical sections of the phase diagram for alloys A and B.

that all the alloys precipitated a face centered cubic phase in a face centered cubic matrix. He suggested a common ageing sequence as a result of his work:

(i) Pre-precipitation stage - characterised by side bands around the F.C.C. X-ray lines.

(ii) Intermediate phase distorted as a result of coherency with the matrix.

(iii) The stable F.C.C. phase ( ) incoherent with the matrix.

Manenc described two classes of alloy:

(i) Alloys forming precipitates as platelets.

(ii) Alloys forming cubic precipitates.

The second process was observed when the lattice parameter difference between the and was less than 0.01A; his nickel- aluminium and nickel-aluminium-titanium alloys came into the first class. It should however be noted that the morphological observations were made on replicas of alloys aged for long times. In a later investigation Manenc et al. (4) showed that rafts of cubes were formed in the early stages of precipitation in nickel-aluminium alloys.

Williams postulated a similar model for his Ni-Al alloys:

(i) Change in atomic configuration, presumed to be an increase in short range order.

(ii) Actual precipitation of Ni_3Al in the form of coherent plates on (100) planes.

Similar morphological observations to those of Manenc were made.

Buckle, Genty & Manenc (5) showed that rafts of cubes were formed at earlier stages prior to plate formation.

Discontinuous precipitation has been observed in this system but only at high ageing temperatures and after long ageing times,(for example see Phillips (6)).

A systematic study of the Ni-Al-Ti system was made by Mihilasin and Dekker (7) who showed that in a nickel-12.2 at.percent titanium alloy the initial phase to form is the F.C.C. γ' phase, confirming some earlier results of Buckle and Manenc (8). The hexagonal η phase was found to form discontinuously at longer ageing times. They showed further that aluminium additions delayed the onset of discontinuous precipitation. Morphological studies were not extended in this paper.

Mihilisin and Dekker investigated the effect of lattice parameter differences on the mechanical properties of alloys in the system and these results will be referred to later.

Detert and Pohl (9) made a number of indirect measurements on Ni-Ti-Al alloys but again they only used replicas for structural studies; the indirect measurements again confirmed a short range ordering stage prior to γ' precipitation. The indirect observations will be referred to in more detail later.

Thin foils of Ni-Al alloys have been studied by Ardell and Nicholson (10) and

Phillips (6) and the following features were established:

(i) The γ' particles were in the form of cubes with sides parallel to the (100) directions in the matrix.

(ii) The cubic particles were aligned in (100) directions after long ageing times.

(iii) After long ageing times the γ' cubes coalesced into 'rafts' which may be identified with the plates observed in the earlier investigations.

(iv) No loss of coherency was observed even after long ageing times.

Ardell and Nicholson (10) suggested that the aligned and modulated structure arose from an elastic interaction between the particles in the matrix.

Nickel-titanium alloys have been investigated by Dewance, Ben-Israel and Fine (11) (12) and they propose the following sequence for a 10 at.% alloy:

(i) Decomposition begins inside the spinodal giving a periodic fluctuation in composition with respect to position in the solid solution.

(ii) Discrete γ' particles, matastable face-centred tetragonal, nucleate and grow. The particles are coherent with the matrix and are periodically spaced.

(iii) The η hexagonal close packed phase appears at long ageing times.

A definite shape change during ageing is reported by Hornbogen and Chakraborty (13) for

a Ni-Si alloy; the particles were spherical at short ageing times changing to cubic at longer ageing times. Ardell and Nicholson (10) also showed some evidence of a similar shape change in their Ni-Al alloy.

The following features appear to have been established:

(i) There is a pre-precipitation stage showing the features of short range order, and quenching would seem to be unable to prevent the onset of this stage.

(ii) The γ' precipitate forms as a spherical precipitate, changing to cubic or rectilinear as ageing proceeds.

(iii) The particles coalesce at long ageing times.

(iv) The particles are initially, or become, aligned in [100] directions.

The nature of the pre-precipitation stage is in some doubt as is the origin of the aligned structure.

3. Experimental procedures:

3.1. Alloy manufacture:

The two alloys were selected by considering the phase diagram and the work of other investigators. The alloys were melted in 30kg. melts and the ingots were homogenized, forged and fabricated by Messrs. Henry Wiggins Limited, Hereford, according to established practises. The alloys were supplied in the following forms:

(i) 0.030" cold rolled and annealed strip. (The annealing treatments were carried out under protective atmospheres).

(ii) 0.5cm. dia. extruded rod.

(iii) 0.064" dia. cold drawn wire.

(i) was used mainly for electron microscopy and for hardness measurements.

(ii) was used for dynamic modulus measurements and for some of the preliminary magnetic work.

(iii) was used for tensile tests and for the majority of the magnetic work.

3.2. Analysis:

The analysis provided by Wiggins showed the following:

	Ni	Al	Ti	C	Al	Ti
Alloy A	Bal	1.22	6.55	0.01wt%	2.58	7.8 At%
Alloy B	Bal	3.5	3.37	0.01wt%	7.3	3.94 At%

Other elements were present only in trace quantities.

The magnetic results confirm the analysis and were reproducible between different batches of specimens indicating the effectiveness of the homogenization treatments given.

3.3 Solution treatment:

Examination of the literature on similar alloys showed solution treatment temperatures in the range 1000 - 1400°C, temperatures above 1275°C being used to obtain very large grain sizes. Treatment times of the order of 1 hour were generally used. Treatments were carried out in argon, hydrogen, or vacuum and samples were quenched into water or iced brine, the more recent investigations showing that a lower hardness could be obtained using the more effective quenching medium. Some of the results in the literature may be criticised because of the poor quenching conditions employed. The solution treatment initially employed was 1100°C for 1 hour in a furnace with an argon atmosphere followed by drop quenching into cold water. The treatment resulted in a grain size of about 0.9mm and the hardness and tensile results were reproducible. Changing the temperature in the range 1000 - 1200°C. and substituting iced brine for the water caused little difference in the properties of the solution treated alloy.

As the investigations proceeded it became apparent that there was little, if any, incubation period in the development of the aged structure, and as spinodal decomposition had already been suggested for this type of

alloy it was decided to try the effect of quenching from lower temperatures; but still above the anticipated spinodal and precipitation temperatures.

Specimens were treated for 1 hour as before and were then furnace cooled to about 875°C, prior to rapid quenching into iced brine; the result was a considerable lowering of the yield stress and a lowering of the Curie temperature. These Curie temperatures did not correspond with the results on the binary alloys in the literature used to construct the initial Curie temperature-composition calibration curves (fig.5.7.1)and it is suggested that the earlier values were obtained on specimens which were not quenched rapidly enough. The more recent results of Ben-Israel & Fine [11] also show this effect and confirm the above interpretation.

The alloys treated as above also showed a narrower Curie temperature spread than those given the standard 1100°C treatment, and this feature will be considered in more detail in later chapters. The effect of the low temperature/iced brine quenching treatment on subsequent ageing is only important at low ageing temperatures and for short ageing times. The powerful quenching technique was only effective on the wire and strip materials; because of their size the modulus specimens could not be produced in this condition.

Table (3.3) summarizes the different treatments and their effects.

TABLE 3.3.

The effect of different solution treatments:

Treatment	Yield stress, Kg/mm^2.
Alloy B.	
1100°C. ½ hour W.Q.	30
1100°C. 1 hour W.Q.	30
1100°C. 1 hour I.B.Q.	29
1200°C. ½ hour I.B.Q.	27
1000°C. 2 hours W.Q.	32.
1100°C. 1hour furnace cool to 875°C.I.B.Q.	22
Alloy A.	
1100°C. 1 hour W.Q.	30
1200°C. ½ hour I.B.Q.	27
1100°C. 1 hour furnace cool to 875°C.I.B.Q.	24

3.4. Ageing treatments.

Long ageing treatments were carried out in a horizontal tube furnace in air. The temperature was controlled to within $\pm 3^{\circ}C$. of the stated temperatures. Short ageing treatments were performed in salt baths and again the temperatures were within $\pm 3^{\circ}C$.

Treatments were observed, under certain conditions, to give very large spreads in Curie temperature and it was thought initially that this could be due to a loss of Aluminium or Titanium from the surface of the specimen during heat treatment. A check was made by traversing wire specimens across a diameter with an electron probe micro-analyser. The results indicated that the composition fluctuations were on a smaller scale than the limit of resolution of the probe (1μ). The probe showed a composition gradient only over a distance of about 10μ from the surface of the specimen and further indicated that the oxide layer was very narrow. Oxidation at temperatures below $700^{\circ}C$. was extremely limited.

Specimens were quenched from the ageing temperatures to prevent further precipitation at lower temperatures.

3.5. Electron Microscopy.

Thin foils were prepared from the alloys after various thermal and mechanical treatments, and were examined in an EM6G electron microscope operated at 100kv.

Foil preparation:

Stock material was reduced from 0.030" to 0.008" by cold rolling. The strip was then solution treated in an argon atmosphere and drop quenched into iced brine. It was then cleaned with silicone carbide paper to remove all traces of oxide and then 3mm. discs were punched out. The discs were given the stated heat treatments in an air furnace and further cleaned with fine abrasive paper.

The discs were profiled using a modified Blankenburg and Wheeler technique. The specimen was placed on a platinum gauze and a 1mm. jet of 40% HCl was allowed to fall on it from a height of about 3mm. A potential of 75volts was applied between the specimen and the jet (the specimen being the anode). A suitable profile was obtained after jetting each side of the disc for about 12 seconds. The foils were subsequently electro-polished in a 20% solution of perchloric acid in ethanol at a potential of 5volts. Polishing was stopped when a small hole appeared in the centre of the disc.

After careful washing and drying using distilled water and ethanol alternately the foils could be inserted directly into the EM6G specimen holder and examined.

The majority of micrographs were taken under bright field operating conditions. The tilting facilities available only rarely allowed the use of dark field illumination employing superlattice reflections; in addition certain features of the microstructure made the use of refined techniques somewhat difficult - these will be discussed later.

Foil orientations and directions were determined by standard methods from selected area diffraction patterns corrected for rotation at different magnifications. Foils were tilted within the limits of the stage available to obtain the most useful contrast conditions and to bring into contrast such features as dislocations and grain boundaries.

Particle size measurements:

Consideration of the orientation relationship between the precipitate and the matrix shows that sizes are best measured in [100] directions in foils having a (100) plane parallel to the foil plane; foils in this orientation were not however very often obtained. Foils of (110) and (310) orientation were frequently found and sizes were measured in the [100] directions in these planes, making the assumption of cubic rather than rectilinear particle shape.

Histograms were constructed for some conditions to check the applicability of coarsening theory and for these 100 to 400 measurements were made. All the particles on a given print were measured to avoid sampling problems. For most of the conditions the

particle size was taken as the arithmetic mean of 40 to 50 particles, and the values obtained agreed closely with those obtained from the histograms. Corrections were made for the true magnification of the microscope as calibrated with standard grids but were not made for the small variations in objective lens current due to the variations in specimen position. This latter factor introduces an error of $\pm 5\%$ or less since the lens current varied only by 3mv. in 150 between different foils.

Checks made when possible using dark field micrographs gave similar sizes and distributions to those obtained from the bright field micrographs.

Particle sizes less than c.100 Å are included but these are subject to large errors because of the strong masking effect of the strain fields.

The particle size measurements are included in the results section for foils aged for various times at a number of ageing temperatures.

3.6. Mechanical property measurements:

Wire specimens heat treated as described in section 3.4 were tested in an Instron testing machine at a cross head speed of 0.2cm. per minute, equivalent to a strain rate of approximately 3.3% per minute.

The specimens were 0.064" in diameter giving a cross section close to 2 sq.mm., and the specimen length between grips was kept close to 6cm, the actual length being measured in each

case. After heat treatment some of the wires showed a layer of oxide on the surface, but this did not affect the reproducibility of the results; removal of the oxide did produce some scatter in the tensile strength.

The specimens were rigidly clamped in heavy jaws attached to the Instron; these held the specimen well and there was no evidence of slipping prior to yielding on any of the tests, and only rarely did slipping occur prior to fracture. The wires in 80% of the tests broke in the measured regions between the grips, thus allowing values of tensile strength and elongation to be obtained. The absence of a standard gauge section does however contribute to an error in the values of these quantities.

A check was made on the wires to see if there was any evidence of preferred orientation in the wires. Laue back reflection photographs failed to show any evidence of preferred orientation after solution treatment. Checks on the possibility of solute loss are reported in section 3.4.

Table 3.6 shows values of mechanical properties on several specimens heat treated in an identical manner. These values show that although the technique was somewhat primitive, in view of the very constant cross section of the wires the values of the mechanical properties are reproducible.

Yield stress values were obtained by extrapolating the elastic portion of the curve to meet the extrapolation of the initial linear

TABLE 3.6.

Reproducibility of tensile tests:

Alloy B solution treated at 1100°C 1 hour W.Q.

Specimen no.	Extrapolated yield stress kg/mm^2.
1	30
2	30
6	29
24	30
43	31
56	32
Solution treated at 1100°C.1 hour furnace cooled to 875°C.Iced brine quench.	
69	23
92	24
116	21.5
139	22

plastic portion of the curve. The values approximate to an 0.2% proof stress; the procedure was more reproducible than proof stress determinations because of the uncertainty in gauge length.

Some 200 tensile tests were performed and without exception gave yield stresses within 1 or 2 Kg./mm.^{2} of a smooth curve drawn through all the points. Any scatter could be traced by checking the Curie temperature curve of the specimen, this generally indicating an irregularity in heat treatment procedure.

Curves are shown in the results section of yield stress versus ageing time at 400,500, 600,700,750,^{o}C for both alloys, and the results of other workers are included where applicable. The effect of the more rapid quenching technique is also shown.

3.7. Curie Temperature Measurements.

A technique was required that would provide information on the Curie temperatures of the alloys and it was realised that this could be done more simply than by using the refined apparatus of the physicist.

The principle of the technique is that a ferromagnetic material when inserted into an air-cored coil causes a significant change in the self inductance of the coil. If the material is caused to become non-ferromagnetic by raising the temperature to above the Curie point then a change in impedance of the coil takes place as the permeability of the specimen changes. A change in impedance may be observed by noting the change in voltage across the coil when connected to a stabilised a.c. supply.

A block diagram of the apparatus is shown in fig.3.7.1. The stable a.c. supply is an a.f. oscillator and the voltage across the coil is measured by an a.f. millivoltmeter; as both these instruments have a very high impedance they have little effect on the changes taking place in the circuit. A thermocouple is attached to the specimen to enable the relationship between voltage and temperature to be found. The output of the thermocouple is fed to the X channel of a function plotter and the voltage across the coil is fed via a rectifying and dividing circuit to the Y channel, thus enabling a continuous plot of voltage versus temperature

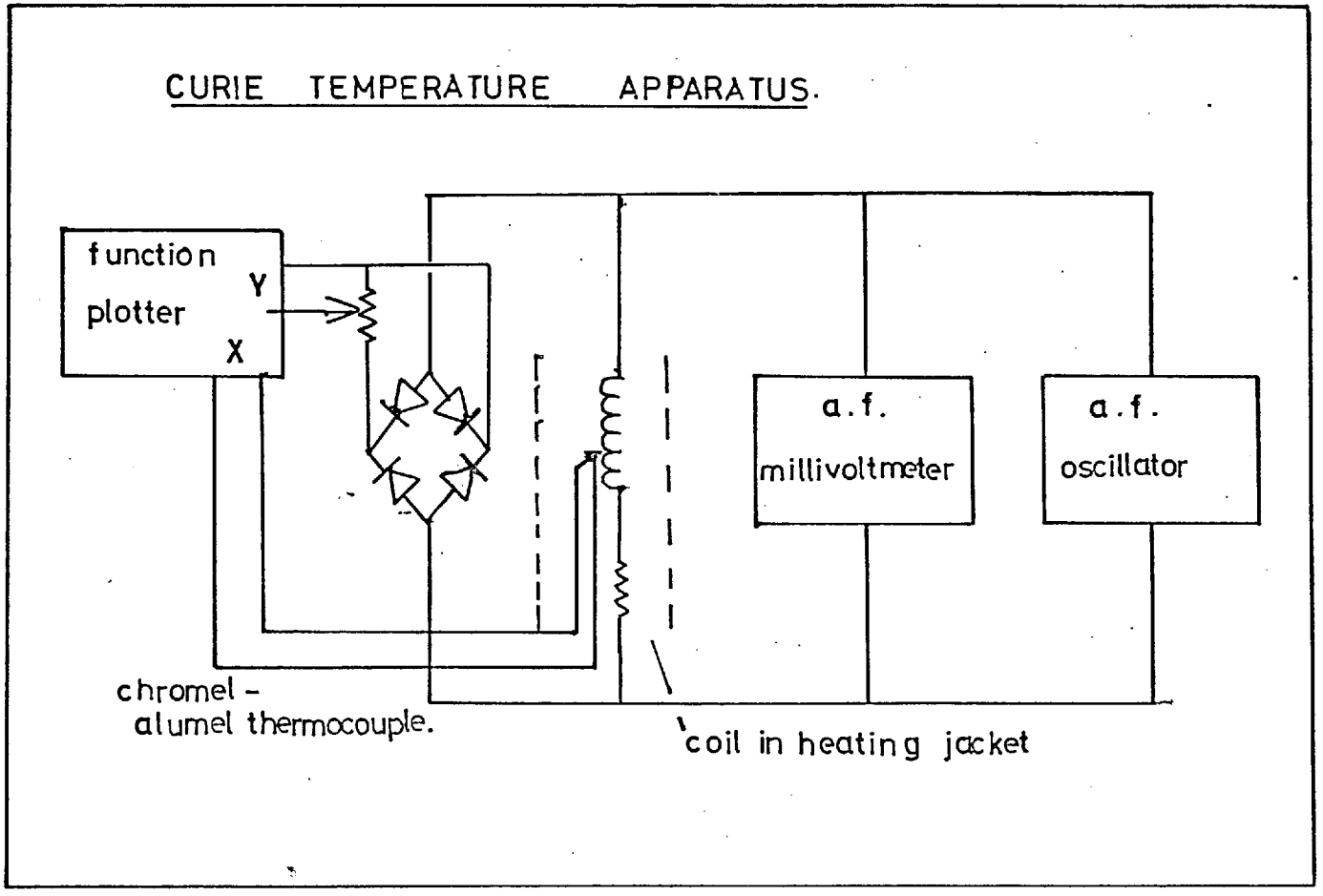

Fig.3.7.1. Schematic circuit diagram Curie temperature apparatus.

to be made.

The coil used in the latter stages of the work (and for all the results reported here) was a Radiospares No. 3 reed coil, the characteristics of which were known from data given by the manufacturer:

length 1.15"
diameter 1.27 cm.
d/c resistance 1.6k ohm.
ampere turns per volt 4.3.

For most of the measurements a potential of 150 mv. was used giving a field of 0.5 oersted.

The coil, specimen and thermocouple were placed in a pyrex tube with one end closed. This tube could be placed in high or low temperature baths. A silicone oil bath was used for temperatures above room temperature and for low temperatures the tube was surrounded by dry ice/acetone mixtures, liquid nitrogen or a freezing mixture.

A frequency of 3kc/s, well away from the fundamental and harmonic resonant frequencies of the coil, was used for the measurements and the output of the oscillator was maintained at 150 mv. without a specimen in the coil. Care was taken to ensure that the circuit conditions remained constant for the duration of a test and also that they were essentially similar for all tests.

Plots of voltage versus temperature were made as the specimen cooled or heated after being placed in the baths. Examples of the curves obtained from the apparatus, and graphs of Curie

temperature versus ageing time are given in the results section.

Limitations and sources of error in the apparatus

The following must be considered so that the results can be interpreted in detail, particularly as the apparatus described is essentially original in design.

(i) The constancy of temperature along the specimen.

(ii) The effect of specimen size on the curve shapes.

(iii) The relation between the voltage across the coil and the magnetic properties of the specimen.

(iv) The effects of field strength and frequency on the shape of the curves.

(i) As the specimens were also used in the tensile tests they were in general somewhat longer than the coil and it was thought that this might give rise to an effect due to a non-uniform temperature distribution. Long specimens some three times the length of the coil when given suitable ageing treatments to produce a sharp change at the Curie temperature, showed negligible differences in their behaviour from shorter specimens which could be contained completely within the coil. This indicates that only those parts of the specimen within the coil were affected by the field, the temperature gradient along the length of the coil was negligible.

(ii) The effective permeability of the

ferromagnetic core depends slightly on the position of the coil around the core and thus the amplitude of the curves could be changed slightly by using different specimen lengths. The curve shapes are not affected.

(iii) If all the circuit parameters were held constant so that only the inductance of the coil changed then the voltage variations across the coil would reflect accurately the change in permeability of the ferromagnetic core via the relation:

$$V = I \cdot 2\pi f \cdot 4\pi \times 10^{-7} \cdot \frac{a N^2}{l} \times \mu.$$

In the circuit described however, a change in voltage across the coil produces a change in current in the circuit. This will produce curves slightly different from true permeability/temperature curves because of the presence of resistive loads in the circuit. The general trends of the curves will however be maintained and no allowance has been made for this effect.

(iv) The permeabilities of ferromagnetic materials are not constant but depend on the field strength at which they are measured. The effects on the curve shapes are somewhat complex and so additional experiments were conducted over a range of field strengths (all of which were relatively low). The curves at different field strengths are included in the results section and are discussed at a later stage with all the factors which might affect the curve shapes.

The measurements were made at a frequency of 3 kilocycles and it is necessary to consider

briefly how the results might differ from more normal methods of measurement in non-varying fields. The permeability at low fields is a measure of the ease with which a ferromagnetic domain boundary may be moved. As the frequency of measurement increases the magnetization of the specimen will lag behind the field by an increasing amount; at a constant frequency however, there will be no effect on the relative differences between each specimen. As the frequency increases the depth of penetration of the field into the specimen decreases; however these alloys have a fairly high resistivity and the skin-depth is very large compared with the small inhomogeneous regions at the specimen surface at the frequency used.

The changes in structure that give rise to changes in the initial permeability because of their effect on domain wall mobility will be discussed in detail at a later stage.

It should be noted that none of the above effects (apart from those due to temperature gradients) will influence the temperature at which the permeability reaches zero. The effects are discussed with relevance to their effect on the interpretation of the shapes of the curves obtained.

3.8. Electrical resistivity measurements.

As discussed in section 5.6 there is some ambiguity regarding the features controlling the shape of the permeability/temperature curves in the early stages of ageing. Further information on the behaviour of the material close to the Curie point may be obtained by measureing the electrical resistivity as a function of temperature.

Wire specimens, aged to produce a range of permeability/temperature curves, were used. Potential leads were spot welded to the specimen, 2 cm. apart, and current leads were attached to the ends of the specimen. A current of 2 amperes was passed through the specimen and a 0.001 ohm standard resistance; the resistances were compared using a Tinsley potentiometer and a sensitive galvanometer[73]. The current was reversed at each temperature in order to balance out the effect of any thermal e.m.f.s. present.

The specimen and leads were immersed in a silicone oil bath for high temperatures and in freezing mixtures or liquid nitrogen for low temperatures. A chromel-alumel thermocouple was attached to the centre of the specimen.

Measurements of the potentials across the specimen and standard resistance were made while the specimen heated or cooled in the oil bath at a rate of about 20^{o}C per hour. The measurements at low temperature were made after allowing the

specimen to come to equilibrium in the low temperature baths. The results are compared with the Curie temperature curves from the same specimens in section (4.6).

3.9. The measurement of dynamic elastic moduli.

The apparatus is described in Appendix 1. It is not included in this section because a number of features of the apparatus are not directly relevant to the results reported here.

Measurements were made on 0.5" diameter rod cut in 10 cm. lengths from stock material. All the modulus results reported here were taken at room temperature without the use of the vacuum system. As shown in the Appendix, measurement of specimen dimensions is one of the limiting factors on the accuracy of the results and for this reason ageing sequences were carried out on single specimens, the specimens being quenched after each time interval in the furnace and then re-aged after measurement. Care was taken to ensure that the specimen was located in a similar position on the suspension on each occasion in order to counteract any effects of imperfect specimen geometry.

Each measurement was corrected for changes in the ambient temperature, as a change of $1^{\circ}C$ produces a change of 4 parts in 10^5 in the resonant frequency which can be measured by the apparatus to within 2 parts in 10^5. The limitations and errors involved in the measurements are indicated in the Appendix; it should be noted that absolute values

of the modulus are not used in the interpretations of the results and thus the major sources of error are eliminated.

Graphs are shown in the results section of $\frac{\Delta E}{E}$ where E is Young's elastic modulus; these are directly related to the measured frequency changes by the relation $\frac{\Delta E}{E} = \frac{2\Delta f}{f}$ where f is the measured resonant frequency. Corrections were not made for the fractional dimensional changes taking place during ageing as these are considered to be negligible.

3.10. Lattice parameter determinations.

Solution treated rod specimens were filed with a fine file and the powder was passed through a 300 mesh sieve. The powder was sealed in an evacuated silica tube and annealed at 700°C for 60 hours. The powder was placed in a pantax tube which in turn was placed on the axis of a Straumanis loading Debye-Scherrer camera. Nickel filtered copper K radiation was used and exposures of about 3 hours duration made. Longer exposures were tried to attempt to locate the superlattice lines but these were unsuccessful. The lattice parameters were determined by plotting the values obtained from the x-ray film against the Nelson-Riley extrapolation function.

4. Experimental Results.

4.1. Electron Microscopy.

Solution treated alloys were readily thinned and gave good areas for electron microscopy. However difficulties were encountered in producing good micrographs of the aged structures; these were considered to arise from complex electron scattering and absorbtion effects due principally to the similarity in the crystal structures of the precipitate and matrix and to the extensive strain fields in the matrix. These conditions also led to difficulties in obtaining simultaneous dislocation and precipitate contrast in deformed alloys.

In order that some of the later micrographs may be compared it is useful to consider initially the various contrast effects observed at the precipitates in these alloys. Figs. (4.1.1) and (4.1.2) show the same area of specimen tilted with different amounts with respect to the electron beam. The diffraction patterns show the foil orientation to be (110). In fig. (4.1.1) the principal operating reflections are (100) and ($\bar{1}$00) and in fig. (4.1.2) the principal operating reflection is (100). In fig. (4.1.1) the precipitates appear dark against the light background of the matrix, the intensity of the images depending on the depth of the particles in the foil. In fig. (4.1.2) a more complex pattern is observed, the precipitates appear somewhat in relief and many are traversed by a light line, all the lines being in the same direction and

perpendicular to the operating g-vector.
Fig. (4.1.3) and (4.1.4) show other contrast effects, and the foil orientations and operating reflections are indicated. Fig. (4.1.11) shows good dislocation contrast with poor precipitate contrast.

These contrast effects have been discussed in the literature and the results will be briefly summarised with relevance to alloys A and B in the discussion section.

Solution treated alloys.

Fig. (4.1.5) shows alloy B in the solution treated condition, a mottling of the background and contrast at the bend contour is observed having an 'orange peel' appearance. Faint superlattice spots were observed in the selected area diffraction pattern of this specimen. Areas of the specimen oriented differently and with different operating reflections did not show evidence of this structure. Dislocation pairs were frequently observed in foils in the solution treated condition. Fig. (4.1.6) shows alloy A in the solution treated condition; in addition to a few dislocation pairs, groups of dipoles may be seen

It should be noted that the electron microscope foils were not given the rapid quench from 875°C and therefore correspond essentially with material quenched from 1100°C. The Curie temperature measurements show some evidence of decomposition in material given this treatment.

Ageing at 300, 400 500°C Fig. (4.1.7) Foils of material that had been given low temperature ageing treatments showed little difference from the solution

treated material and the 'orange peel' effect was again observed. Paired dislocations were observed more frequently.

600°C. The mottling effect observed at lower temperatures became more pronounced, and superlattice spots were always observed for ageing times of 2 hours and longer. In Fig. (4.1.8) which shows alloy B aged 2½ hours at 600°C, some evidence of discrete precipitation may be seen. Fig. (4.1.9) shows alloy B aged for 238 hours and the particles are now more clearly seen; there was no evidence of grain boundary denudation in any foils aged at this temperature.

700°C. For ageing times up to about 7 hours the structures were similar to those in foils aged for longer ageing times at 600°C. Fig. (4.1.10) clearly shows the γ' particles together with some denudation along a grain boundary. Evidence of grain boundary denudation was observed after ageing times of about 7 hours. By indexing diffraction patterns and observing foils in different orientations, the particles were established as cubes with (100) faces parallel to and coherent with (100) in the matrix. The cubic particles may be observed to line up in [100] directions in the foils. There is some difficulty in deciding the particle shape for particle sizes less than about 120 Å; similarly the particle alignment was less pronounced at small particle sizes.

Ageing at 750° and 800°C. Figs. (4.1.1) and (4.1.2) show alloy B aged 2 hours at 800°C. There is some evidence for grain boundary denudation in these foils.

Fig. (4.1.4) shows alloy B aged 5½ hours at 800°C and fig. (4.1.11) shows alloy A aged 50 hours at 800°C; there was no evidence for a general loss of coherency at the particle/matrix interface but some of the dislocations in this micrograph do appear to have arranged themselves so as to accommodate some of the lattice strain. The average particle size was about 1300 Å. The shape of the particles may be very clearly seen in fig. (4.1.3) which is of alloy B aged 24 hours at 750°C.

The features described above were essentially similar for both alloys. Particle shapes, sizes (see section 4.3) and volume fractions appeared very much the same. The only difference between the microstructures of the two alloys was that the particles aligned in [100] directions were somewhat closer together in alloy A than in alloy B, particularly after long ageing times.

Grain boundary denudation.

Neither alloy showed evidence of grain boundary denudation until overageing occurred and the particle size reached approximately 300 Å, at which stage a small denuded zone was observed, which increased in width as particle coarsening proceeded. A few large particles were observed in the boundary at this stage, (fig. 4.1.10).

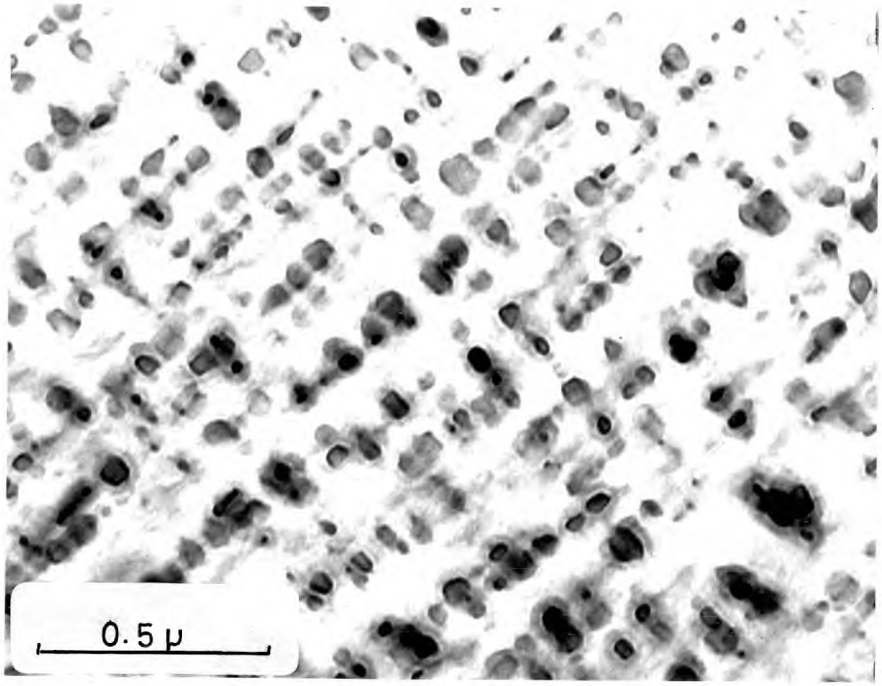

Fig.4.1.1. Alloy B. aged 2 hours at 800°C.
Foil orientation (110)
Operating reflections 200, $\bar{2}00$.

[100]

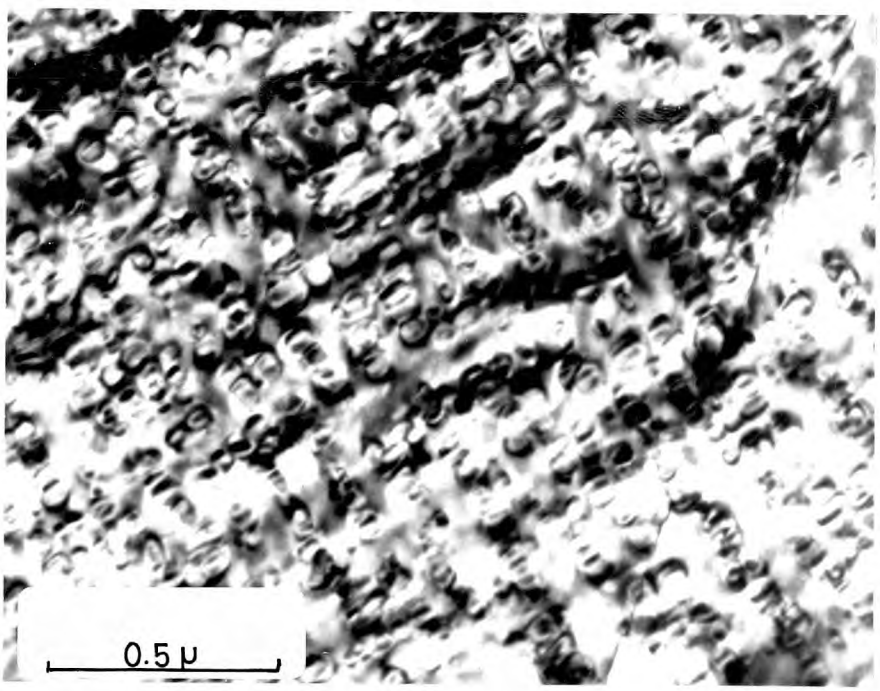

Fig.4.1.2. Same area as above tilted with respect to the electron beam.
Operating reflection (200)

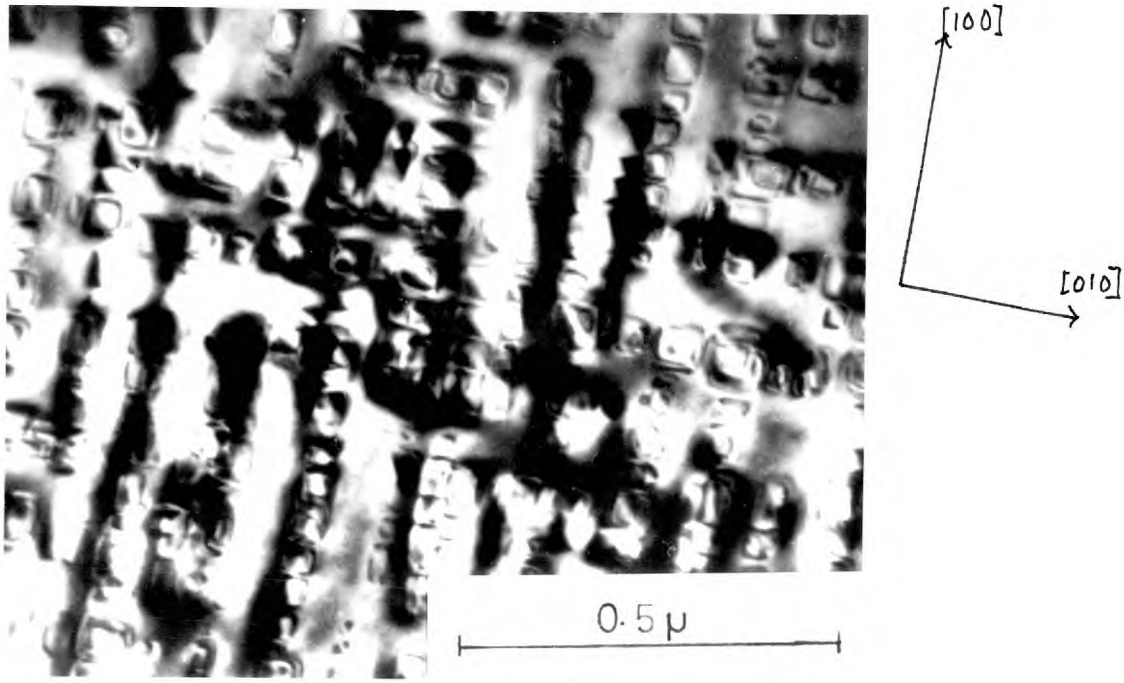

Fig.4.1.3. Alloy B. aged 24 hours at 750°C.
Foil orientation (100).
Operating reflections ($2\bar{2}0$)

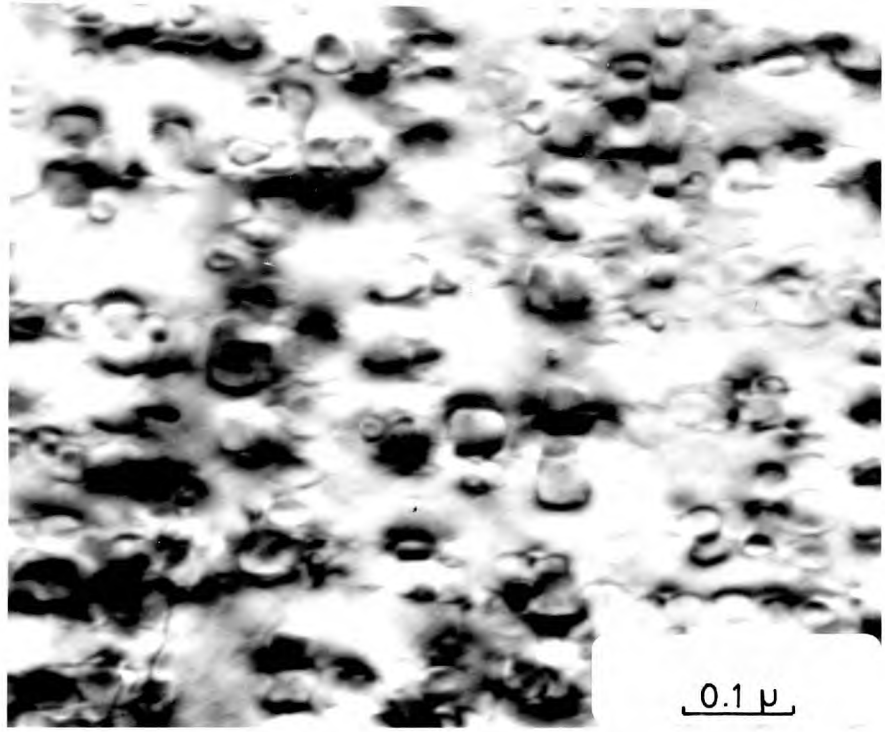

Fig.4.1.4. Alloy B. aged $5\frac{1}{2}$hours at 800°C.
Foil orientation (100)
Operating reflections 200 (+ $2\bar{4}0$ + $\overline{44}0$)

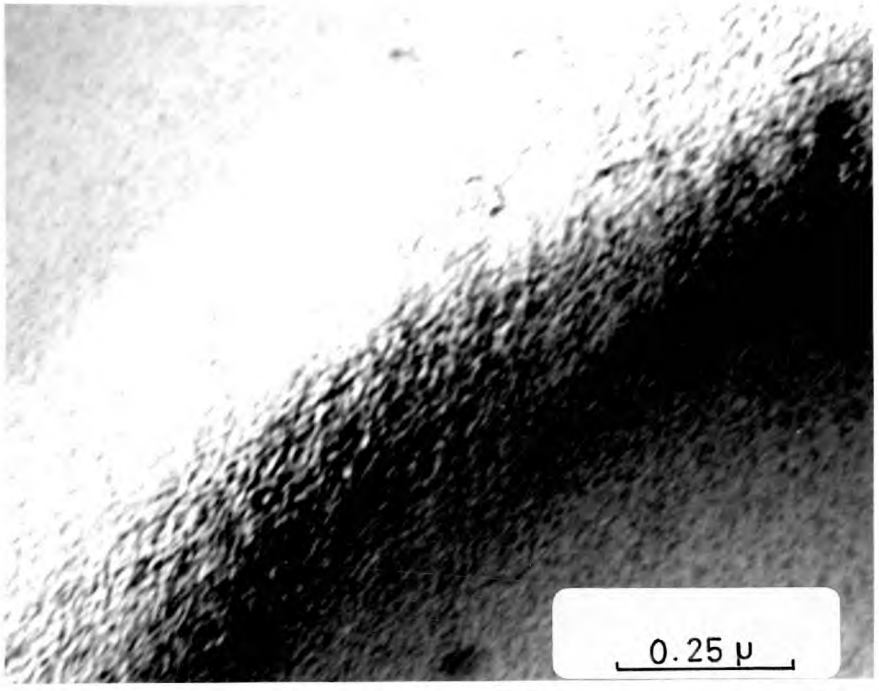

Fig. 4.1.5. Alloy B. Solution treated 1100°C. 1 hour, iced brine quench.

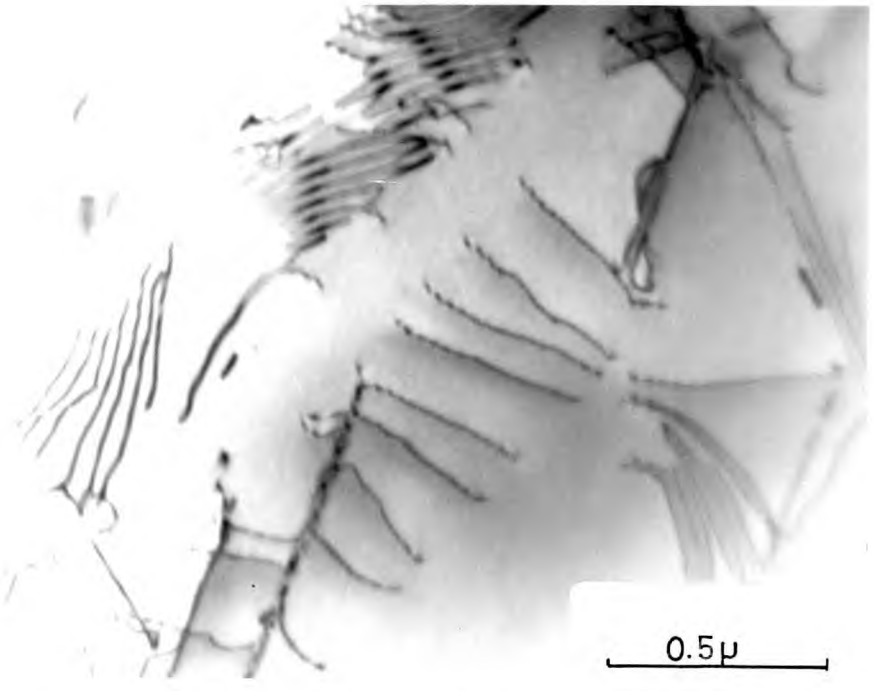

Fig.4.1.6. Alloy A. treated as above.

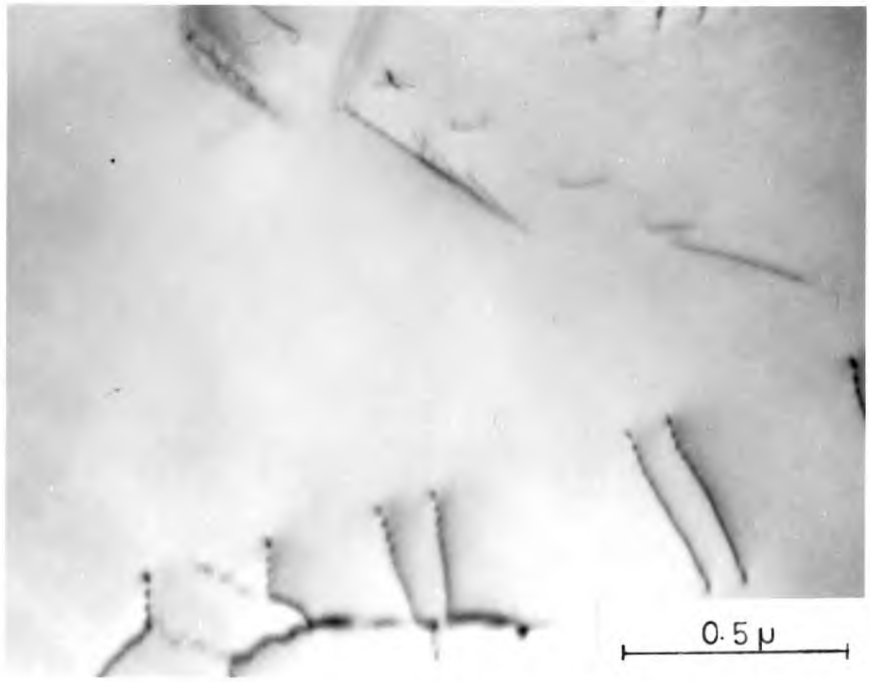

Fig.4.1.7. Alloy B. Aged 50 hours at 300°C. Foil orientation (211).

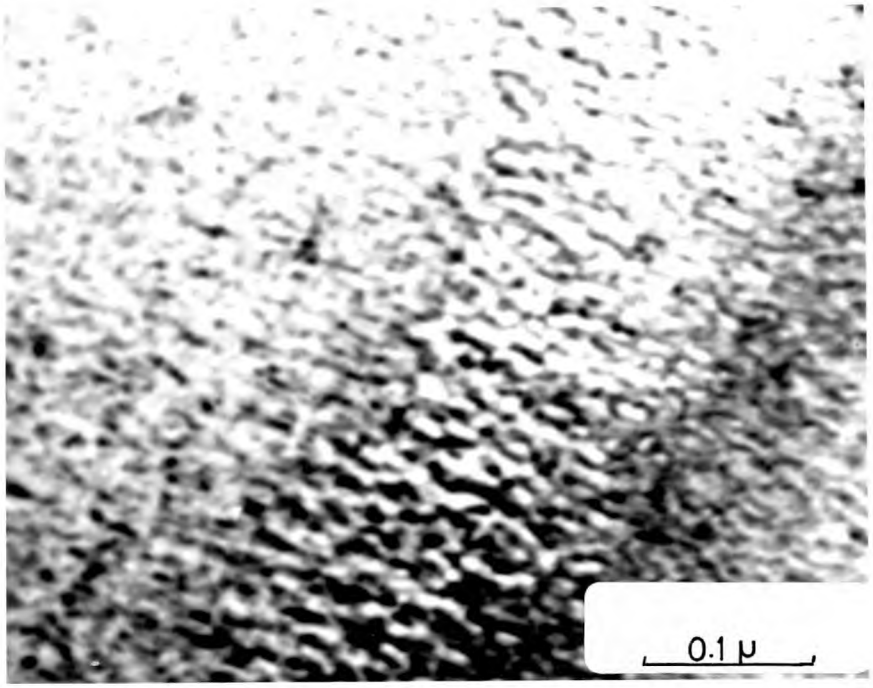

Fig.4.1.8. Alloy B. Aged 2½ hours at 600°C.

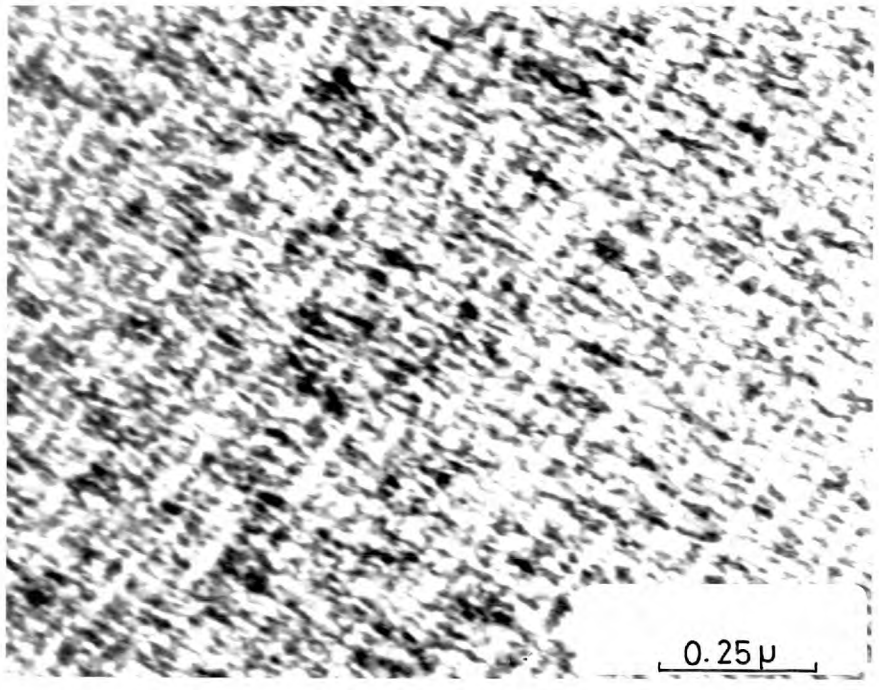

Fig.4.1.9. Alloy B. aged 238 hours at 600°C.
Foil orientation (110)

Fig.4.1.10. Alloy B. aged 43 hours at 700°C.
Foil orientation: L.H.S. (211) R.H.S. (110).
Operating reflections: L.H.S. (T11)
R.H.S. (200).

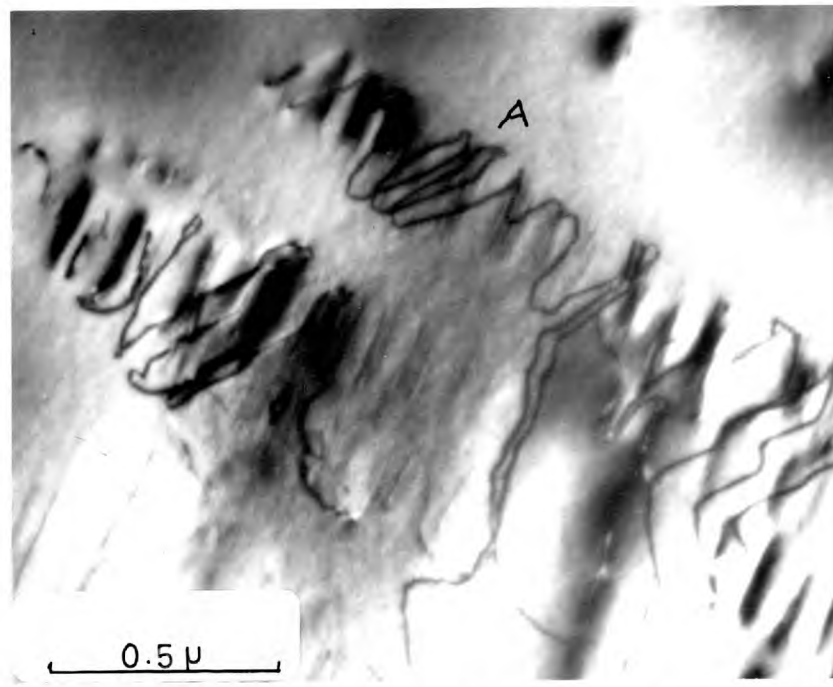

Fig.4.1.11. Alloy A. aged 50 hours at 800°C.
Foil orientation (100)
Operating reflection (200)

4.2. Dislocation arrangements after deformation.

The dislocations moved in pairs in all cases where the particles were cut and these conditions existed for all particle sizes less than about 200 Å (see figs. 4.1.6 and 4.1.7). The spacing of the dislocations in a pair decreased with ageing time and fig. (4.2.1) shows closely spaced pairs in alloy A aged 95 hours at 650°C.

When dislocation pile-ups were observed it was noted that only some of the dislocations from the head of the pile-up were paired. The number of pairs along the pile-up increased with ageing time. Suitable pile-ups were not observed frequently enough for quantitative measurements of the number of pairs and their spacing to be made.

At a particle size of about 200 Å not all the dislocations appeared straight along their full length, and in certain cases separation of the two dislocations in a pair, and dislocation loops were observed around a few γ' particles (figs. 4.2.1 and 4.2.2). At larger particle sizes the dislocations were no longer present in planar pairs, but rather looping of the dislocations was observed. Complete dislocation loops around γ' particles were frequently observed (see figs. 4.2.3 and 4.2.4). It should be noted that the dislocation configurations in these foils were the result of localised deformation during foil preparations). When the particle size was small the dislocations moved in widely spaced slip bands which were densely populated with planar

dislocation pairs (fig. 4.2.5). At larger particle sizes another effect is observed on deformation as shown in fig. 4.2.6, and although it is difficult to make out the details of this complex picture it would appear that some of the particles have lost coherency on deformation.

4.3. Particle size measurements.

Fig. (4.3.1) summarises the particle size measurements which are plotted as a function of the cube root of the ageing time. Straight lines are obtained showing agreement with a $t^{\frac{1}{3}}$ law. Alloy A coarsens somewhat faster than Alloy B. This plot is used to display the results so that the different rates of particle growth at the different temperatures may be clearly seen; there is however a limitation on its use because (a_o) the particle size when coarsening starts, has been ignored.

In fig. (4.3.2) the data are replotted as log (a) against log time and the slope of the plots is close to $\frac{1}{3}$. The lines are drawn to a fitted slope of $\frac{1}{3}$ to allow values of the coarsening rate constant to be obtained at the different temperatures assuming that a $t^{\frac{1}{3}}$ law holds. Most of the points represent the mean of 50 measurements, in a few cases 400 measurements were made and histograms were constructed to check the particle distribution. At the smaller particle sizes (less than 200 Å) the maximum error is considered to be $\pm$ 20% decreasing to $\pm$ 10% for the larger particles. Values of the rate constants, activation energies and other calculations are shown in the discussion (section 5.5).

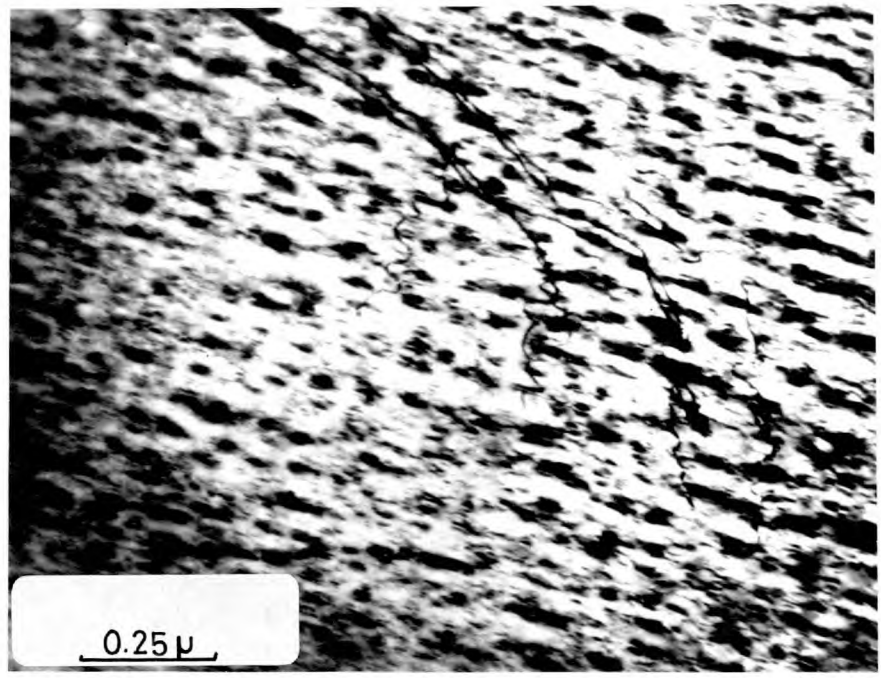

Fig.4.2.1. Alloy A. aged 95 hours at 650°C. 2% deformation.

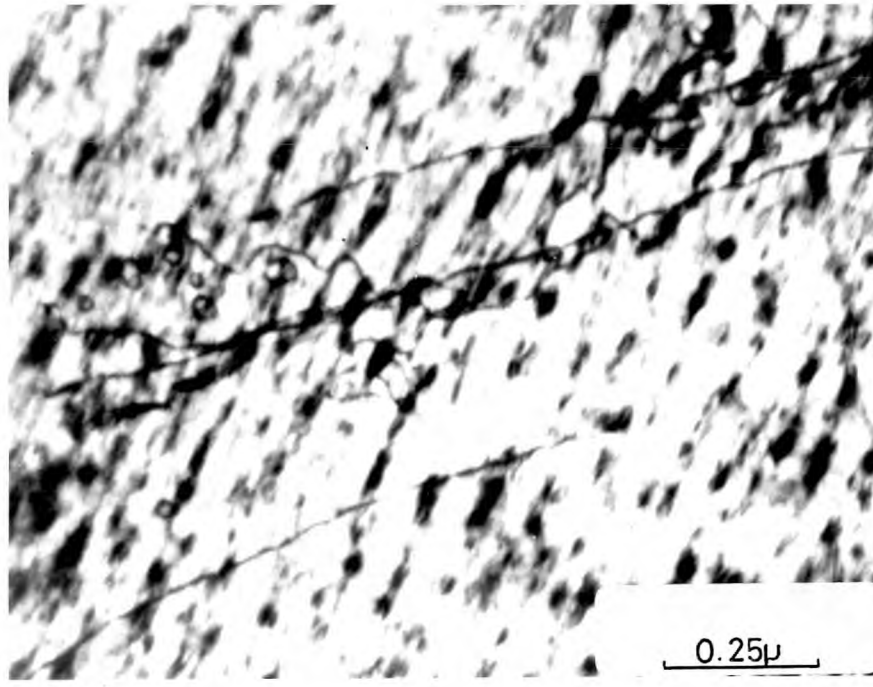

Fig.4.2.2. As above.

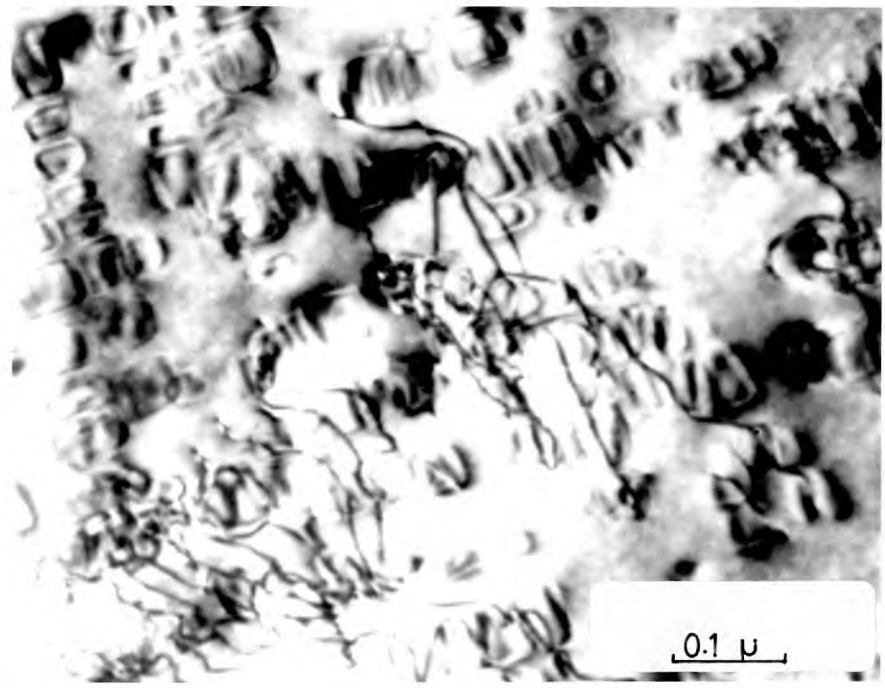

Fig.4.2.3. Alloy A. aged 24 hours at 750°C.
Foil deformed during preparation.

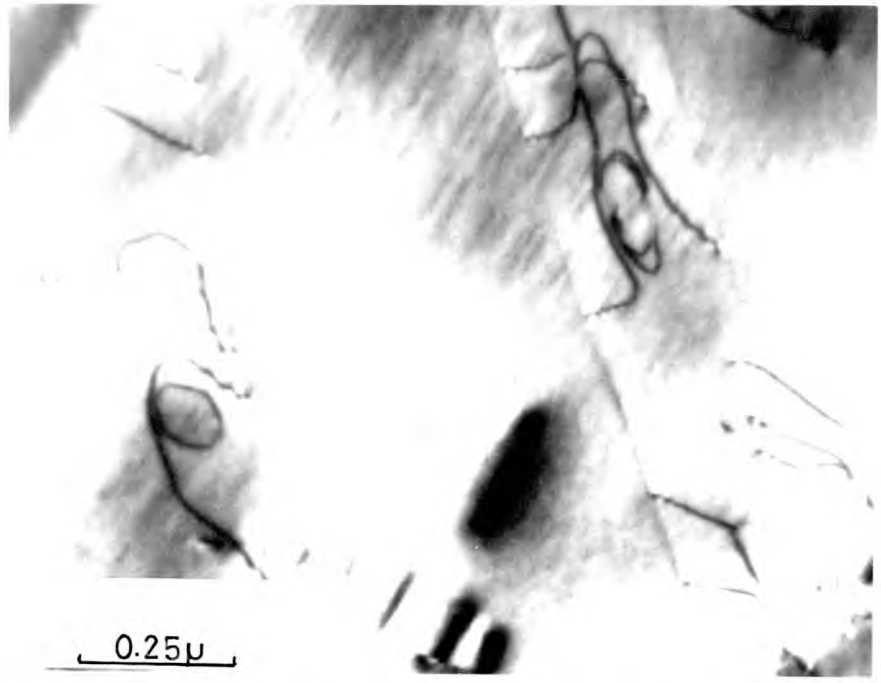

Fig.4.2.4. Alloy A. aged 50 hours at 800°C.
Foil deformed during preparation.

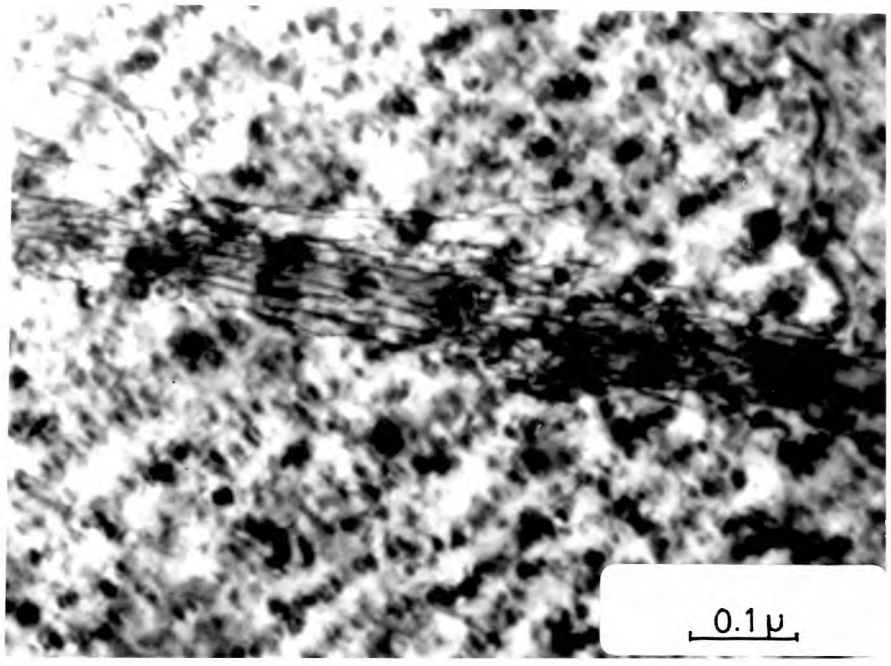

Fig.4.2.5. Alloy A. aged 7½ hours at 700°C. 3% deformation.

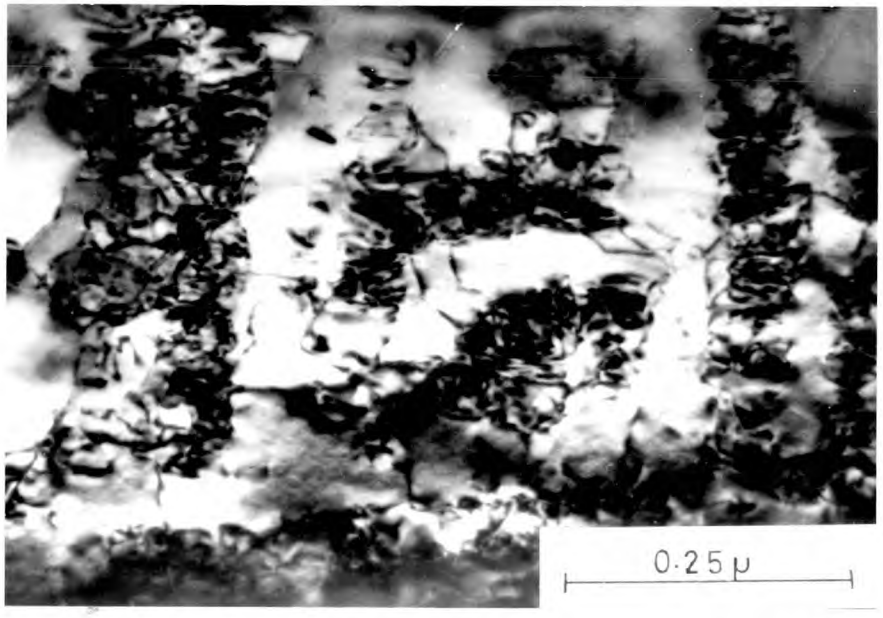

Fig.4.2.6. Alloy A. aged 100 hours at 700°C. 3% deformation.

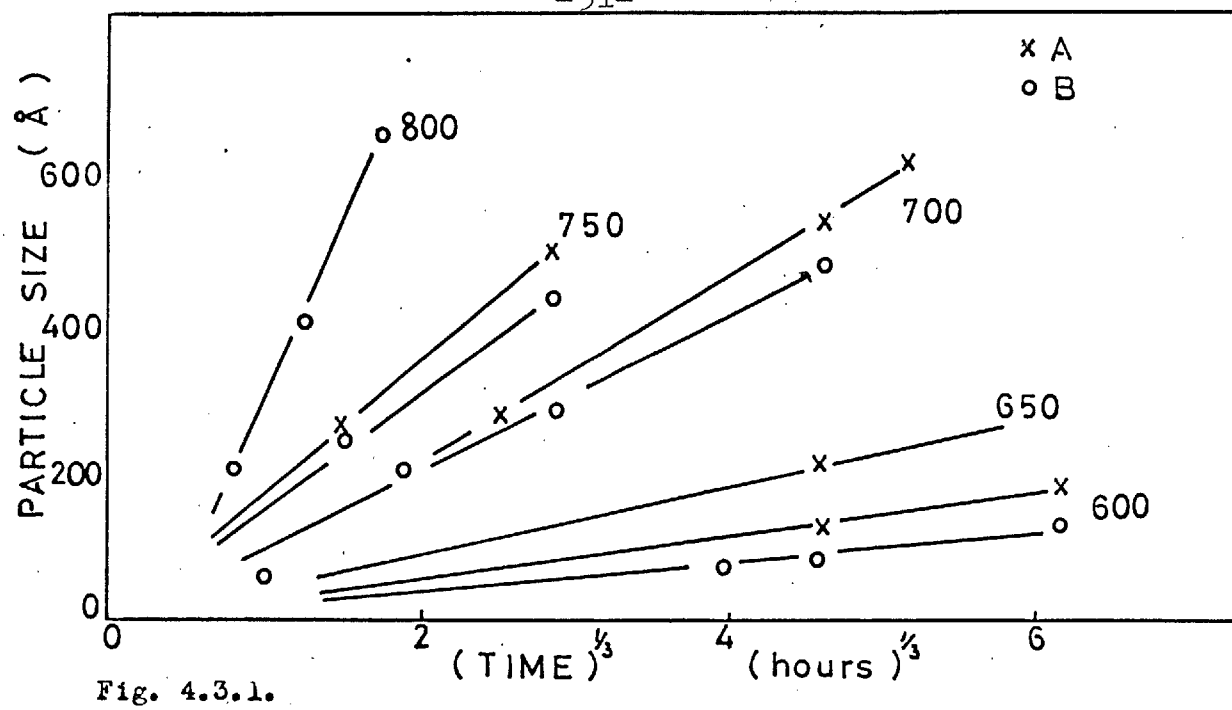

Fig. 4.3.1.

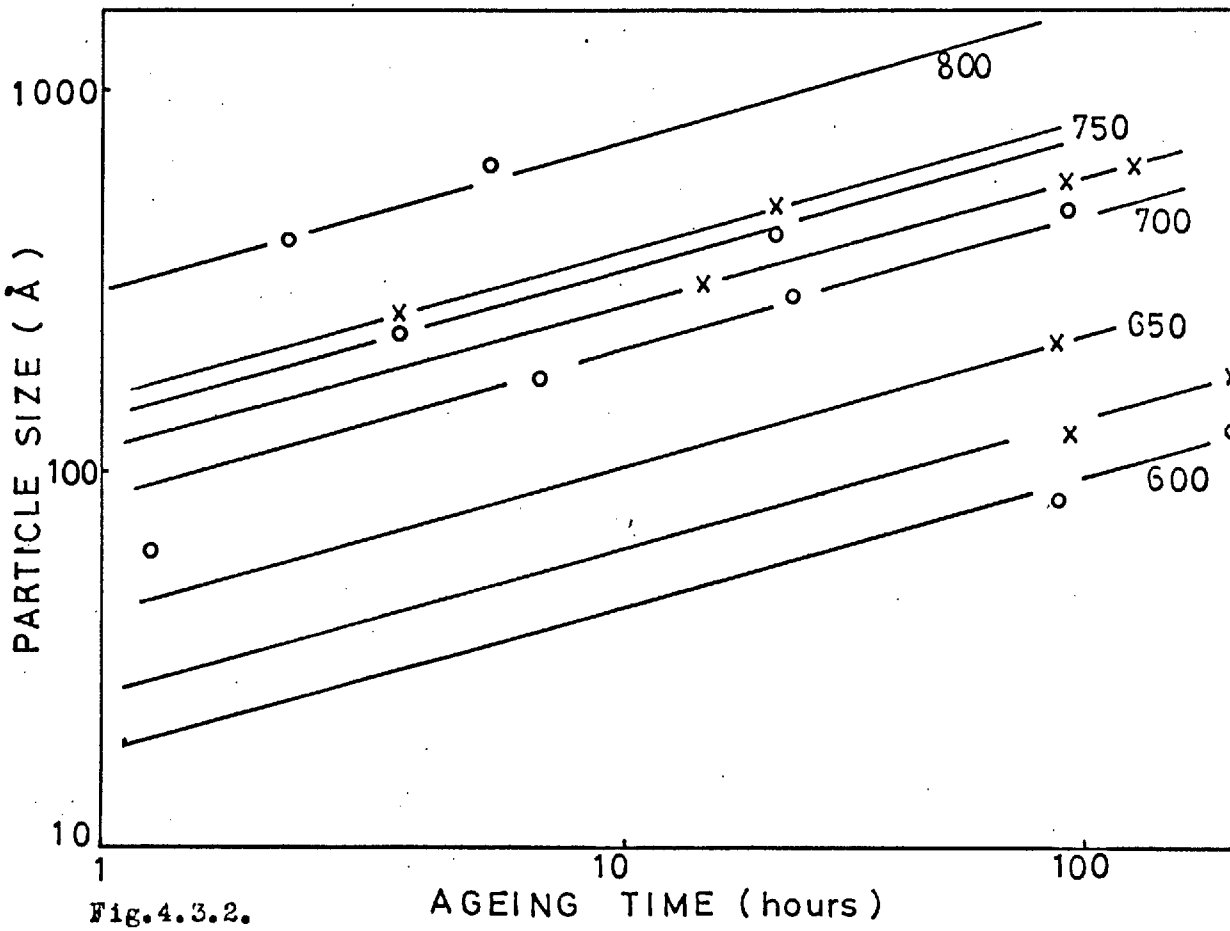

Fig.4.3.2.

Fig.4.3.1. Mean particle edge length versus $(\text{time})^{1/3}$

Fig.4.3.2. Mean particle edge length versus time (logarithmic plot)

4.4. Mechanical property results.

A number of different mechanical property parameters may be obtained from the tensile tests. The results reported here are of the extrapolated yield stress (close to an 0.2% proof stress) and the work hardening rates. These two parameters are the most easily interpreted in terms of the dislocation motion and the microstructure.

Yield stress.

Ageing at 400°C. Fig.(4.4.1).

There is an initial rise in the flow stress in the first few minutes which is more marked for alloy A. The hardening rate decreases over the range 10 to 150 minutes, increases again up to about 3000 minutes and then tends to level off. The curve is very similar in shape to the locus of the Curie temperature maxima on ageing at 400°C (fig.4.5.1). Alloy A has a much higher flow stress than alloy B at all stages at this ageing temperature. The inflexions in the curves occur at approximately the same ageing times for both alloys.

500°C. Fig (4.4.2).

The results of Jurkowitz and Fine [14] on a nickel 10 at.% titanium alloy aged at 525°C are replotted on this graph. There is a rapid initial hardening during the first few minutes of ageing for alloys A and B quenched from 875°C. The hardening rate with time is then low and gradually increases up to the longest ageing times; at very long ageing times the yield stress values approach those of

material quenched from 1100°C and aged for similar lengths of time. Specimens quenched from 1100°C show a slower rate of hardening from their solution treated values followed by a plateau prior to a rise in yield stress at longer ageing times; similar behaviour is shown by the nickel-titanium alloy.

Alloy A is again stronger than alloy B and the variation of yield stress with ageing time again follows the same form as the Curie temperature/ageing time curves.

600°C. Fig (4.4.3).

The results of Phillips [6] on a nickel 12.7 at % Al. alloy are included. Specimens quenched from 1100°C. show a steady increase in flow stress with time after a rapid initial rise in the first minute. There is no decrease in the flow stress at the longest ageing times. The effect of the 875°C quenching treatment is to reduce the hardening rate after the initial rise up to an ageing time of about 20 minutes at which stage the curves rise to join those of the 1100°C quenching treatment. Phillips' curve is of the same shape except that the initial rapid rise in the first minute is not observed; possibly his quenching treatment was not rapid enough to prevent some decomposition. A similarity between the yield stress and Curie temperature curves may again be seen particularly in the case of specimens aged following the 875°C quenching treatment. The

difference in strength between alloy A and alloy B is less marked, particularly at the shorter ageing times. The nickel-aluminium alloy is much less strong although it has approximately the same volume fraction of γ' at equilibrium.

700° and 750°C. Figs. (4.4.4 and 4.4.5).

Phillips' [6] results are again included on the 700°C curve. The effect of quenching treatment is not marked at these ageing temperatures. The flow stress values at the two temperatures are similar for ageing times up to 10 minutes. At 700°C the strengths of alloys A and B increased up to ageing times of about 300 minutes after which they showed a slight fall on ageing up to 10,000 minutes. The nickel-aluminium alloy shows a definite fall in strength after the peak at 300 minutes. At 750°C the peak is reached after 10 minutes ageing and the strength then remains constant up to about 100 minutes before falling. Alloy A does not appear stronger at these ageing temperatures mainly because the phase diagram shows a lower equilibrium volume fraction for this alloy at these temperatures.

It should be noted that the true yield stress may be considerably below the values obtained for overaged alloys because of the very rapid initial work hardening rates of these specimens. Measurements of the 0.1% proof stress were compared with the extrapolated yield stresses and these showed a somewhat greater loss of strength on overageing; the 0.1% proof stress results were not, however, reproducible.

The explanation of the change in yield stress with ageing time depends much on the variation of the volume fraction and nature of the precipitate. In the discussion therefore the yield stress will be related to the nature of the precipitate and its distribution rather than its variation with time. The sections on the phase transformation and kinetics will explain many of the inflexions shown by the curves, which are determined more by the phase transformation than any change in the yielding mechanism.

The features to be discussed are:

(i) The marked increase in yield stress with alloy composition for a given volume of precipitate.

(ii) The strengthening for ageing treatments which do not show γ' particles in the electron microscope.

(iii) The increase in strength with particle size when the volume fraction of precipitate becomes essentially constant.

(iv) The effect of alloy composition on the overageing after peak hardness.

Work hardening rates.

The parameter used for the work hardening rate is the difference between the flow stress at 5% strain and that at 0.1% strain. This gives a measure of the average work hardening rate over this range of strain, but the measurements are subject to some scatter for the reasons given in the experimental section. Figs. (4.4.6 and 4.4.7) show the work

hardening rates of the two alloys at 600 and 700°C. Tests at 500°C showed a small rise in work hardening rate for ageing times in excess of 10,000 minutes, but otherwise the work hardening rate was constant with ageing time. At 600°C the work hardening rate is constant up to 1100 minutes after which it rises steadily with ageing time. At 700°C a similar rise is observed after about 30 minutes and at 750°C after about 10 minutes.

The important feature of these results is that the rise in work hardening rate occurs before the time at which peak hardening occurs. If it is supposed, on a simple model, that a high rate of work hardening is associated with a looping of dislocations around the particles then this rise should be associated with a loss in strength. This point will be considered in the mechanical properties discussion.

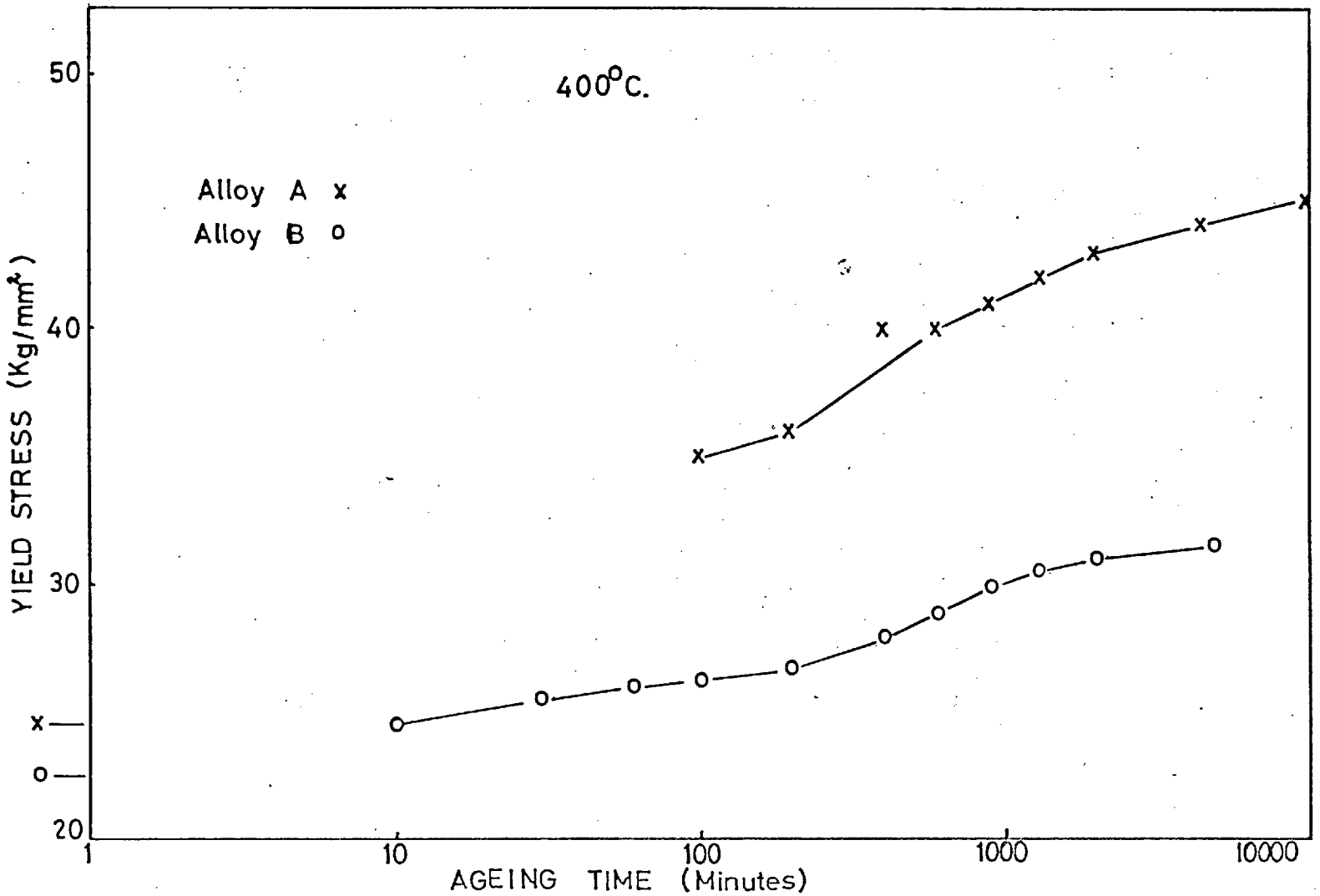

Fig.4.4.1.Yield stress versus ageing time after ageing at 400°C.

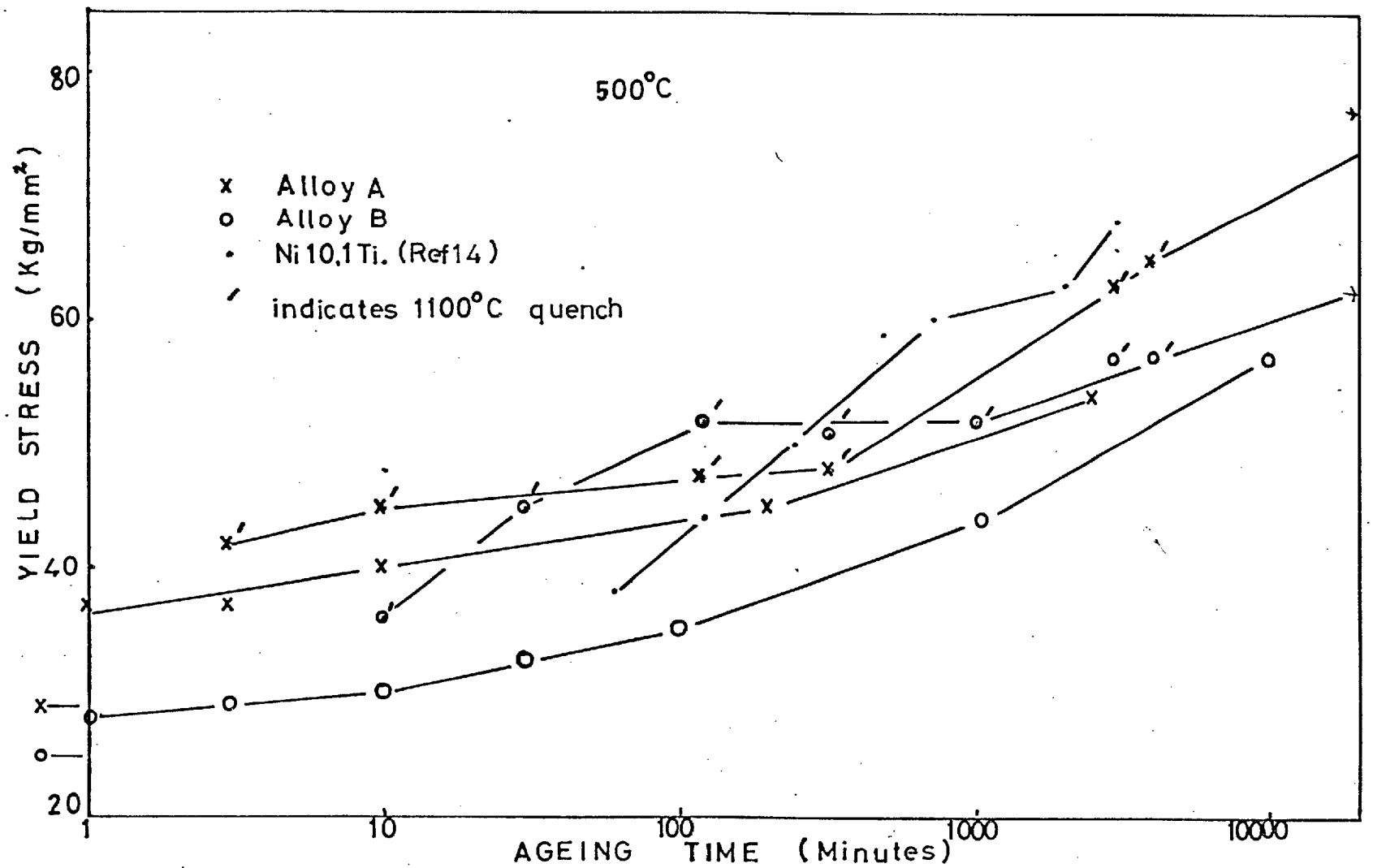

Fig.4.4.2.Yield stress versus ageing time after ageing at 500°C.

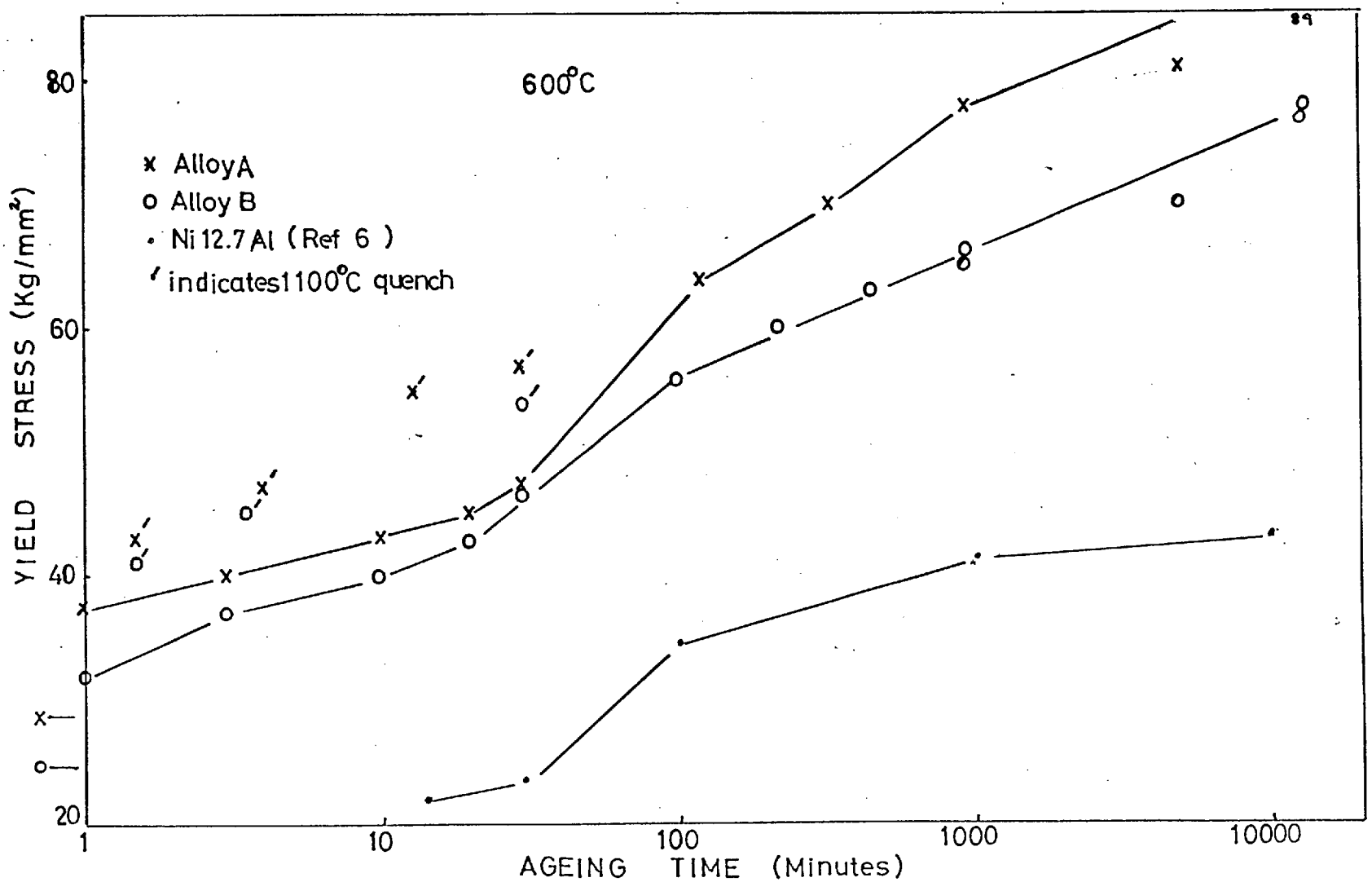

Fig.4.4.3. Yield stress versus ageing time after ageing at 600°C.

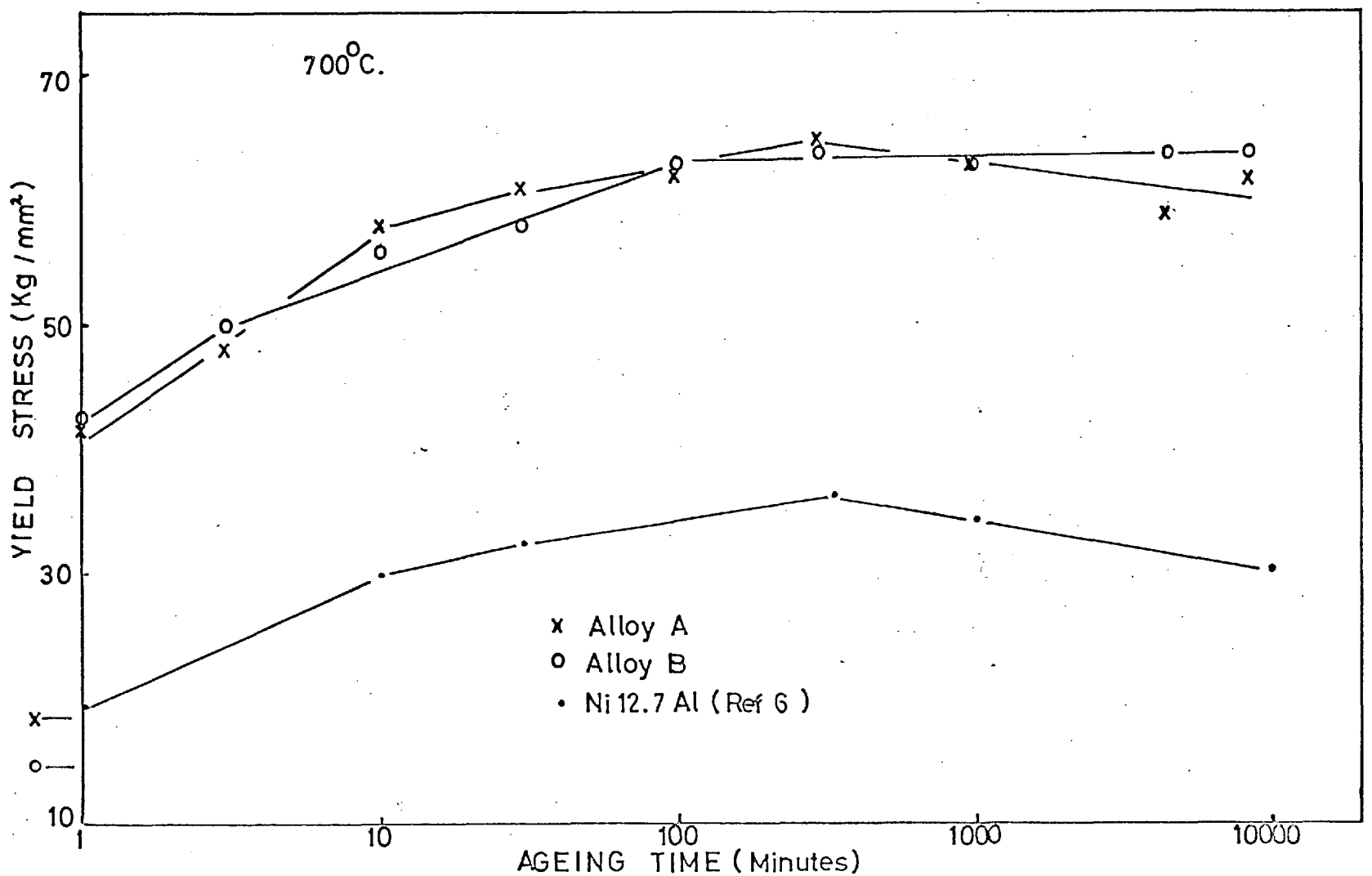

Fig.4.4.4. Yield stress versus ageing time after ageing at 700°C.

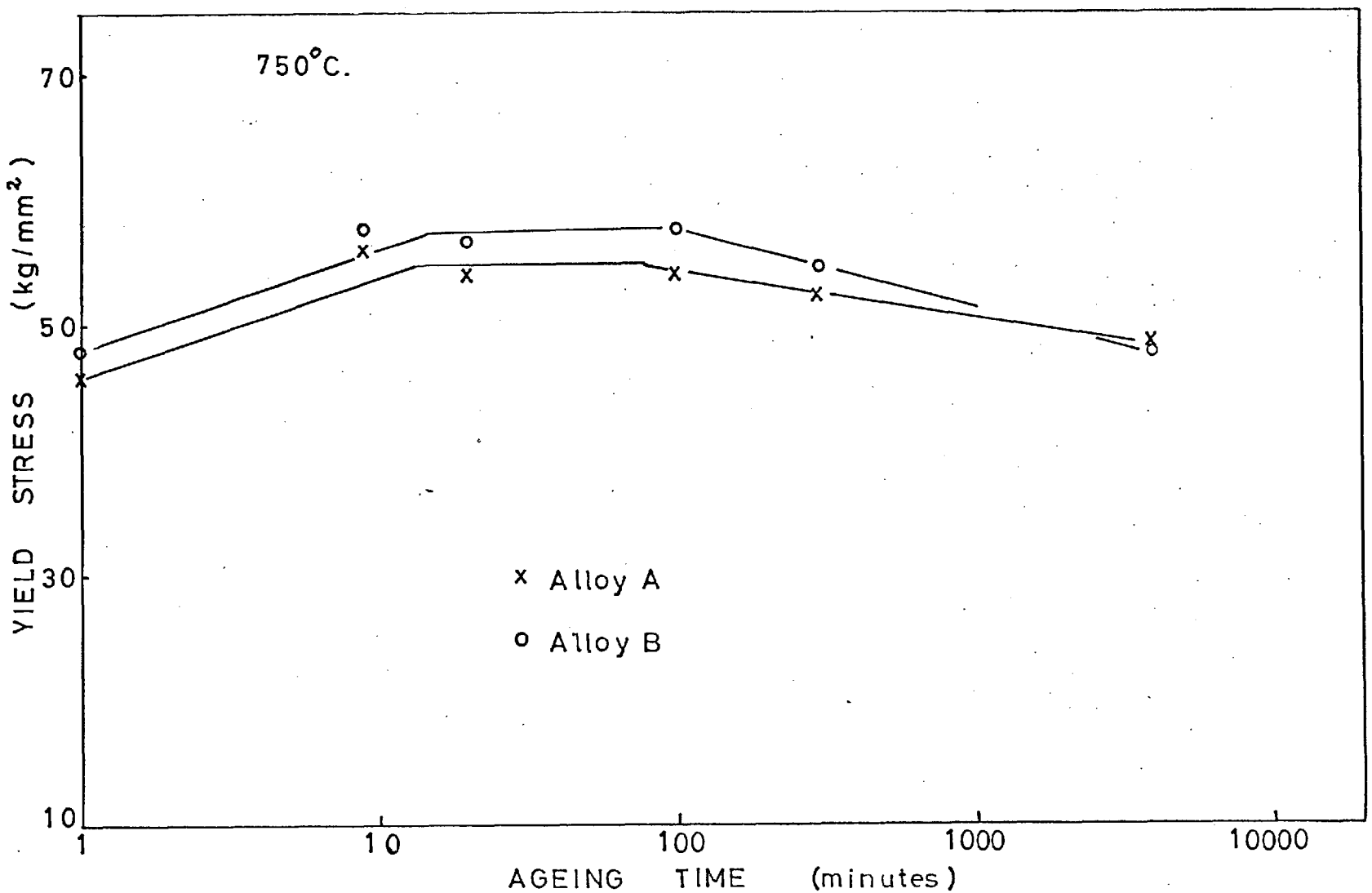

Fig.4.4.5. Yield stress versus ageing time after ageing at 750°C.

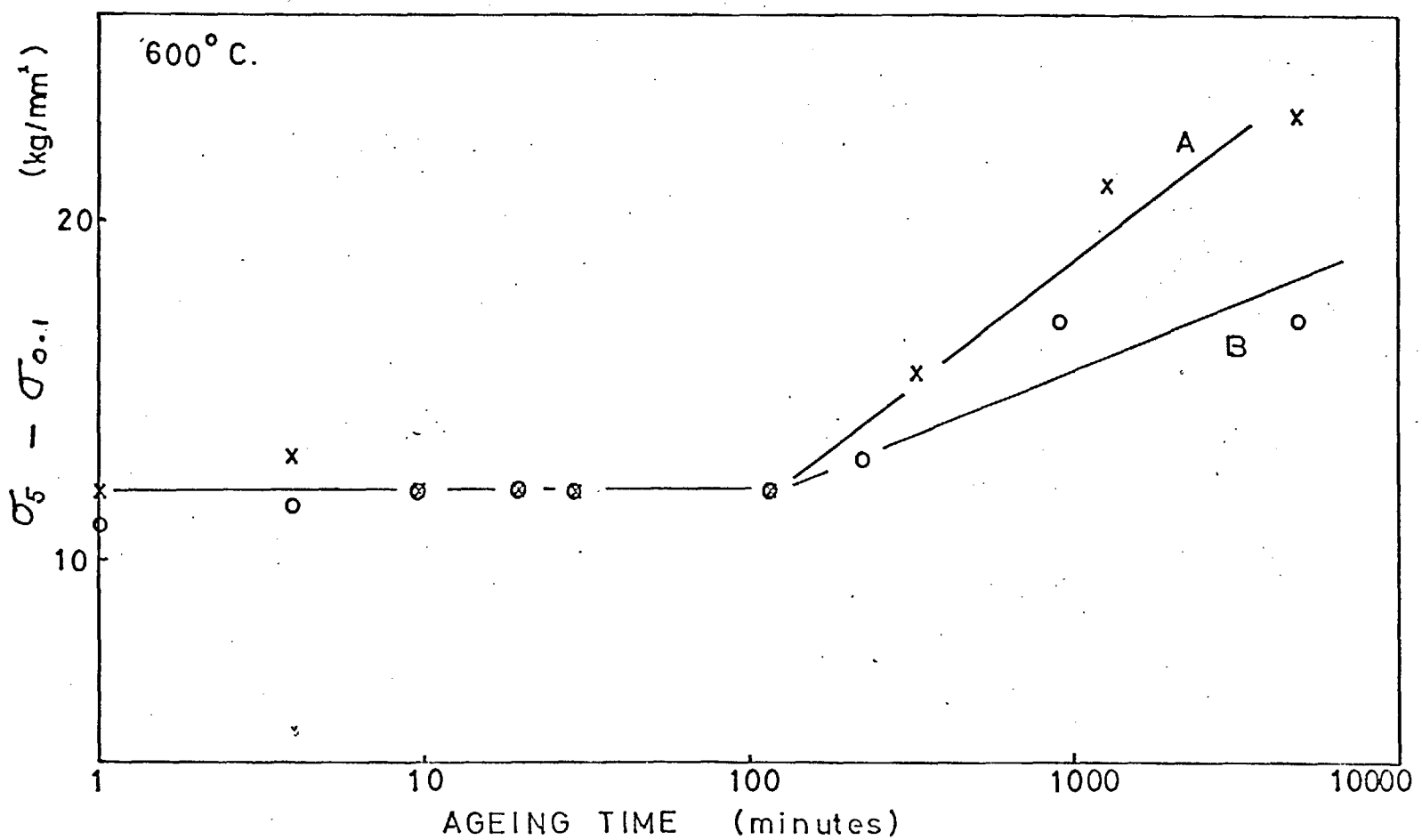

Fig.4.4.6 Work hardening rate versus ageing time after ageing at 600°C.

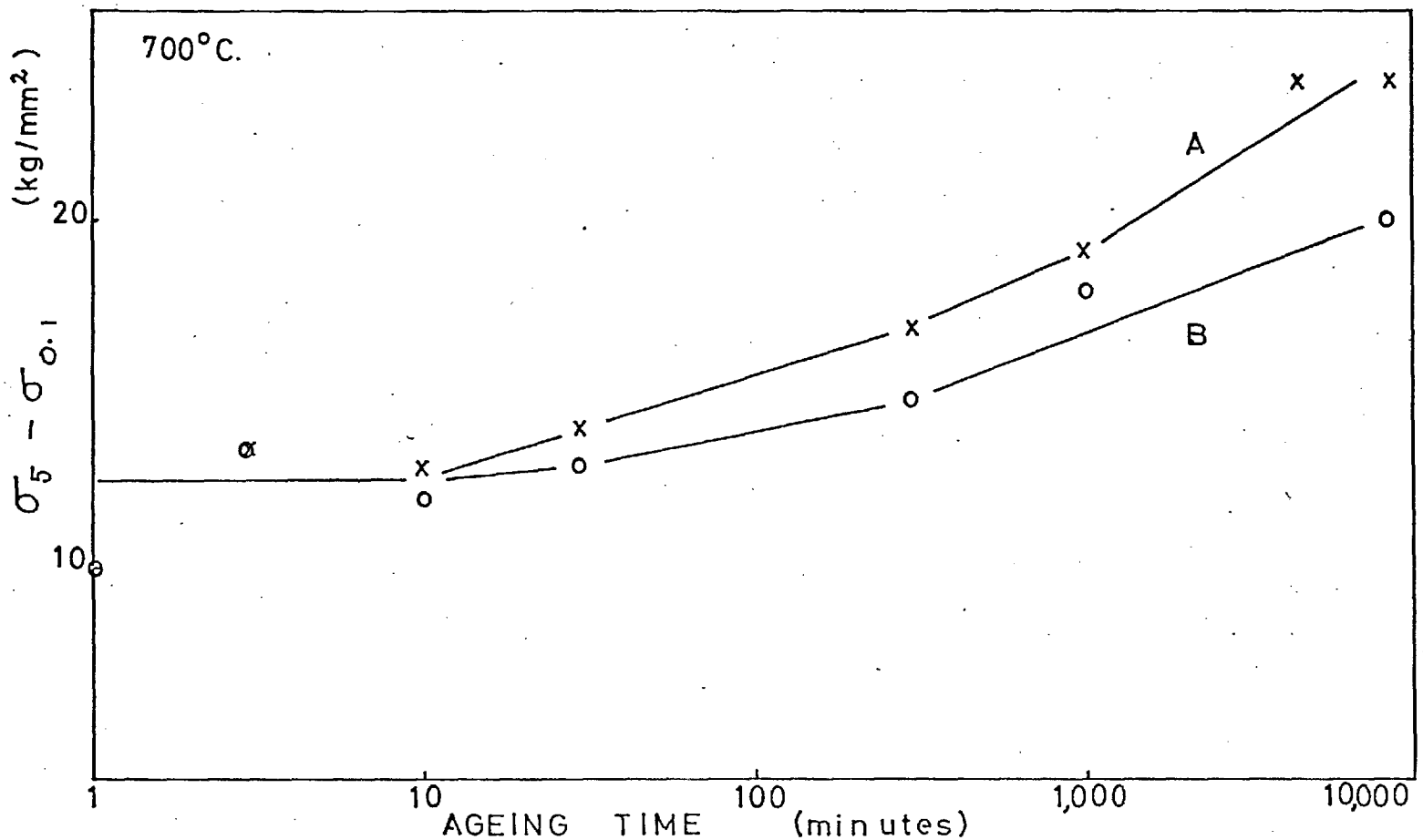

Fig.4.4.7. Work hardening rate versus ageing time after ageing at 700°C.

4.5. Curie temperature results.

Typical sequencies of permeability/temperature curves are shown in figs. (4.5.1 and 4.5.2). The sequence in figure (4.5.1) is of specimens of alloy A aged at 750°C and that in fig. (4.5.2) is of alloy B aged at 400°C. It may be seen that the curves vary between two extremes, one showing a sharp drop in permeability with temperature and one showing a gradual fall in permeability over a range of temperature. The latter curves are characteristic of ageing at lower temperatures or for short times at intermediate temperatures.

Ageing at the higher temperatures:

750°C Fig. (4.5.3).

Both alloys showed sharp changes of permeability with temperature from the shortest ageing times. The maximum range of temperature over which the transformation took place was about 8°C. The Curie temperature rose very rapidly in the first minute of ageing and then increased slowly up to an ageing time of about 100 minutes. For ageing times greater than 100 minutes the Curie temperature was constant.

700°C Fig. (4.5.4).

The temperature range after 1 minute of ageing was 10°C for alloy A and 20°C for alloy B. These ranges dropped to 5°C after 10 minutes ageing. The Curie temperature rapidly rose in the first minute of ageing and continued to rise steadily up to ageing times of about 100 hours.

600°C Fig. (4.5.5).

The effect of the different quenching treatments may be seen for ageing times less than about 100 minutes at 600°C. The Curie temperature change in the first minute of ageing was again very marked. The Curie temperature ranges for both alloys changed from 15°C to 6°C over the first 30 minutes of ageing; there was however some evidence of a small fraction of each sample having lower Curie temperatures; the figures given represent 90% of the total magnetic change. The Curie temperature continued to increase steadily up to the longest ageing times.

Summarising the effects at the higher ageing temperatures; the initial rise in Curie temperature is greater at 600°C than at 750°C, suggesting that this initial process is very rapid and dependent on the supersaturation. The lower the ageing temperature the longer the time it takes before the alloys show narrow ranges for the magnetic change and the longer the time required for the Curie temperature change to go to completion.

Lower ageing temperatures:

500°C Fig. (4.5.6).

The effect of the prior quenching treatment is pronounced and the ageing curves after the two quenching treatments only come together at very long ageing times. The slopes of the ageing curves after the 875°C quenching treatment increase with time over the first 1000 minutes of ageing. The Curie

temperature ranges were about 10°C after 1 minute ageing, increased to about 20°C after ageing for 3 minutes and then decreased steadily to about 6°C on ageing up to 200 minutes for alloy A and 1000 minutes for alloy B. The rise in Curie temperature during the first minute of ageing was still large and was greater than that at 600°C.

400°C Fig. (4.5.7).

At this temperature the initial large rise was not observed although a small change took place in the first minute. The range over which the magnetic change took place increased from about 30°C after 1 minute ageing to 145°C after 10,000 minutes ageing for alloy A and from 20°C to 110°C for alloy B. The lower limit of the range remains essentially constant whilst the upper limit steadily increases with ageing and the rate of change of Curie temperature decreases at long ageing times. The shapes of the ageing curves are similar for both alloys except that alloy A has a larger increase in Curie temperature during the first minute.

The lower ageing temperatures show increases in the Curie temperature ranges on ageing; at 500°C these ranges are reduced as ageing proceeds, becoming similar to those observed at the higher ageing temperatures. The results at 400°C show that the initial rapid decomposition is retarded at this temperature.

The effect of field strength on the shapes of the permeability temperature curves.

In general, the shape of a permeability temperature curve is a function of field strength, and the effect is discussed in section 5.6. In order to see whether the results in this work could be partly interpreted in terms of a field strength effect, measurements were made over a range of field strengths. The voltage across the coil was varied through the range 50 to 1050 mv (giving fields from 0.2 to 4.5 Oe) and the results are shown in fig. (4.5.8). The shape of the curve is essentially unaffected by fields considerably larger than that used for the majority of the results. The effects observed at very low fields were due to a lack of sensitivity in the apparatus.

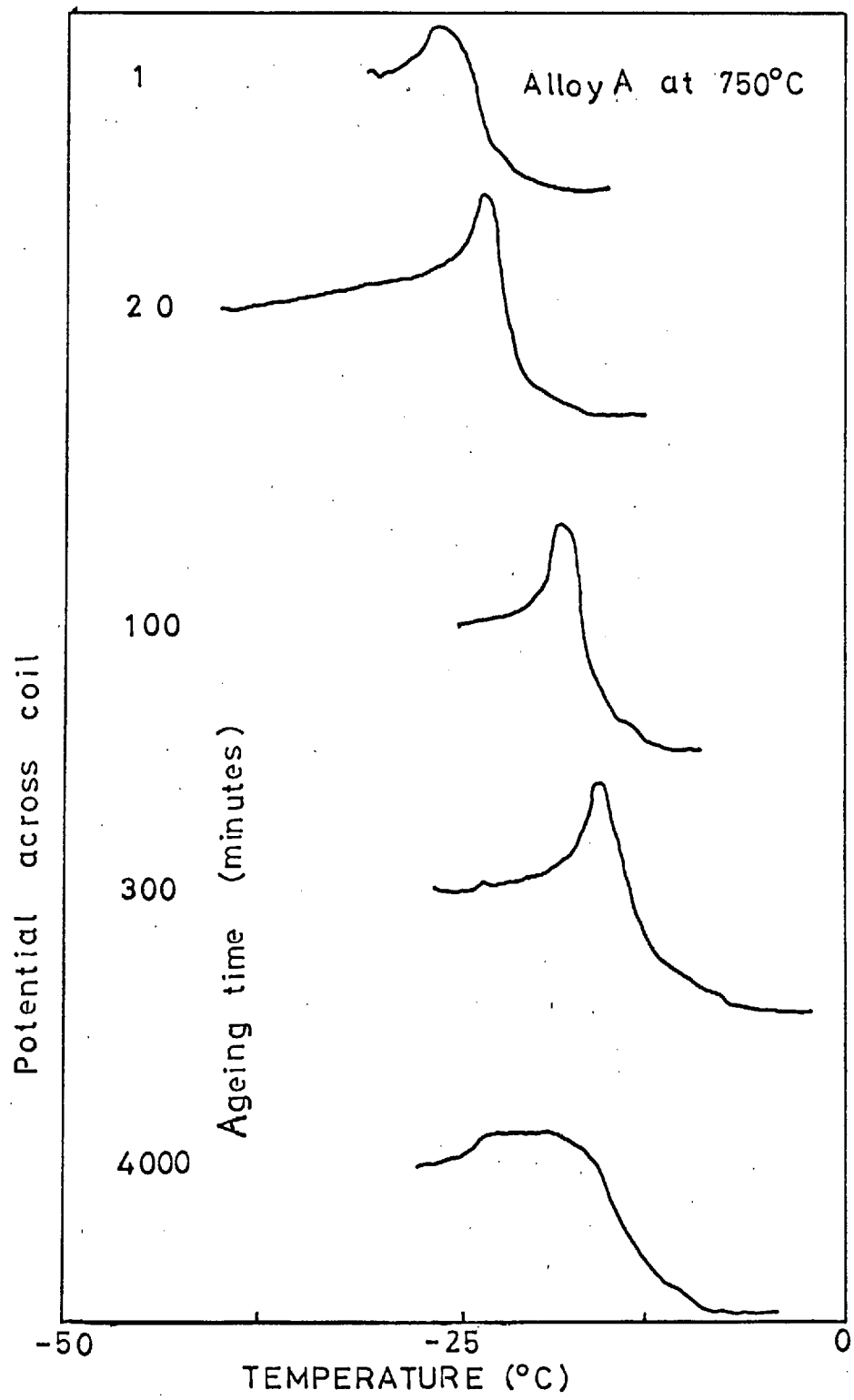

Fig.4.5.1.Typical permeability/temperature curves:

Alloy A aged at 750°C.

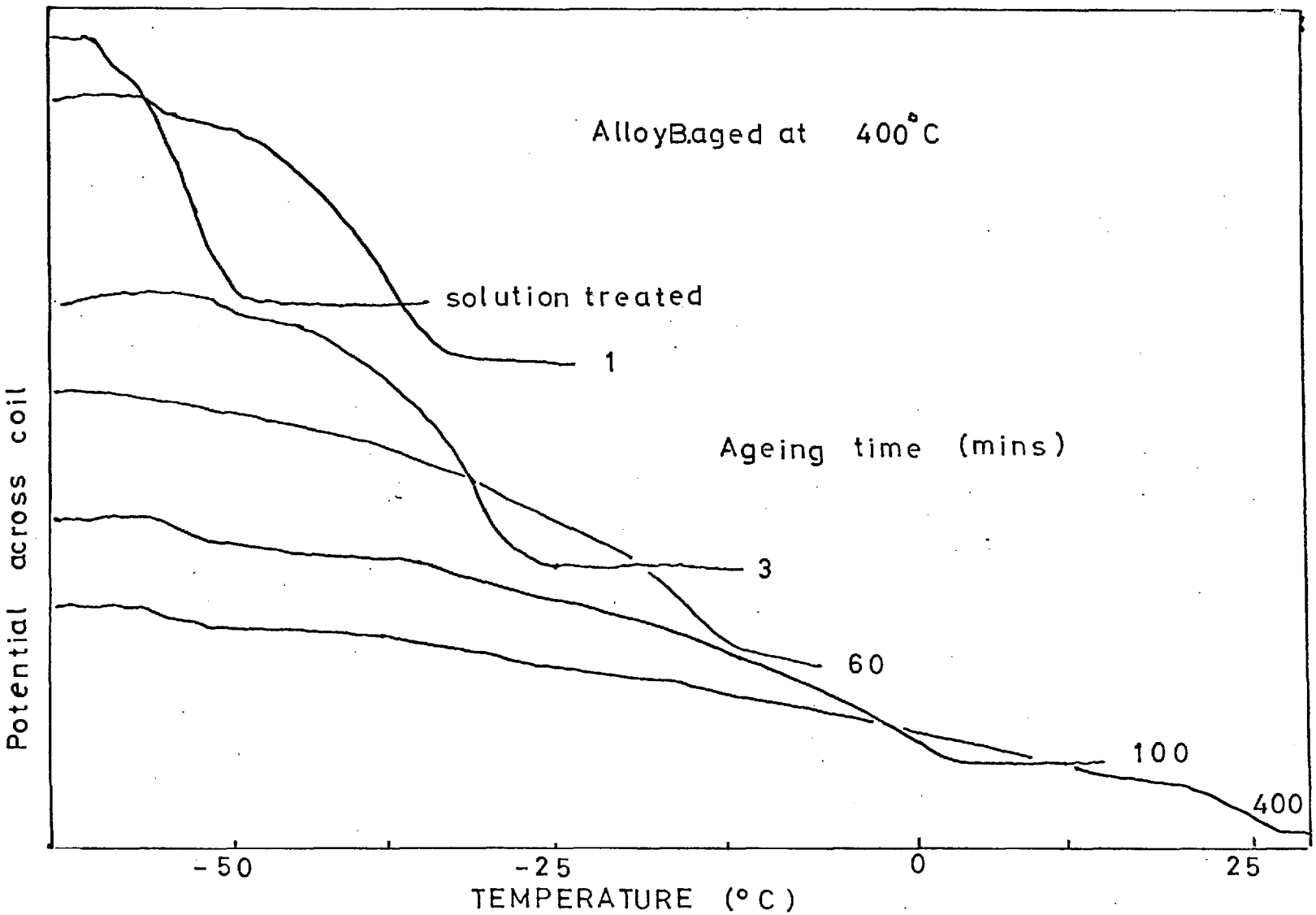

Fig.4.5.2 Typical sequence of permeability/temperature curves : Alloy B aged at 400°C.

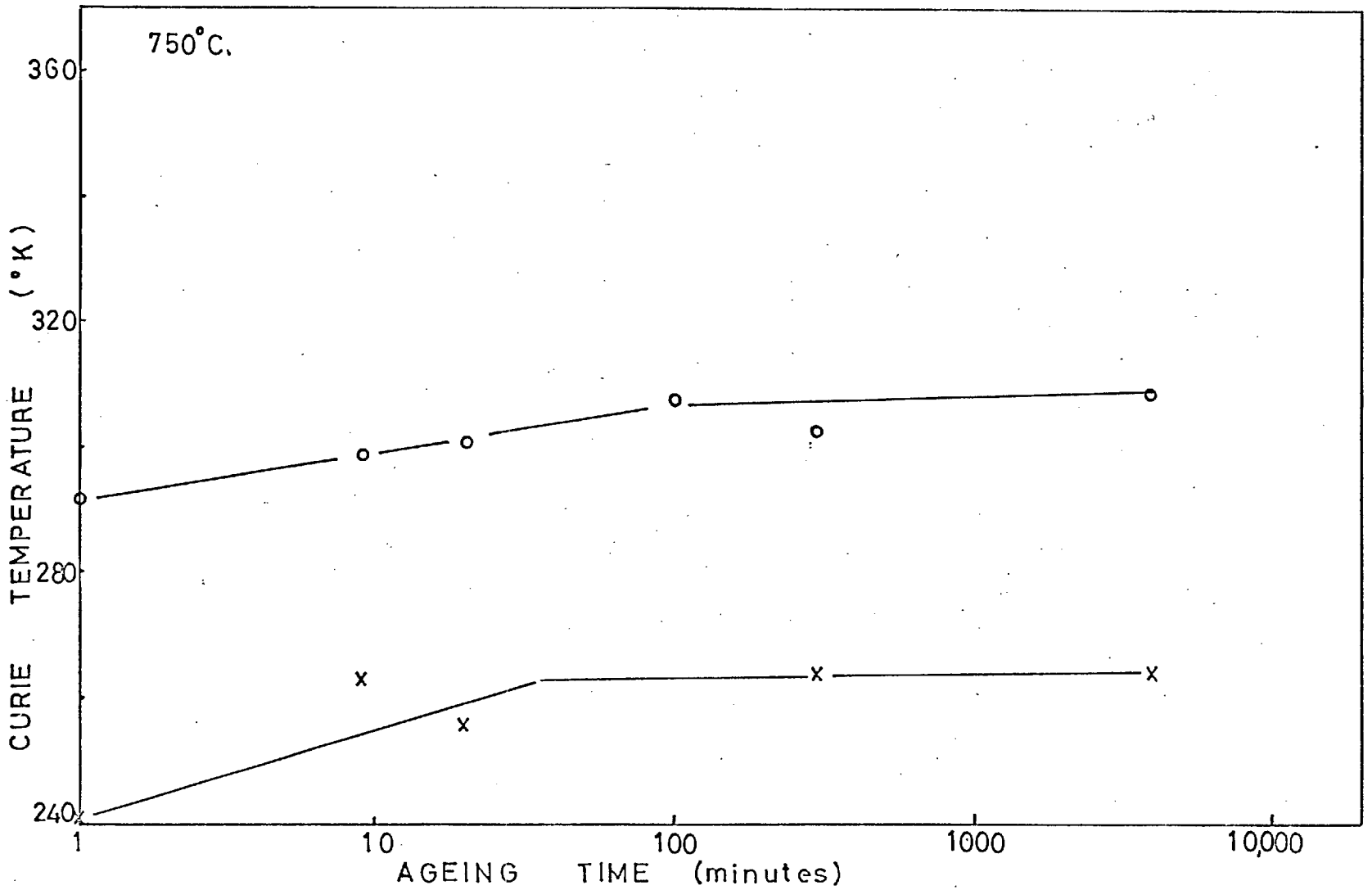

Fig.4.5.3.Curie temperature versus ageing time after ageing at 750°C.

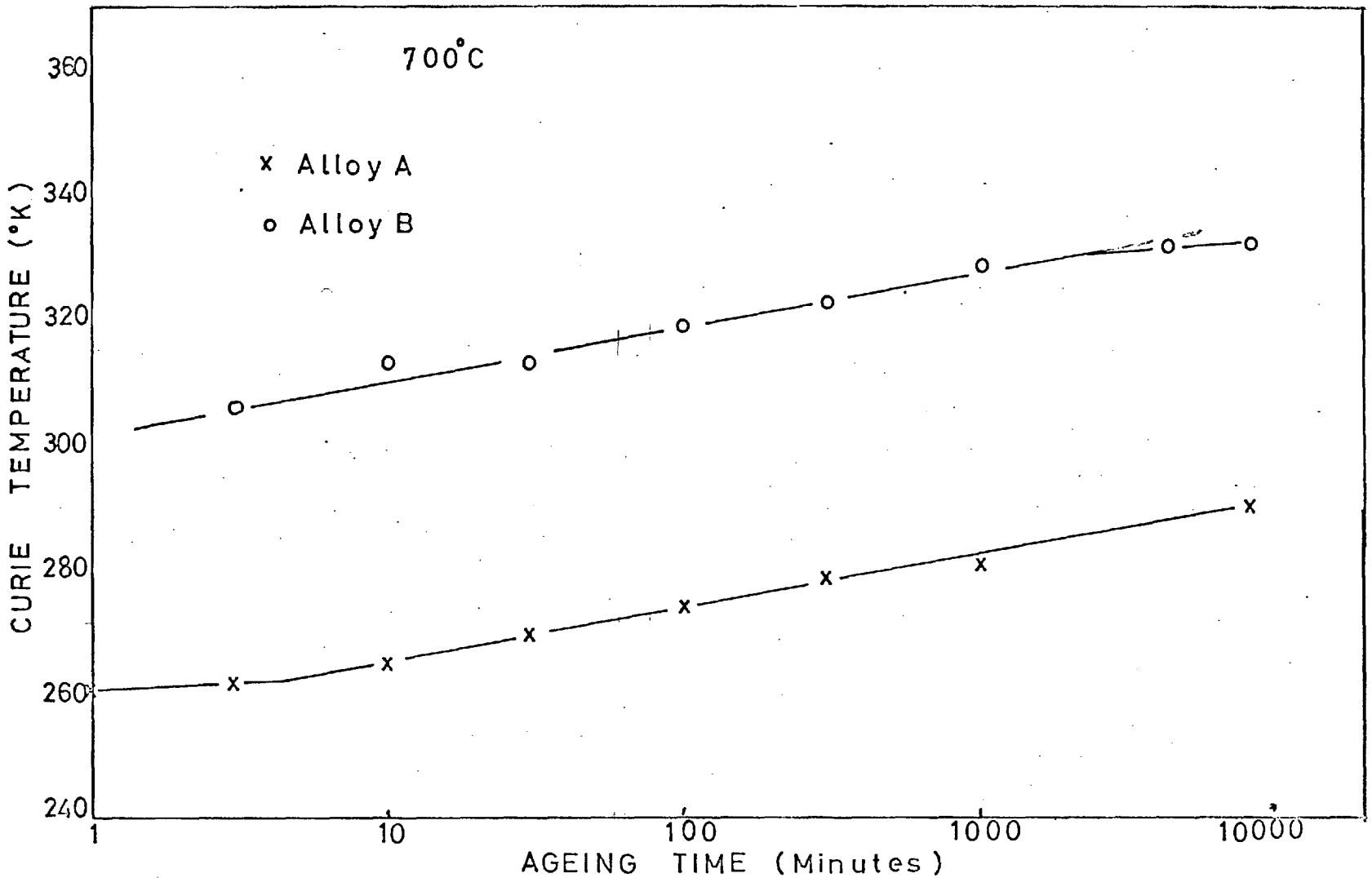

Fig.4.5.4.Curie temperature versus ageing time after ageing at 700°C.

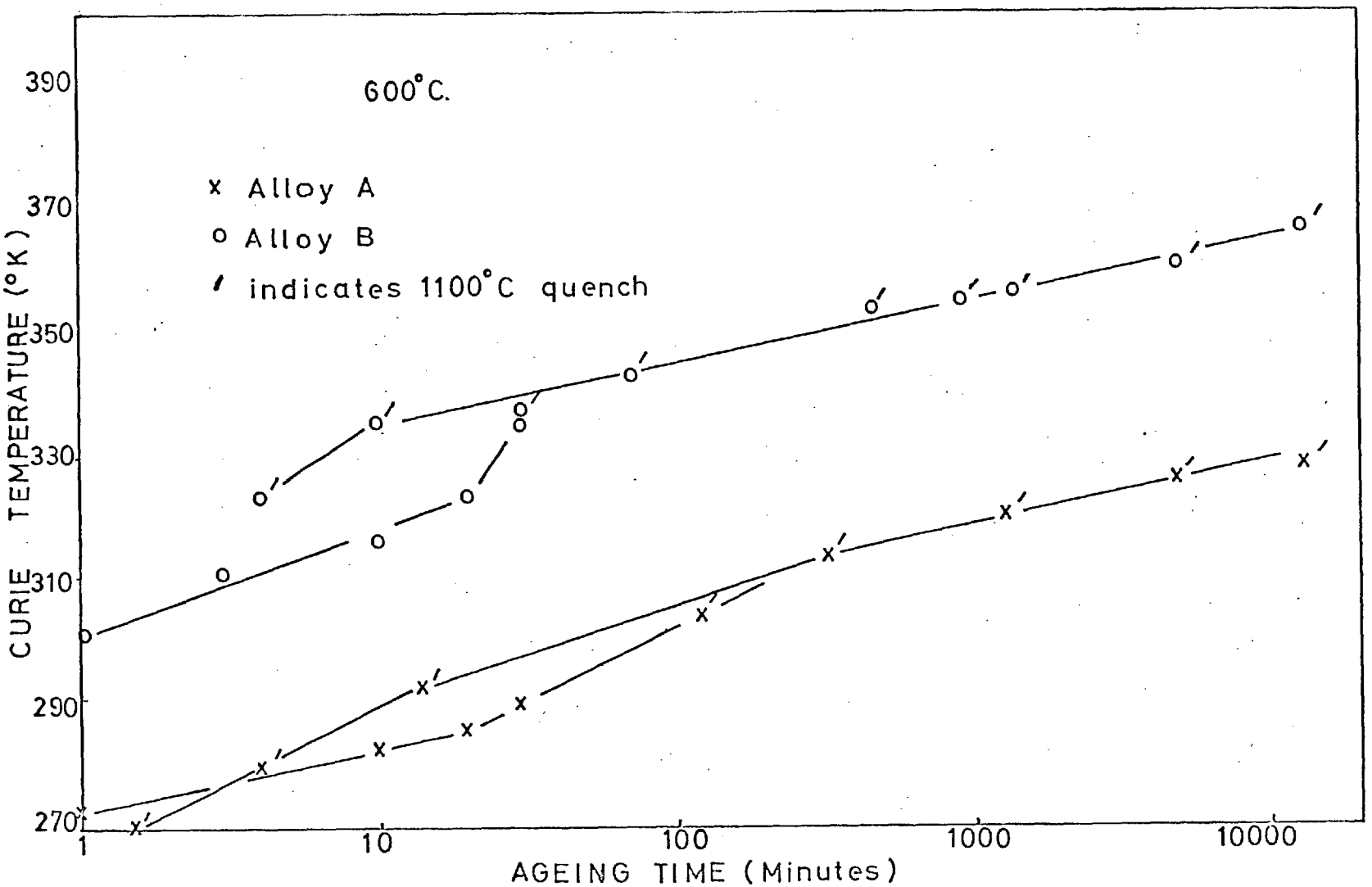

Fig.4.5.5. Curie temperature versus ageing time after ageing at 600°C.

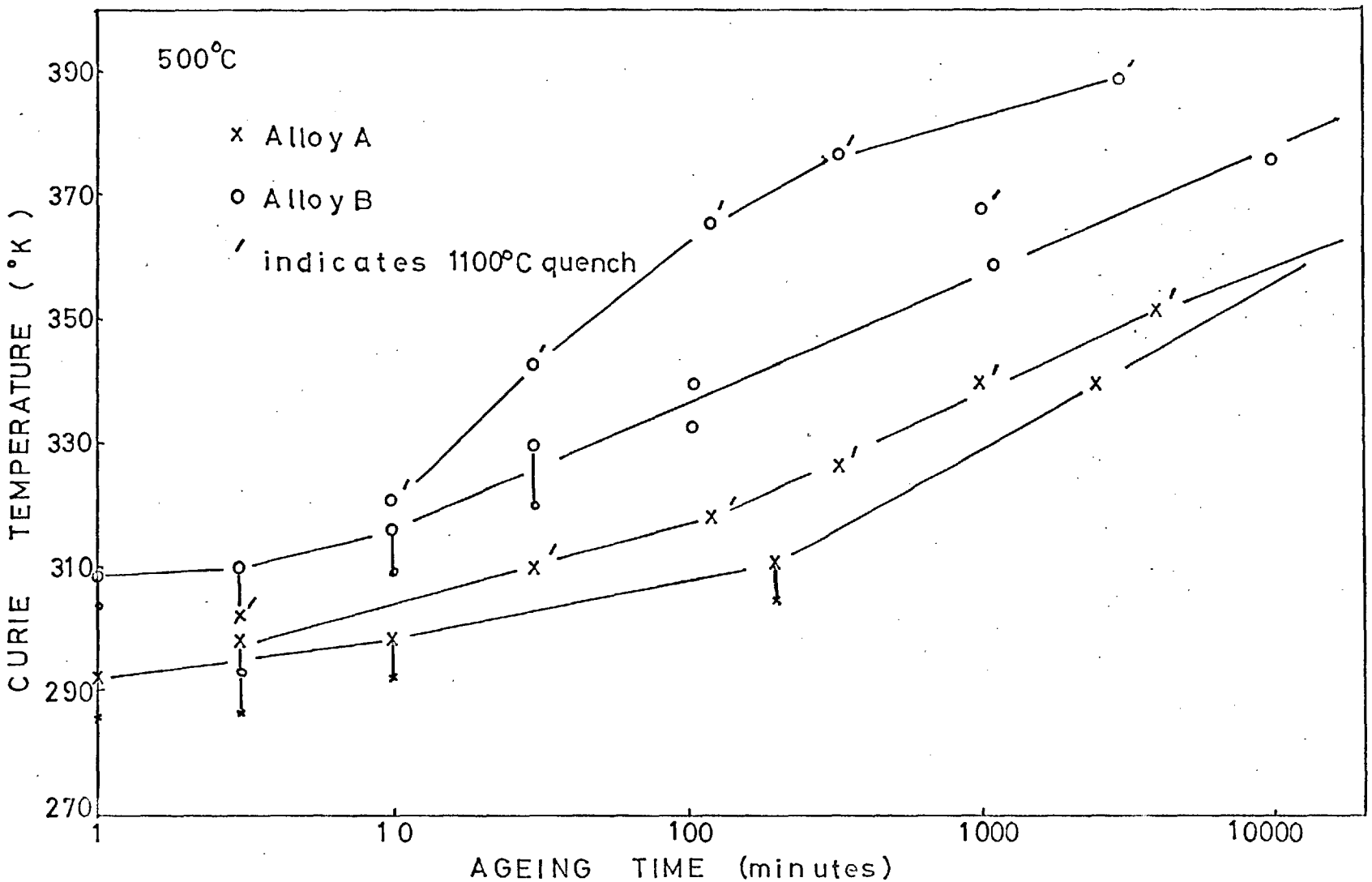

Fig.4.5.6. Curie temperature versus ageing time after ageing at 500°C.

(bars indicate Curie temperature ranges)

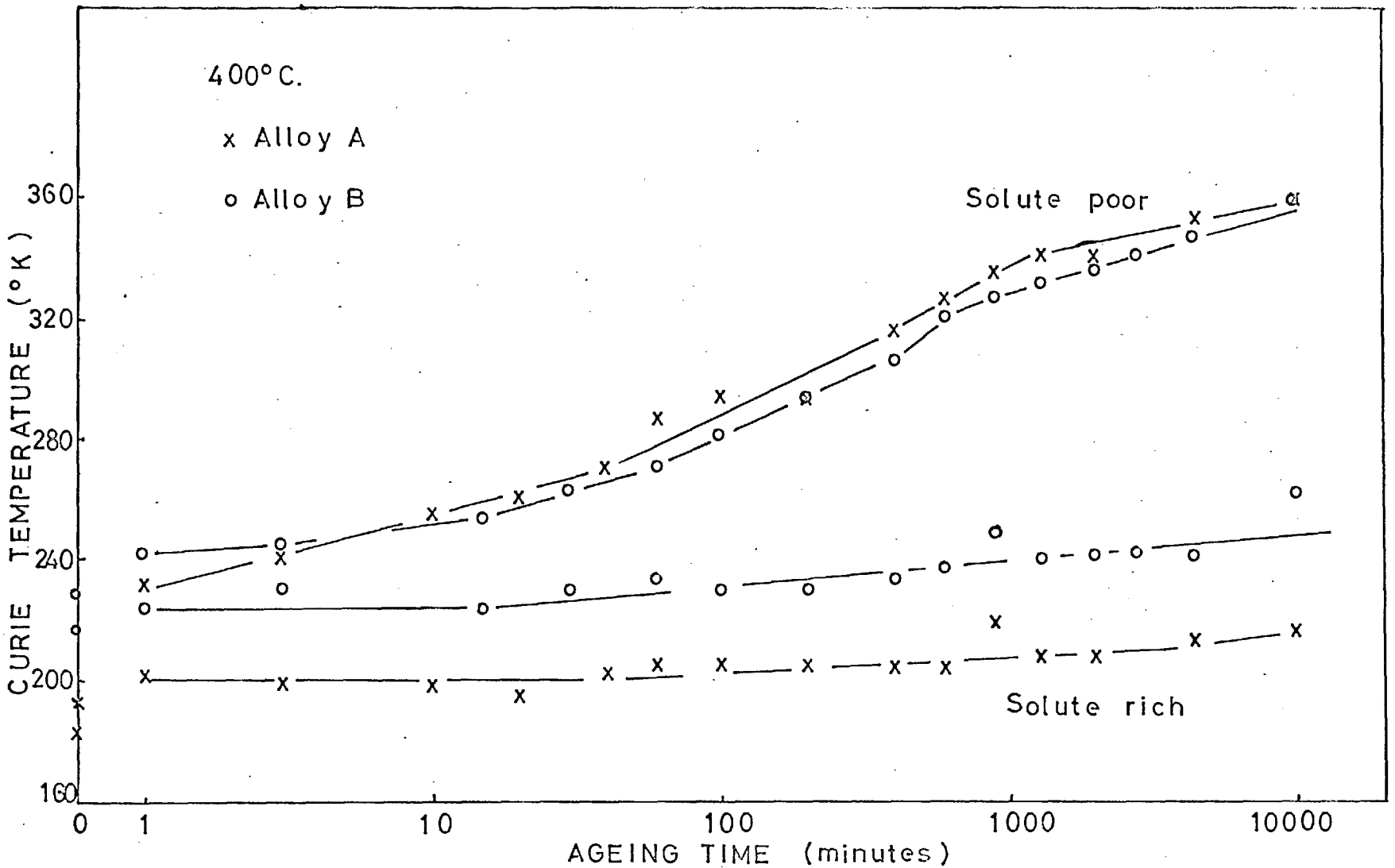

Fig.4.5.7. Curie temperature ranges versus ageing time after ageing at 400°C.

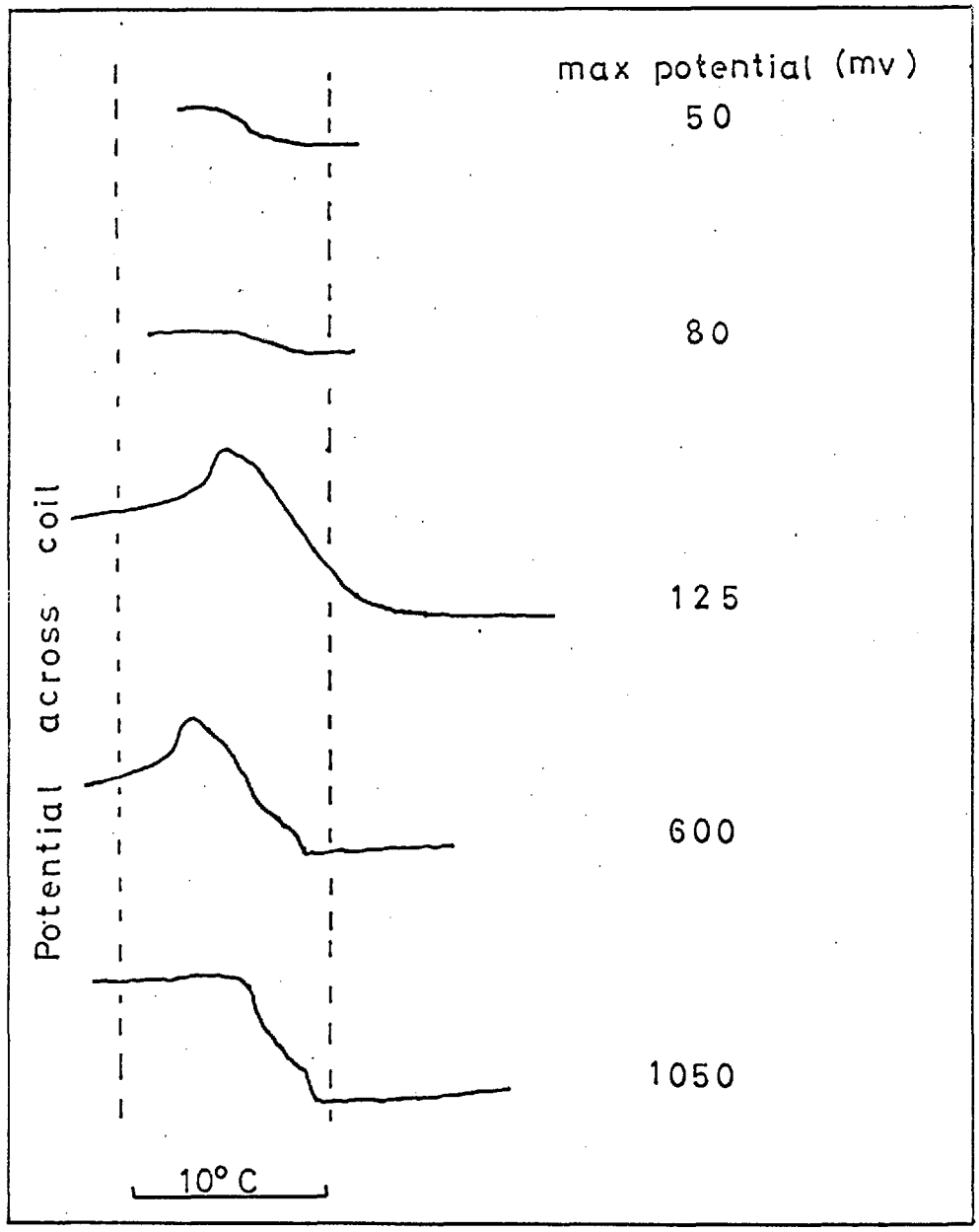

Fig.4.5.8.Effect of field strength on permeability/temperature curves.

4.6. Temperature dependence of the electrical resistivity.

Figs. (4.6.1 and 4.6.2) show the variation in resistivity with temperature compared with the permeability/temperature curves for the same specimens. Fig. (4.6.1) is of a specimen of alloy B aged for 184 hours at 300°C to produce a wide range of Curie temperatures; and fig. (4.6.2) refers to the same alloy aged for 125 hours at 700°C to produce a narrow range of Curie temperatures.

The 700°C specimen shows a sharp change in slope in the resistivity temperature curve at a temperature close to that at which the change in permeability takes place. For the specimen aged at 300°C the slope of the resistivity plot decreases at a point somewhat below that where the permeability starts to drop, and reaches a constant value at a temperature close to that where the permeability reaches zero.

If similar curves in the literature are considered an increase in the slope of the curve should be observed prior to a decrease at the Curie temperature, but this effect has not been observed in this work. It is very likely that the rise would be masked in the case of the specimen having a range of Curie temperatures (see also Williams [3]) but at present the absence of a rise for the other specimen cannot be explained. The results show that a change in resistivity occurs over a similar range of temperatures to the change in permeability, and

therefore confirm that the gradual change in permeability with temperature is a consequence of a range of matrix compositions giving rise to a range of Curie temperatures.

4.7. Elastic modulus results.

Values of $\frac{\Delta E}{E}$ $(= \frac{2\Delta f}{f})$ measured at room temperature are shown in figs. (4.7.1 and 4.7.2) for alloys A and B aged at 500, 600 and 700°C. It should be noted when comparing these results with the other measurements that the modulus specimens did not receive the 875°C quenching treatment.

Ageing at 500°C.

A steadily increasing slope is observed in the early stages for both alloys; the slope of the curve becomes constant after about 10 minutes ageing for both alloys. The initial values of $\frac{\Delta E}{E}$ are lower for alloy A but the overall slope of the curve is greater for this alloy.

600°C.

The curves for both alloys show an increase in slope after 2 to 5 minutes ageing, followed by a decreasing slope which reaches a constant value after about 20 minutes ageing. The slope of the curve for alloy A is again greater than that for alloy B.

700°C.

Both alloys showed a steady increase in modulus for ageing times up to about 20 to 30 minutes and the modulus then remained constant with ageing time.

The shapes of the modulus curves, particularly in the early stages of ageing, are similar to the Curie temperature/ageing time curves obtained from specimens aged following quenching from 1100°C. This suggests that the phenomena giving rise to the changes in these parameters are closely related. An increase in modulus on the precipitation of γ' from the supersaturated solid solution is clearly shown by these results.

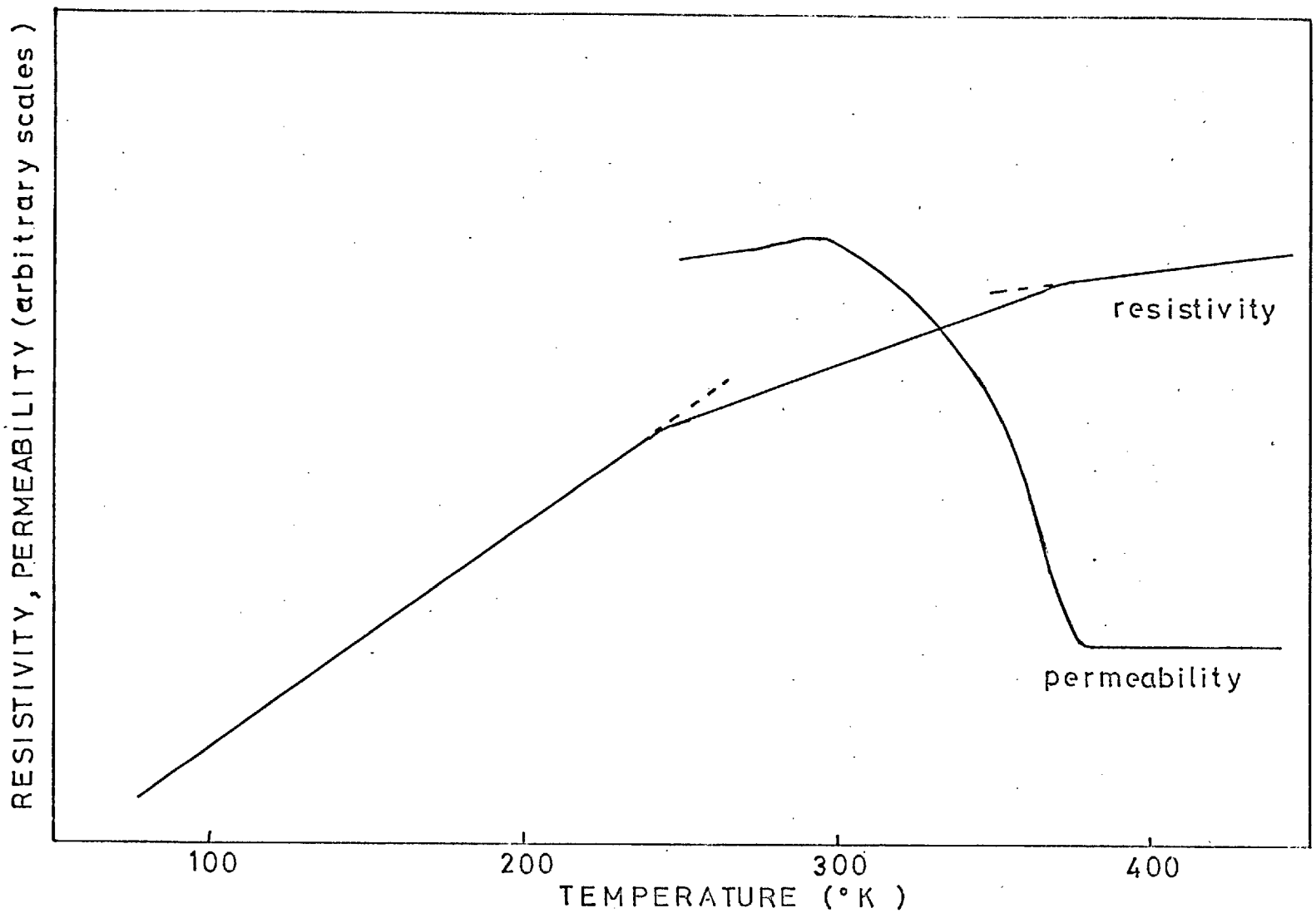

Fig.4.6.1. Temperature dependence of the electrical resistivity : Alloy B aged at 300°C. for 184 hours.

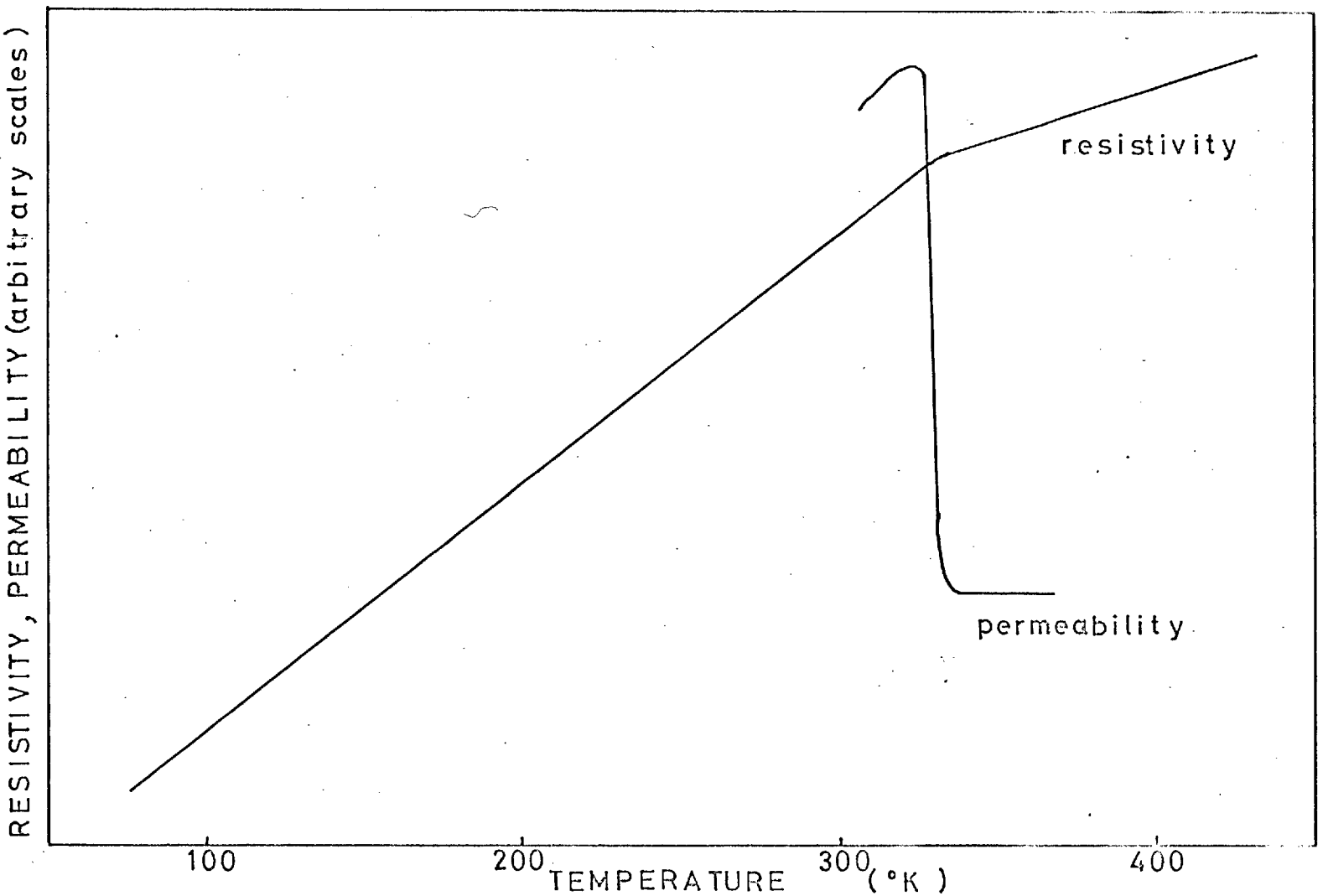

Fig.4.6.2.Temperature dependence of permeability and resistivity:Alloy B aged 125 hours at 700°C.

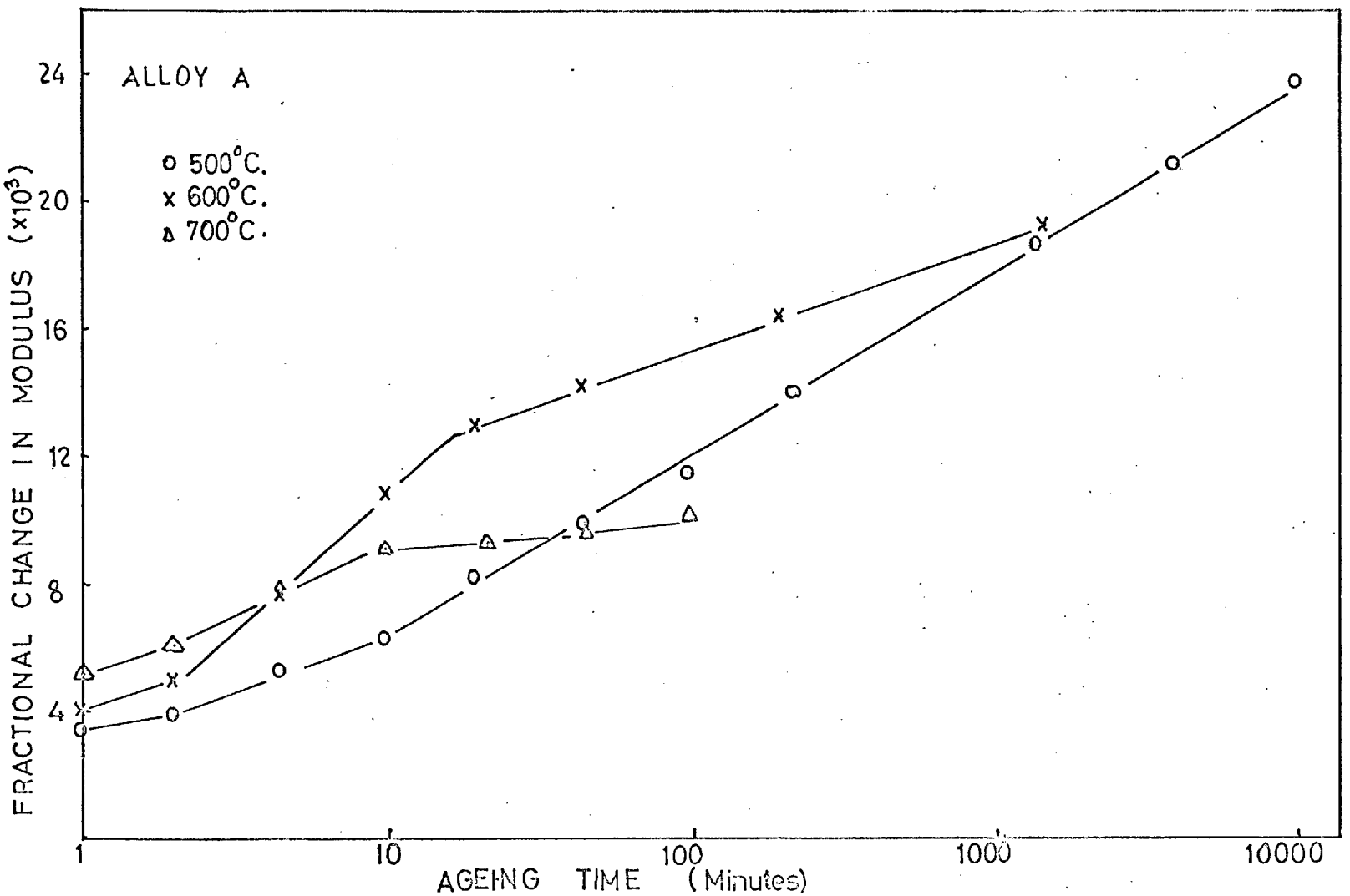

Fig.4.7.1. Fractional change in modulus versus ageing time at 500, 600, and 700°C. Alloy A.

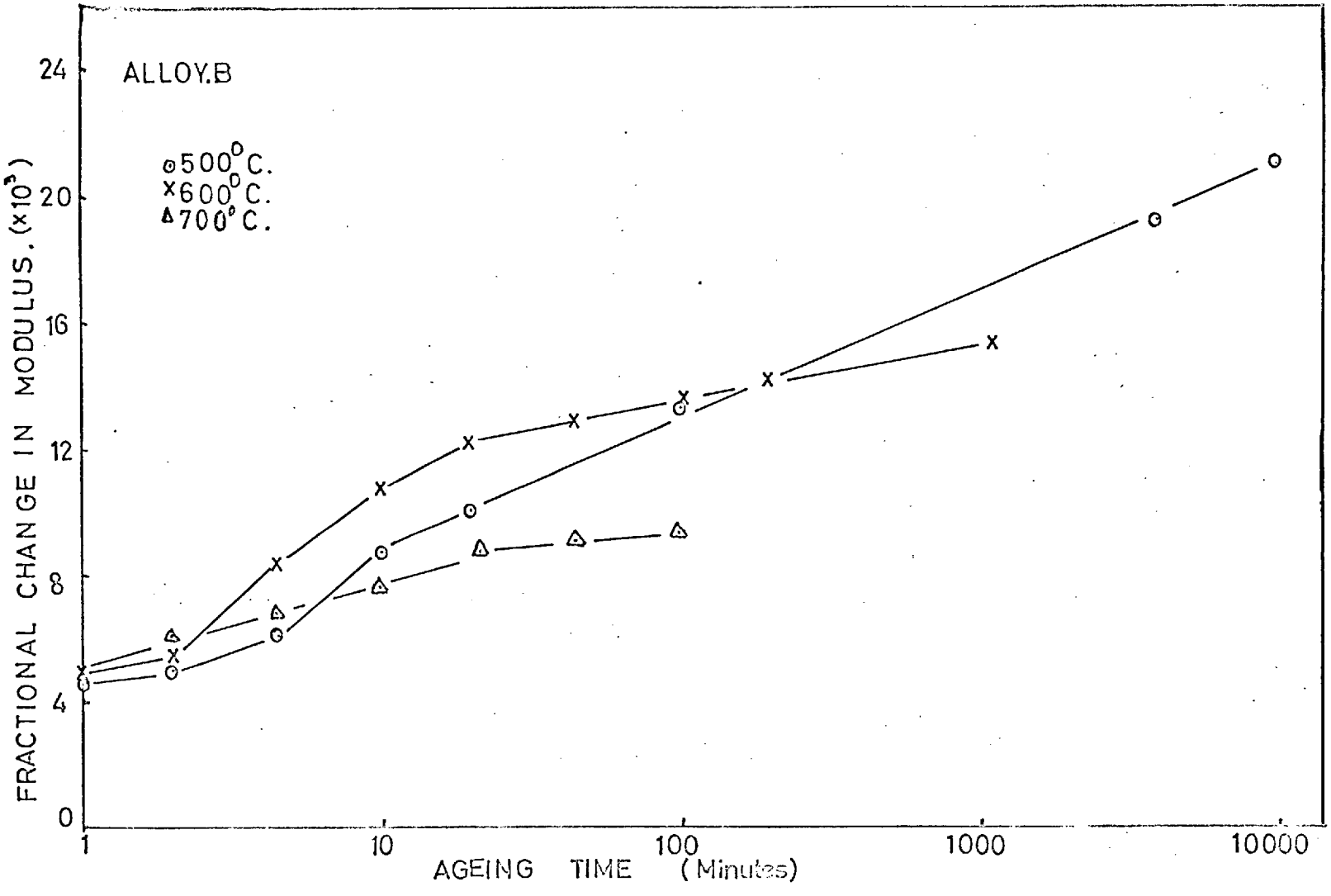

Fig.4.7.3.Fractional change in modulus versus ageing time at 500,600 and 700°C. Alloy B.

4.8. X-ray lattice parameters.

The values of the matrix lattice parameters obtained in the present work for the alloys aged at 700°C for 25 hours

Alloy A = 3.544 Å
Alloy B = 3.538 Å

In order for the mismatch values to be obtained the values of the lattice parameters of the γ' phase determined by Taylor and Floyd [1] are assumed. For alloys having aluminium to titanium ratios similar to those of alloys A and B the following parameters are shown:-

Alloy A 3.587 Å
Alloy B 3.571 Å

giving mismatches (at 700°C) for Alloy A of 1.2% and alloy B of 0.93%.

The lattice parameter of the matrix depends on the concentration of solute in the matrix; the misfit will therefore be a function of the precipitate volume fraction and will be greatest at the lower ageing temperatures.

5. Discussion of Experimental Results.

5.1. Electron microscopy - contrast effects.

The precipitates may be observed by precipitate contrast or by matrix contrast due to their perturbing effect on the surrounding matrix whilst they remain coherent.

(i) Precipitate contrast

As the γ' is of ordered f.c.c. structure coherent with the matrix there is no possibility of contrast arising from the f.c.c. reflecting planes as these will be essentially continuous throughout the matrix and the particles (except for the lattice distortions giving rise to the matrix contrast effects). As the γ' is ordered it has reflections that are forbidden to the matrix (100, 110) and these reflections can give rise to contrast due to interference with the f.c.c. reflections. If the diffraction conditions are such that superlattice and f.c.c. reflections are operating so as to interfere, then the particles appear dark against the light background of the matrix. (Fig. (4.1.1) is a good example of precipitate contrast).

Even when conditions are not such as to show precipitate contrast, the particles may still be seen because of the effect of the elastic strain fields on the scattering of the electron beam.

(ii) Matrix contrast

The results show that, amongst other effects, lines of no contrast may be observed when only one strong reflection is operating. The work

of Ashby and Brown[15] established the theory of matrix contrast from coherent precipitates and their work allows the interpretation of the various contrast effects that are observed around γ' particles embedded in the matrix. The theory shows that there are five principle features that affect the image profile:

(1) Thickness of the foil

The fringes in the image become less pronounced as the foil thickness increases, but the overall width of the image is relatively independent of the foil thickness.

(2) Depth of the particle in the foil

The shape and symmetry of the image varies with the depth of the particle in the foil. When precipitates are within one extinction distance of the foil surface wide asymmetric images are formed (for example see fig. (4.2.4).

(3) Order of the operating reflections

The width of the image increases and the particles become less sharp for low order reflections. A number of fringes cross the image when low order reflections operate and the intensityof the image relative to the unstrained matrix is reduced.

(4) Particle size

The image width decreases relative to the true particle size as the particle size decreases, and it is possible for very small particles to be invisible.

(5) Magnitude of the strain field

The image widths increase with mismatch for a given particle size.

The image profiles computed by Ashby and Brown are for diffraction conditions when only one strong reflection is operating, and when there is no deviation from the Bragg condition. The presence of a number of operating reflections alters many of the effects, but the results do serve to show how a number of different patterns may be obtained from the same area of a foil. The work also serves to show that there are strict limitations on the conditions under which particle sizes may be measured, particularly in bright field conditions.

The particles in the present work were cubic, whereas the Ashby-Brown analysis is derived for spherical particles with spherically symmetric strain fields. The strain fields around cubic particles will however closely approximate to a radial form and the qualitative observations of the analysis still hold. One effect will be present for cubic particles however; the particles present different thicknesses to the electron beam when the foil is not in a (100) orientation, which will affect the images observed in a different manner to those from spherical particles.

5.2. Particle shape and alignment.

Particle shape:

In an isotropic medium, precipitates nucleate and grow such that they have a minimum surface energy to oppose the free energy of the transformation associated with the volume of the precipitate. The particle size which satisfies the condition of minimum surface area for maximum volume is the sphere. In crystalline solids the elastic anisotropy of the matrix and the variation of surface energy with crystallography must be included in the calculations (16).

In those nickel-based alloys in which there is a low lattice parameter misfit between the γ' and the matrix, the γ' particles are spherical in shape. For systems where the misfit is higher, cubic particles are observed and it may be inferred that the shape is a function of the mismatch at the interface; various examples are given by Manenc [2]. The mismatch contributes to the energy at the interface through the elastic energy associated with the coherency strains.

The elastic anisotropy of nickel is such that the lowest strain energies are associated with coherency strains at (100) interfaces and this would seem therefore to adequately explain the variation in particle shape as the misfit increases. Another observation made by Ardell and Nicholson [10] and Hornbogen and Chakraborty [13] is that there is a change in the early stages of ageing from spherical to

cubic shape. This is less easy to explain, since if it is supposed that the small particles are pure γ' with a sharp interface, then the strain energy per unit area of the interface will be independent of the particle size. Ardell and Nicholson have suggested that they observe spherical particles at small sizes because the elastic strains are less effective at these sizes but they do not indicate the reason.

In the discussion that follows it is suggested that the alignment results from an elastic interaction between the particles, and that the alignment process is one of selective coarsening with chemical potential gradients favouring alignment in (100) directions. The work of Ardell and Nicholson shows that there is no elastic interaction between the particles and the solute atoms; however the chemical potential gradients set up for selective coarsening in (100) directions may affect the diffusion rates, thus allowing a shape change to arise, not from surface energy effects, but rather from anisotropic diffusion. Alignment is observed in all systems that show a shape change.

In the case of nickel-aluminium alloys (and the present alloys if the particles are considered to be spherical at small sizes) the shape change takes place at very small particle sizes. When the particle size is small the interface will be diffuse and a number of the constraints at the interface will be relaxed, and this might also allow

spherical particles at small particle sizes even when the strain energy controls the particle shape. The diffuse interface will also affect the particle image in the electron microscope and it will be difficult to decide the particle shape; Hornbogen and Chakraborty observed the shape change at somewhat larger particle sizes and it is unlikely that the same argument can apply.

Particle alignment

The observation that the particles are aligned in (100) directions immediately suggests an aligned distribution of nucleation sites in the matrix. Such a distribution is not normally observed for classical homogenous nucleation and growth processes since the probability of achieving a nucleus of critical size is, to a first approximation, equal in all parts of the matrix.

Aligned nucleation sites may be observed as a result of spinodal decomposition in systems which have elastic anisotropy in the same sense as nickel [17]. It is therefore interesting, particularly in view of the later discussions on the phase transformation, to suppose that the aligned structure is the result of spinodal decomposition in the early stages of ageing.

Ardell and Nicholson [10], working on nickel-aluminium alloys, showed that the aligned structure could arise even when the ageing treatment was such that the alloys were not within the supposed spinodal; further they showed that the alignment was

much less pronounced when the particle size was small and the supersaturation of solute low. This latter observation is confirmed in the present work although alignment is observed at smaller particle sizes than those quoted by Ardell and Nicholson.

Ardell and Nicholson suggested that the alignment was a function, not of the nucleation, but rather the coarsening process, the alignment depending on an elastic interaction between the particles. Other experimental observations confirm this idea in that in similar alloys having a low misfit, alignment of the particles is not observed (see for example Gleiter and Hornbogen [52]) whereas as the misfit increases, the alignment becomes more pronounced and is observed at smaller particle sizes. The latter feature is shown by comparing the microstructures in the present work with those shown by Ardell and Nicholson, and further confirms the idea that the alignment is a function of the elastic strain energy at the particle/matrix interface.

Eshelby [18] has derived an expression for the elastic interaction between particles showing that an interaction exists if the mismatch and/or the modulus differences between the two phases are sufficiently large. Ardell and Nicholson applied Eshelby's expression to their nickel-aluminium alloy and showed that a large interaction existed at larger particle sizes; the higher mismatch in the present alloys would give a greater interaction for a given particle size.

Ardell and Nicholson suggested that the alignment of the particles arises as a result of selective coarsening, pointing out that the elastic interaction energy will be minimised by alignment in the (100) directions. Their model is that particles which find themselves aligned, by chance, in (100) directions will have a chemical potential gradient between themselves and particles which are not so aligned; solute passes down this gradient and assists the growth of the aligned particles at the expense of unfavourably located particles. Calculation of the interaction between a particle and a solute atom showed that there was no effect on the diffusion rate.

The model explains the present experimental observations very well and the supposition that the aligned structure originates from a spinodal decomposition process is therefore untenable.

5.3. The precipitate/matrix interface.

The particles appear to remain coherent up to the largest sizes observed (1500 Å) although there is some evidence for a few interfacial dislocations in fig. (4.1.11); these dislocations may, however, have been introduced during foil preparation. The dislocation marked A in the micrograph does appear to have the form which would accommodate some of the strain associated with a row of particles. It is also suggested that some of the deformed structures show incoherent particles although in the undeformed state the particles were coherent (fig. 4.2.6).

There is an elastic shear strain in the matrix due to the lattice parameter misfit at the interface. It has been suggested by some workers [38] that as the particle grows a stage will be reached at which the strain is of such a magnitude that the associated stress is able to nucleate dislocations to accommodate the strain. Brown [39] has shown that this argument is fallacious and that if a (spherical) particle starts to grow coherently with the matrix then it will remain coherent up to an infinite size unless an external stress is applied to nucleate the interfacial dislocations.

Brown's argument is that the stress required to nucleate an interfacial dislocation is independent of the particle radius and depends only on the mismatch. The equation for the nucleating stress is $\sigma_p = 2\mu\frac{\Delta a}{a}$; for a 1% misfit this

gives a possible nucleation stress of 0.16 $\times 10^3$ kg/mm^2. If the critical stress to nucleate a dislocation is taken as $\frac{\mu}{30}$ = 0.26 $\times 10^3$ kg/mm^2 then it may be seen that there is no reason why the particles should lose coherency. As the mismatch increases the additional shear stress that has to be provided by an external load to nucleate interfacial dislocations decreases and it would therefore be possible for alloys with a high mismatch to go incoherent under low applied stress, even during the preparation or examination of thin foils.

5.4. Grain boundary denudation.

Grain boundary denudation is generally observed from the beginnings of the appearance of a second phase. It is generally attributed to vacancy or solute depletion in the region adjacent to the grain boundary, the grain boundary acting as a sink. In alloys forming G.P. zones, the zones frequently ignore the presence of vacancy depleted regions when they form. On the dissolution of the zones and the growth by diffusion of an intermediate precipitate, growth is impeded in the depleted regions and a denuded zone appears.

In the present alloys no denudation is observed in the early stages because of the nature of the phase transformation (see section 6). The interesting feature is that the depleted zones only appear after considerable ageing times and after the χ' precipitate is readily observable in the electron microscope.

The origin of the zones must therefore be a function of the coarsening process and may be explained on the basis that particles in the boundary are able to coarsen faster than those in the matrix close to the boundary. This increase in the coarsening rate may be due to enhanced diffusion rates in the boundary or to a partial loss of coherence of the particles in the boundary. Vacancy profiles will be unimportant as the ageing times and temperatures are such that an equilibrium vacancy concentration will exist in all regions of the alloys.

5.5. Particle coarsening.

The basic expression for the coarsening of particles is due to Wagner [19] and for cubic particles has the form $\left(\frac{a}{2}\right)^3 - \left(\frac{a}{2}o\right)^3 = kt$ - (1) where k is a rate constant given by $k = \frac{8\ \gamma\ DCe\ Vm}{9\ RT}$.

γ is the interfacial energy of the particle matrix interface, c_e is the concentration of solute in the matrix in equilibrium with a particle of infinite size D is the coefficient of diffusion of solute in the matrix and V_m is the molar volume of the particle.

This equation was originally derived for the coarsening of spherical particles in a liquid matrix; Ardell and Nicholson [10, 20] showed that a $t^{\frac{1}{3}}$ law was still obtained for the coarsening of γ' in nickel aluminium alloys and this is confirmed by the present work. These observations imply that the law may still hold even though the particle distribution is by no means random and the particles have very definite non-spherical shapes.

Oriani [21] has pointed out that the diffusion coefficient D will not simply be the coefficient of diffusion of the solute in the matrix but will be influenced by the properties of the matrix and the shape of the particles. This modified diffusion coefficient is denoted D_{eff}. The uncertainty in the diffusion coefficient means that values of the interfacial energy may not be obtained to any degree of accuracy from equation 1, although sensible values of about 30 ergs/cm^2 were obtained by Ardell and Nicholson using the bulk diffusion data of

Swalin and Martin [22]. This value agrees with the quasi-chemical value given by Williams [3]; Ardell and Nicholson recalculated this value and obtained the result that $\chi = 0$; they however, ignored the presence of solute in the matrix in their calculation. Recalculation considering the solute content of the matrix gives a value close to that of Williams. The value is a first order nearest-neighbour calculation and does not take into account elastic strain energy.

The activation energy for the coarsening process may be obtained from an Arrhenius plot using the values of k at the different temperatures. Ardell and Nicholson obtained a value of 64.4 k.cal/mole which is very close to that of Swalin and Martin for the diffusion of aluminium in nickel implying that D is not much altered by the constraints of the system.

Independent calculation of χ and D_{eff}.

In a very recent paper Ardell [23] has shown that it is possible to obtain independent values of χ and D_{eff} if measurements of the solute concentration are made concurrently with those of particle size, but he points out that there are no data in the literature to support the theory. In the present work solute concentrations have been accurately determined by Curie temperature measurements as a function of time and thus allow Ardell's analysis to be tested. Ardell's paper will first be considered:

The average concentration of solute in a matrix is related to the particle size by the Gibbs-Thompson equation:

$$C - C_e = \frac{2 \gamma C_e V_m}{(\frac{a}{2})RT} \quad - \quad (2)$$

This equation may be rewritten in terms of $\frac{a}{2}$ and substituted into equation 1 giving

$$\left(\frac{1}{C - C_e}\right)^3 - \left(\frac{1}{C_o - C_e}\right)^3 = k't \quad - \quad (3)$$

where k' is another rate constant and is given by

$$k' = \frac{D (RT)^2}{9 \gamma^2 C_e^2 V_m^2}$$

By combining k and k' in different ways it is possible to obtain constants such that

$$\frac{k}{k'}^{\frac{1}{3}} = \alpha = \frac{2 \gamma C_e V_m}{RT}$$

and $$k^2 k'^{\frac{1}{3}} = \beta = \frac{4}{9} D V_m$$

Thus by measuring k and k' from the experimental results, γ and D may be obtained independently.

Calculation of k'

Ardell assumes that at sufficiently long ageing times ($C_o - C_e$) will be much greater than ($C - C_e$) and therefore equation 3 reduces to:

$$C - C_e \simeq (k't)^{-\frac{1}{3}}$$

Hence a plot of C against $t^{-\frac{1}{3}}$ will be a straight line of slope $(k')^{-\frac{1}{3}}$.

Plots of C versus $t^{-\frac{1}{3}}$ at three temperatures for the two alloys are shown in figs. (5.5.1) a and b and exhibit linear behaviour at long ageing times. Values of the constants k and k' obtained from the experimental results together with the calculated values of γ , α , β , C , D_{eff} and D (calculated from Swalin and Martin's work) are shown in table 5.5. The results of Ardell and Nicholson on nickel-aluminium alloys and Ardell (who used the results of Ben-Israel and Fine [11]) on nickel-titanium alloys are included in the table.

The following were assumed in the calculations:

$$V_m = V_m\ Ni_3Al = 27.2\ cm^3/mole.$$

Density = Density for Ni = 7.9 gms/cm^3.

The values of C_e were obtained directly from fig.(5.5.1) where $t^{-\frac{1}{3}} = 0$.

The values for the interfacial energy obtained are in close agreement with the exception of the result from alloy B at 600°C. The k values

at 600°C are subject to large errors and this may account for the discrepancy, the use of a value of D_{eff} of the order of that calculated from Swalin and Martin would give an interfacial energy close to 20 ergs/cm^2. The estimated accuracy of the 700 and 750°C results is±5 ergs/cm^2. although the agreement between the results suggests a somewhat closer tolerance.

The diffusion coefficients (i.e. $D_{eff.}$) are a little greater than those calculated using the bulk diffusion data of Swalin and Martin which suggests that the diffusion is somewhat enhanced by the shape of the particles and the strains in the matrix. The apparent activation energies are calculated in the next section.

It should again be noted that the thermodynamic expressions were derived using a spherical particle model and this places some limitations on the use of the Gibbs-Thompson equation in the present work.

Calculation of the activation energies for coarsening.

From the two sets of rate constants it is possible to obtain two values of the activation energy of coarsening (which should be the same) for each alloy. Arrhenius plots are shown in figs.(5.5.2) a and b for the particle coarsening data and the concentration data respectively. The k values for the particle size measurements are corrected for the small

variation in $\frac{T}{C_e}$ with temperature and the k' values are similarly corrected for the variation in $(\frac{C}{T}e)^2$ From the size measurements the activation energy for both alloys is about 70 k.Cal./mol., there is some scatter on the points and the estimated accuracy is ±10 k.cal./mol. The measurements on alloy B at 800°C did not fit the plot and this may be because the volume fraction of γ' is much lower at this temperature and the effect of impingement of diffusion fields may be much less.

The plots from the concentration data show better straight lines giving activation energies of 72.5 k.cal./mol. for alloy A and 61.4 k.cal./mol. for alloy B. The limits of accuracy are ±5k.cal./mol.

All the values are in good agreement with those given by Swalin and Martin for the bulk diffusion of aluminium and titanium in nickel (Al = 64.4 ,Ti = 61.0 k.cal./mol.) and further confirm that the diffusion characteristics are not much changed by the constraints of the system.

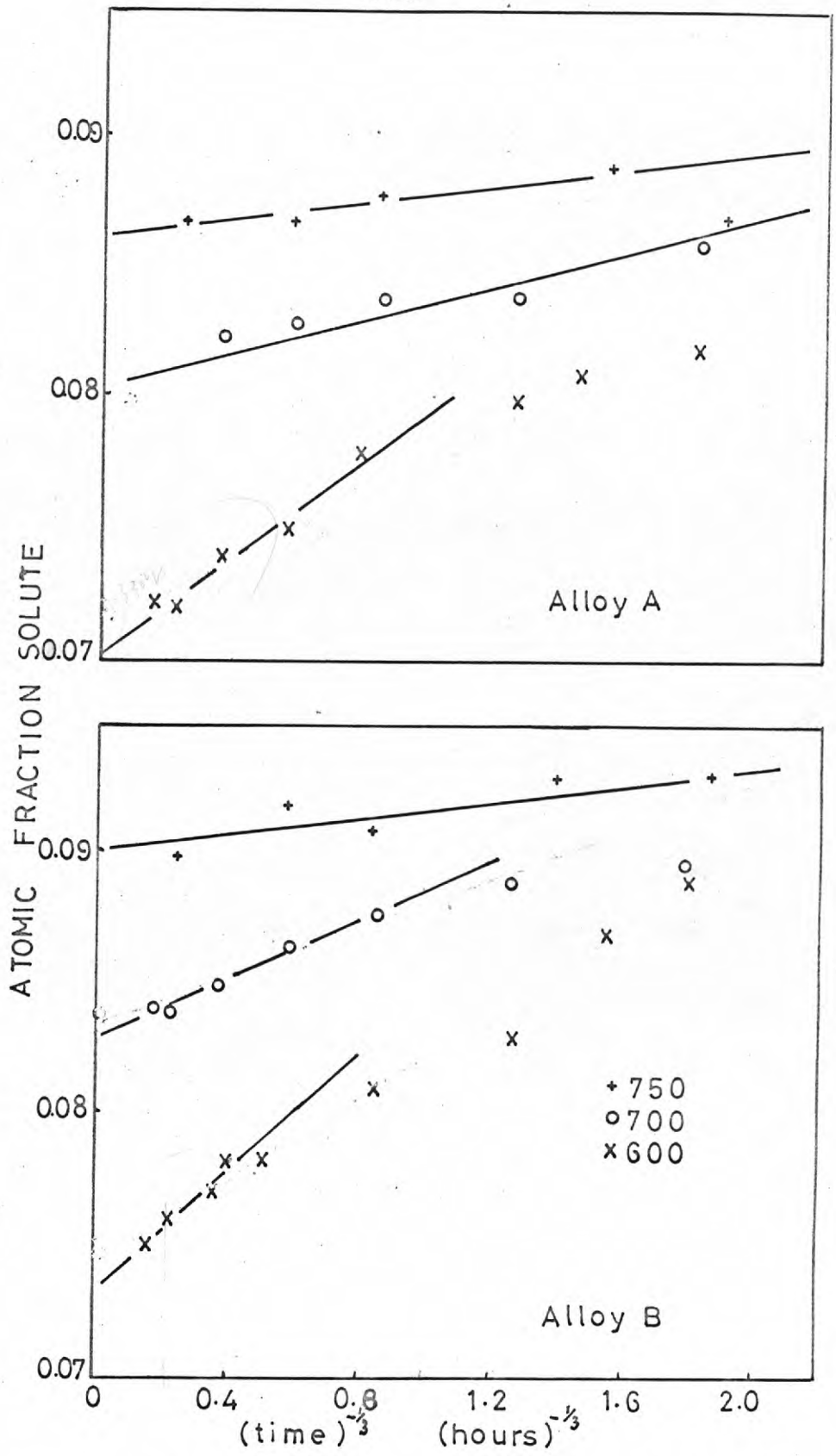

Figs.5.5.1 a and b .Solute concentration versus (time)$^{-1/3}$

Alloys A and B aged at 600,700 and 750°C.

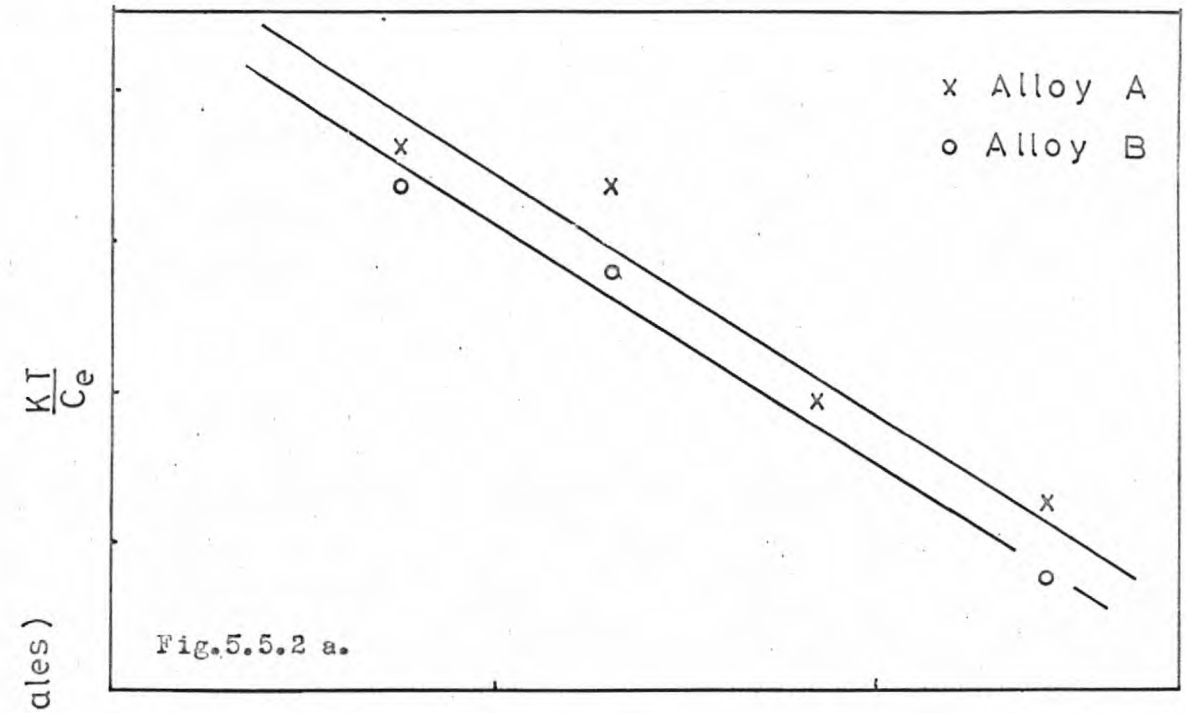

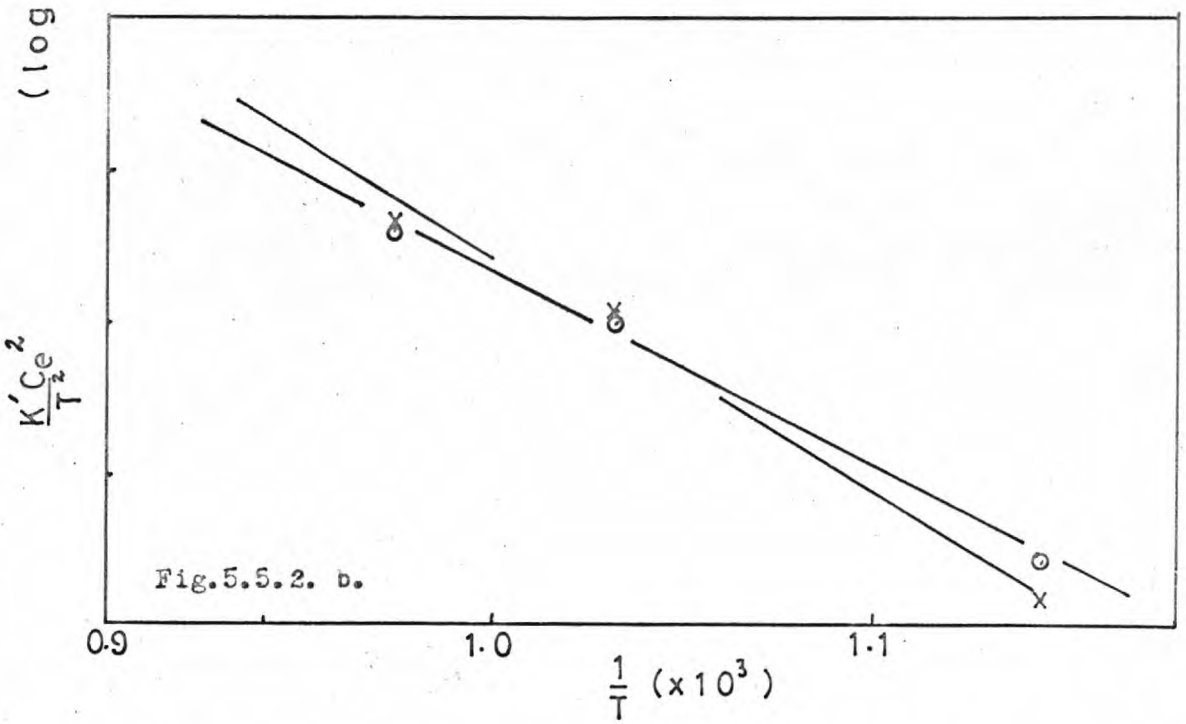

Fig.5.5.2. Arrhenius plots from (a)Coarsening results (b)Concentration data.

Table 5.5

Ageing Temp °C	Alloy	K cm^3/sec $\times 10^{25}$	K' $cm^9/mol^2 sec$ $\times 10^{-5}$	α $\times 10^{10}$	β $\times 10^{-15}$	C_e mol/cm^3 $\times 10^{4}$	γ erg/cm^2	D_{eff} cm^2/sec $\times 10^{16}$
600	A	7.5	1.19	1.85	4.06	0.97	24.8	3.35
600	B	2.6	1.79	1.13	2.30	1.05	14.2	1.90
600	10.1 Ti	-	39.4	-	-	1.30	3.4+	3.5*
700	A	570	86.5	1.87	304	1.12	24.8	250
700	B	280	69.0	1.60	176	1.19	20.0	150
700	10.1 Ti	-	48.0	-	-	1.32	24.5+	133*
750	A	1640	334	1.70	965	1.20	22.1	800
750	B	1100	234	1.67	656	1.31	19.9	550
750	14.5 Al	1590	-	-	-	1.96	25.3+	419*

* D values calculated from Swalin and Martin.

\+ Calculated assuming D values as above.

5.6. Shape of the permeability/temperature curves.

The initial permeability of a ferromagnetic material is highly structure sensitive and therefore its use to measure an essentially structure insensitive property such as the Curie temperature is open to some question. Under conditions of low applied field, homogeneous ferromagnetic materials show permeability/temperature curves which rise rapidly with temperature and then drop sharply to zero at the Curie point. The measurement of Curie temperature using structure insensitive properties such as saturation magnetisation involves complex extrapolations to obtain the Curie point, a procedure that is obviously difficult in the case of a material having a range of Curie points.

It was assumed initially that the gradual fall of permeability from a maximum over a wide range of temperatures for alloys aged for short times and at low temperatures represented a range of Curie temperatures in the alloy. As the initial permeability is structure sensitive, a change in structure may possibly influence the shape of the curves without the necessity for invoking a range of compositions in the alloy.

A second feature that must be considered is the effect of the field strength on the permeability/temperature curves. Bozorth [24] shows a series of curves for pure iron in which, as the field strength increases, the maximum in the permeability/temperature curve becomes less marked

and occurs at lower temperatures. The nett effect is a more gradual fall of permeability as the Curie temperature is approached. The sharp drop at the Curie point is still observed but in other respects the curves look very similar to those aged for short ageing times in the present work. The field strength in the present measurements was kept low and constant for the measurements and it is therefore considered that the field strength has little effect on the curve shapes. This assumption is further justified by the experiments conducted at different values of the field strength and by the measurements of the temperature dependence of the electrical resistivity. In order to consider the effects further it is necessary to consider the phenomena governing the shapes of the permeability temperature curves.

Permeability temperature curves at low field strengths.

The description that is used here is essentially that given by Bozorth. The Weiss theory of ferromagnetism shows that the alignment of atom spins takes place at very low fields (spontaneous magnetisation). Saturation magnetisation is not observed in low field strength conditions because of the arrangement of atoms into misoriented domains. Higher applied fields are necessary to align all the domains in the same direction, the strength of the field required depending upon the mobility of the domain walls.

Domain wall movements are described in

terms of reversible and irreversible movements and under low field conditions only the former take place. At a low temperature and under a given low applied field a few domain wall movements take place and a given magnetization is observed. As the temperature is increased the domain wall mobility increases and thus the magnetization rises and this process continues until the Curie temperature is approached at which point the magnetization sharply drops. This behaviour is not observed at high field strengths because the field aligns all the domains by irreversible wall movements and no further magnetization with rise in temperature is observed. The result at high fields is therefore a steady decrease with temperature at a rate increasing as the Curie temperature is approached.

The effect of structure on the domain wall mobility

Although quantitive measurements were not made it was apparent from the results that specimens exhibiting the slow fall from the maximum also showed a lower value of permeability at temperatures well below the Curie temperature. This is due to the effect of the structure on the domain wall mobility; Bozorth [25] shows that alloying and lattice strains have a marked effect on the initial permeability, both of them reducing it drastically, presumably by the pinning of the domain walls. In the present work it was noted that the processes

taking place in the early stages of ageing lowered the permeability to below the value of the supersaturated solid solution, although the latter value will itself be low because of the strains associated with the solute atoms. As ageing proceeded at higher temperatures the permeability increased and this may be attributed to solute depletion of the matrix, although some effect on the permeability is still to be expected from the strains associated with the coherent precipitates.

In order to describe the curve shapes observed after short ageing times in terms of structural restraints on the domain wall mobility, it would be necessary for the pinning to be so strong that the temperature rise would not increase the mobility of the domain walls. Since the values of permeability obtained are not much lower than those for more 'normal' structures some movement of the domain walls must have taken place; it would therefore be reasonable to suppose that mobility would increase with temperature. The only model that would give curves of the shape observed would be one that supposed the existence of a few highly mobile walls which moved at any temperature under very low fields but which ignored the existence of intermediate walls between the highly mobile and strongly locked ones. It is reasonable to conclude that the slow decrease from the permeability maximum is not a function of structural restraints on the domain walls.

In order to confirm further the

description of the results in terms of a spread in Curie temperatures it was suggested [72] that the temperature dependence of the electrical resistivity should be examined.

Temperature dependence of the electrical resistivity:

In the case of a pure metal, as the Curie temperature is approached, the resistivity starts to rise more rapidly until the Curie point is reached [26] At the Curie point the slope of the resistivity/temperature curve decreases sharply to a constant value. A curve of roughly this form was obtained for specimens that showed sharp changes in permeability at the Curie point. Specimens showing a range of Curie temperatures also showed a wide range of temperature for the slope change, the range extending to somewhat lower temperatures than those indicated by the permeability/temperature curves.

There are no problems of a change in curve shape with field strength when resistivity measurements are made and moreover resistivity measurements are, to a first approximation, structure insensitive. Thus the resistivity curves confirm further the existence of true composition gradients in the material.

It is now possible to conclude that the shape of the permeability/temperature curves after the maximum is governed by the existence or otherwise of a range of Curie temperatures, and hence of

compositions in the matrix. This conclusion will be used in later discussions on the decomposition of the alloys.

5.7. Curie temperature changes on ageing.

Theory of the change in Curie temperature:

The addition of solute atoms to nickel provides electrons which find it energetically favourable to occupy sites in the 3- d electron band. This reduces the number of empty levels in to which electrons may be thermally excited and the Curie temperature is consequently lowered. If the band shape of nickel was unaffected by the solute additions then a linear relationship would be expected between the Curie temperature and solute content. X-ray absorbtion data [27] together with considerations of the behaviour of the solute in solution show that the assumption of a constant band shape is unreasonable and it is necessary to consider experimental evidence for the relationship between Curie temperature and solute content.

This relationship has been studied in nickel-titanium alloys by Marian [28], Taylor and Floyd [29], Stover and Wulff [30] and Fine and Ben Israel [11]. Nickel-aluminium alloys have been studied by Marian [28] and Crangle and Martin [31]. The conclusions are that an approximately linear relationship does exist corresponding to an electron transfer from titanium of 4.2 electrons per atom and from aluminium of 2.78 electrons per atom.

The assumption is made here that as essentially linear relations are observed for solute atoms in their binary alloys with nickel, then a similar relation will hold for the ternary alloys; this assumes that the aluminium and titanium atoms do not interact. The latter assumption is reasonable in view of the nature of the supposed short range ordering reaction in which the solute atoms tend to surround themselves with nickel atoms.

Using the data for the electron transfer per atom from the literature, Curie temperatures were calculated for the two alloys assuming that all the solute was in solution. The values obtained were: alloy A 230°K and alloy B 270°K. These values are close to those at the maximum of the Curie temperature ranges obtained by quenching the alloys from 1100° C . As has been shown, lower Curie temperatures with a narrower range could be obtained by quenching from 875°C and these values did not lie on the interpolated curves drawn from the results in the literature.

The conclusion is drawn that the results in the literature were obtained on material that had not been quenched sufficiently rapidly to prevent partial decomposition of the solid solution. If this is correct then the nickel-aluminium alloy results show the greatest discrepancy. The results of Crangle and Martin for the nickel-aluminium alloys suggest an electron transfer of 2.78 electrons per atom, whereas the number of electrons available for transfer is 3 per atom, as the aluminium atoms have 3 valency

electrons in their outer shell, all of which should find it favourable to enter the 3 - d band.

The above comments suggest that whilst a linear relation is observed for alloys receiving 'normal' quenching treatments, such a relation may not exist for more effectively quenched alloys, as alloys with a high solute content will be more greatly affected by this quenching treatment since they will decompose more readily during the quench. The effect over the range of compositions encountered in this work will be small and a linear relation has been assumed; calibration curves were constructed using the lowest determined values of Curie temperature after the 875°C quenching treatment. Further slight corrections are required for the change in Al/Ti ratio as ageing proceeds but the effect on the curves is again small.

The calibration curves and the results of other workers are shown in fig.(5.7.1).

Discussion of the experimental results.

Higher ageing temperatures.

The calibration curves in fig.(5.7.1) allow the interpretation of the Curie temperatures in terms of the matrix solute content. After ageing treatments producing discrete particles very narrow ranges for the magnetic change are obtained, implying a unique value of the Curie temperature. An application of the lever rule, using the vertical sections in fig.(2.2.2), gives the atom fraction

of the alloy that has transformed. The atomic volumes of precipitate and matrix are very nearly the same (γ' is approximately 3% greater than γ) and the volume fraction of the precipitate may be obtained to a high degree of accuracy.

The continued slow increase of Curie temperature with ageing time at 600° and 700°C must be due to the change in equilibrium solute content as the particle size increases. This is a consequence of the Gibbs-Thompson equation and has recently been discussed by Ardell (23). The change is discussed in greater detail in the section on particle coarsening.

The Curie temperature changes in the first minute of ageing are shown in table 5.7 together with the fractions of the total Curie temperature change which they represent, although the latter are subject to the limitation imposed by the change in solute content with particle size. The figures show that although the initial change in Curie temperature is a function of the supersaturation the actual fraction transformed during the period of this change is not a strong function of the ageing temperature. The conclusion to be drawn is that the initial stage of decomposition is extremely rapid and is not controlled by diffusion kinetics. This will be considered in the discussion on the phase transformation.

The other feature to consider in the later discussion is the plateau followed by an

apparent increase in transformation rate after the initial stage observed at 500 and 600°C. This stage is affected markedly by the quenching treatment.

Ageing at 400°C.

The interpretation of the Curie temperature curves in terms of a range of compositions in the matrix allows the following description of the changes taking place: (The ageing curves are replotted in terms of the matrix compositions in fig.(5.7.2)

As ageing proceeded the nickel-rich Curie temperature increases steadily whilst the solute rich Curie temperature increases only to a very small extent. The significance of these observations in relation to a model of the phase transformation will be discussed in section 6.

Table 5.7.

Curie temperature changes during first minute of ageing.

Ageing temperature		Curie temp. range after 675°C Q	Change from S.T.	Fraction of total change.
500°C	A	284-292 °K	100°C	50 %
	B	303-309	80	57
600	A	268-273	83	41
	B	295-301	70	52
700	A	253-261	70	70
	B	293-304	70	70
750	A	237-241	50	70
	B	289-292	60	75

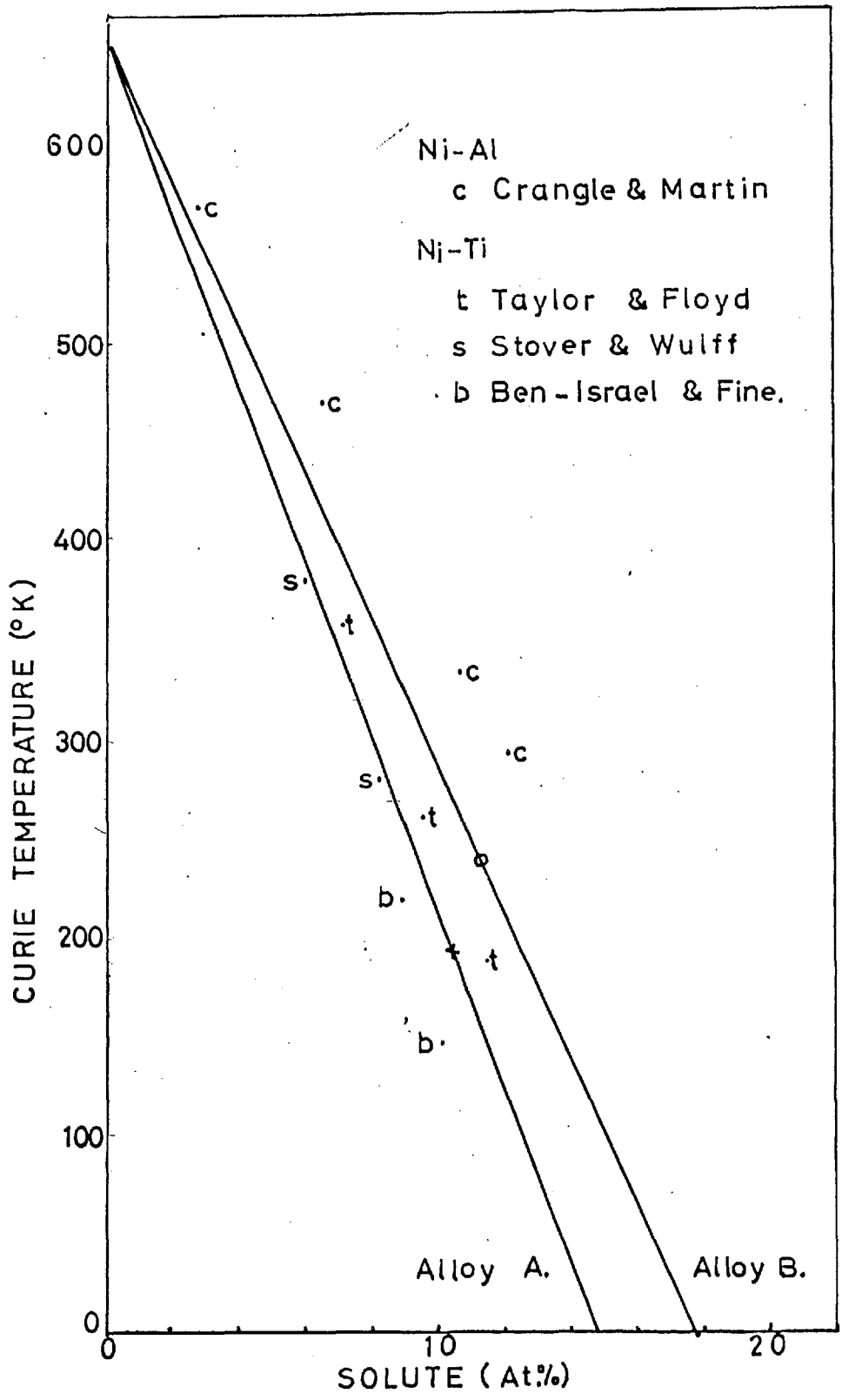

Fig.5.7.1.Curie temperature versus solute content for alloys A and B.

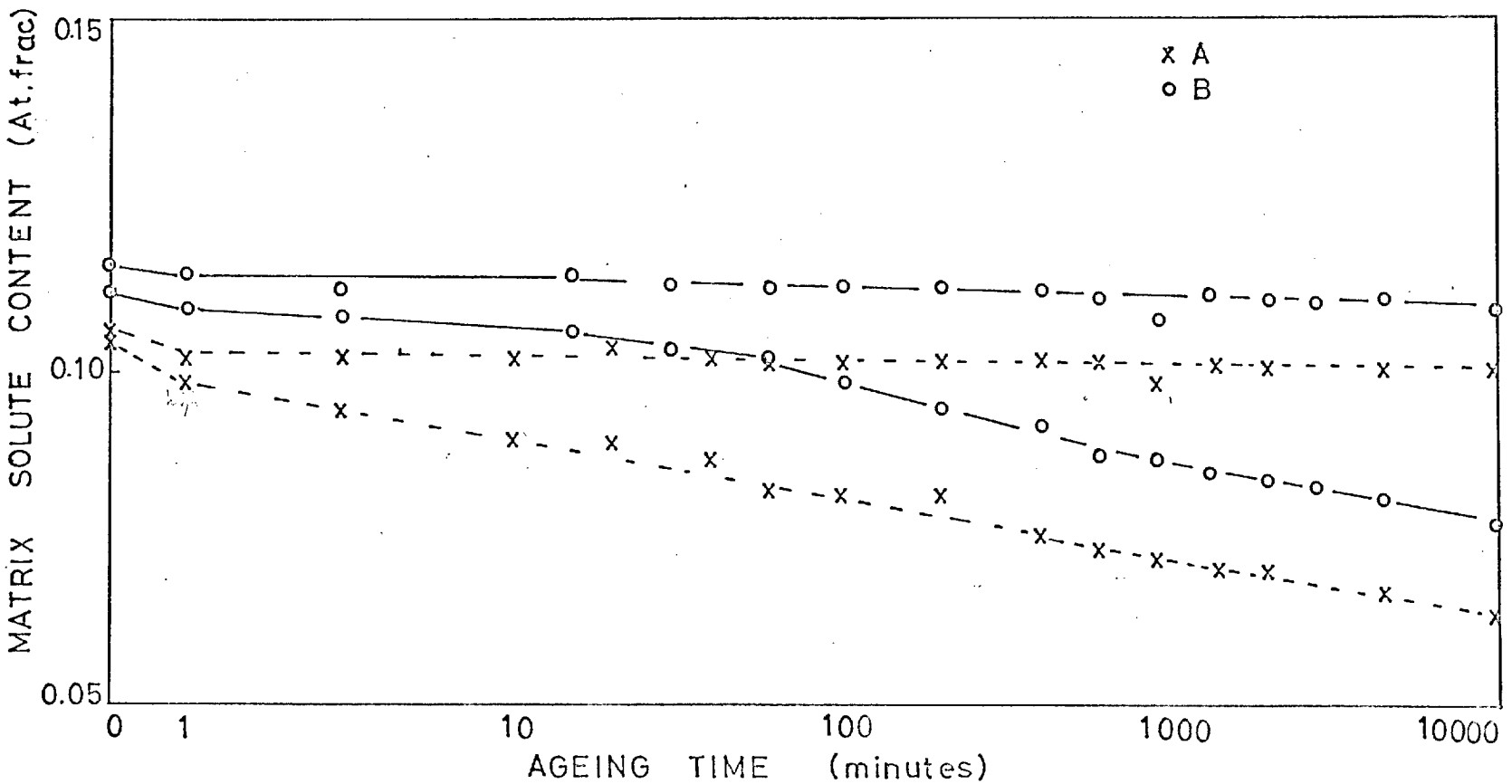

Fig.5.7.2. Matrix composition ranges : Alloys A and B aged at 400°C.

5.8. Elastic modulus results.

The elastic constants of metals depend on the distribution of atoms in the solid, and if a change in this distribution takes place then a corresponding change in the modulus is to be expected. Elastic modulus studies have not been used extensively to follow ageing phenomena. These studies do however provide a useful alternative to resistivity measurements, particularly in alloys that show maxima in their resistivity/ageing time curves. These maxima complicate the quantitative interpretation of resistivity data.

Fine et Al. [44] [45] [46] have studied G.P.zone formation in Al-Cu and Al-Ag alloys by observing elastic modulus changes with a high frequency technique: in the case of the Al-Cu alloys the modulus increases with ageing time whereas the reverse is true for Al-Ag alloys. Fine et al. used their results directly for kinetic studies although they did not indicate precisely the phenomena they assumed to be causing the modulus change. They assumed that the modulus varied monotonically with the amount of precipitation.

Cohen and Fine [47] have reviewed a number of modulus studies relating to local ordering in solid solutions. The modulus of Cu_3Au has been studied on ageing after various quenching treatments; a minimum is observed for a critical quenching temperature somewhat above the order/disorder transformation temperature. The increase in modulus

on quenching from higher temperatures is attributed to ordering during the quench. On ageing specimens quenched from different temperatures the rate of increase in modulus is found to be dependent on the quenching history, interpreted as the effect of the quench on the defect concentration. Similar effects have been reported for Cu-14% Al. alloys and short range order in these alloys has been confirmed by small angle X-ray scattering [48]. There are no data in the literature on changes in the modulus during ageing of nickel based alloys.

From the brief review above the following atom redistributions during ageing processes will affect the modulus:

(i) Solute depletion of the matrix by the precipitation of second phases.

(ii) Ordering in the matrix reducing the elastic distortions due to solute atoms.

(iii) Clustering of solute atoms into zones allowing the remainder of the solution to adopt essentially its non-supersaturated modulus (this is virtually the same process as (i)).

(iv) In addition to (i) above the second phase could have a different modulus and thus the modulus of the whole assembly may be changed through a mixture effect.

In the present alloys it is assumed that (iii) does not take place and that the modulus change on ageing the alloys in this work is governed

by any one or all the other factors.

(i) The effect due to modulus differences:

Davies and Stolloff [50] have measured the modulus of pure Ni_3Al and found it to be 18×10^3 kg/mm^2 at room temperature. The moduli of the quenched solid solution alloys are about 20×10^3 kg/mm^2. The equation for the modulus of a two phase mixture is

$$E = E_{\gamma} (1- f) + E_{\gamma'} (f) \quad - (1)$$

E will decrease according to this equation as the amount of γ' increases, (other equations exist for the modulus of a two phase mixture but the above is adequate for present purposes).

(ii) The effect due to solute redistribution:

An increase in the modulus of the matrix is expected both when solute redistribution to form regions of high local order occurs and when the solute segregates to form discrete precipitates. There is a difficulty in separating the two contributions and both are expected to occur (see decomposition model). For ageing treatments that are known to give discrete γ' particles the net change in modulus of the matrix will be largely due to the depletion of solute since the locally ordered regions will disappear on the formation of γ' particles.

The modulus of the matrix at time (t) will in this case (assuming that the modulus is a monotonic function of the solute concentration) be given by an equation of the form:

$$E^{(t)}_{\gamma'} = E^{(o)} + af^{(t)} \quad - (2)$$

where a is a constant and f the volume fraction of precipitate.

Equation 2 may be substituted into equation 1 so that the matrix and solute depletion effects may be compared. This gives:

$$E^{(t)} = (E^{(o)} + af^{(t)}) (1 - f^{(t)}) + E_{\gamma'} \quad (f)$$

rearranging:

$$\frac{\Delta E^{(t)}}{E_o} = f^{(b)} \left(\frac{a(1-f^{(t)})}{E_o} + \left(\frac{E_{\gamma'}}{E_\alpha} - 1 \right) \right)$$

the left hand side is the experimental modulus fraction value, the first term on the right hand side is the solute depletion contribution and the second term the modulus difference contribution. The magnitude of the two effects may now be determined by considering the experimental results:

From above $\frac{E_{\gamma'}}{E_\alpha} = 0.9$ therefore the contribution to $\frac{\Delta E}{E}$ from the mixture effect will be -0.1 f. For alloy B aged 100 minutes at 700°C f = 0.17 and $\frac{\Delta E}{E} = 0.01$. The contribution from the modulus differences is -0.017 and therefore the

contribution from the solute depletion is 0.027. This shows that the opposing contribution of the mixture effect is of the same order as the change due to solute depletion.

The existence of two effects, equal in magnitude, places a limitation on the use of the modulus results for quantitative studies. The modulus changes are plotted as a function of the solute depletion from the matrix in fig.(5.8.1) and it may be seen that a non-linear plot is obtained; this is expected as a consequence of the equation relating the modulus change to the volume fraction.

The results cannot be used, with any confidence, for kinetic studies because the lower ageing temperature curves do not become asymptotic at long ageing times. Arrhenius plots for the time to 80% of the change observed at the longest ageing times were made and gave activation energies close to those obtained from the coarsening results but this may well be fortuitous.

The results show that elastic modulus measurements are sensitive to the changes taking place on ageing but in the present work only limited use has been made of them because of the availability of the sensitive Curie temperature measurements which may be interpreted directly in terms of solute depletion. In precipitation systems where the volume fraction is low, and the modulus differences small, then the elastic modulus measurements could provide a good measure of the solute depletion and the reaction kinetics.

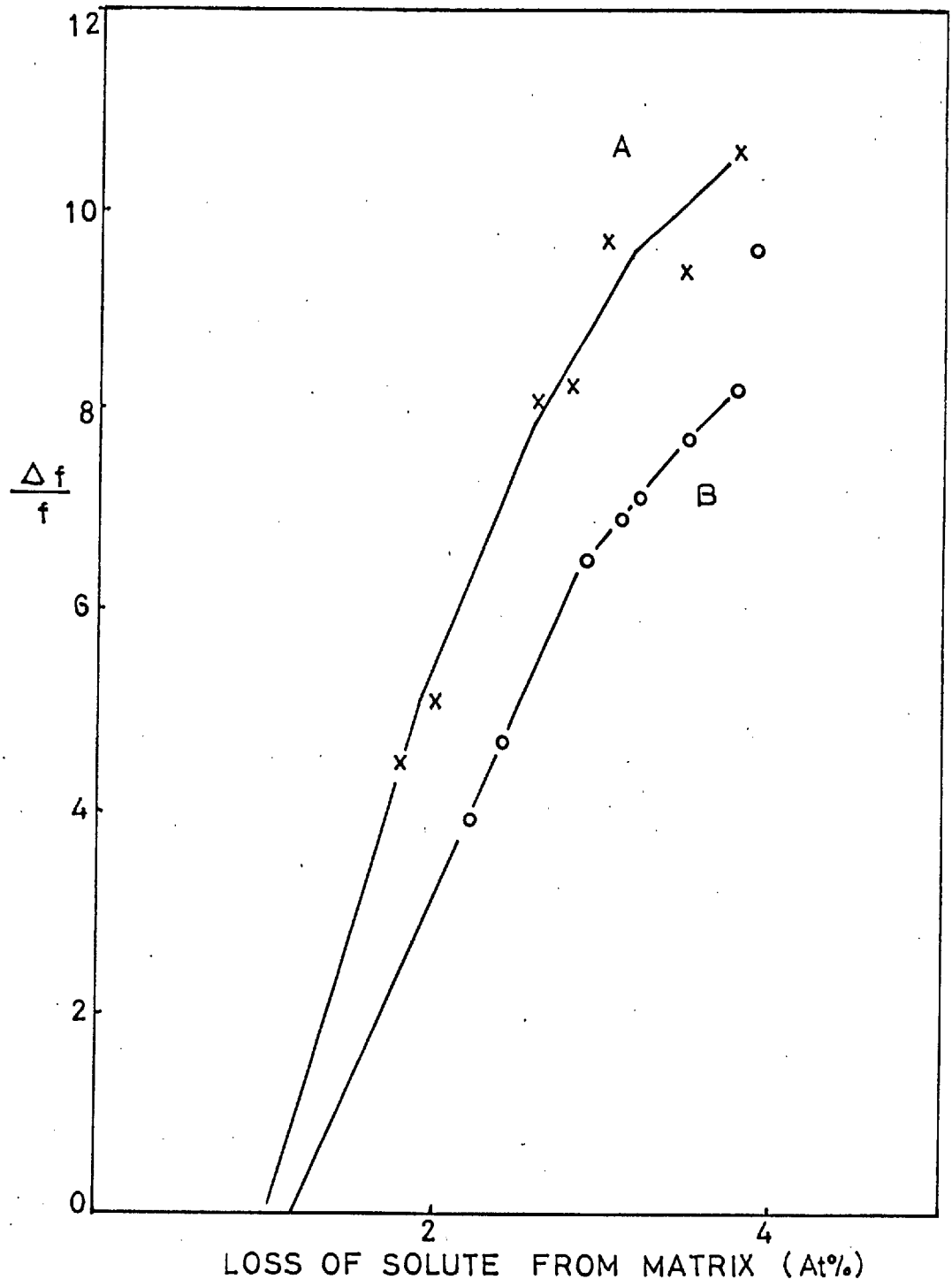

Fig.5.8.1. Fractional change in modulus versus solute depletion from the matrix.

6. The phase transformation from supersaturated γ to $\gamma + \gamma'$.

There is, in the literature, considerable indirect evidence on the structure of nickel-aluminium solid solutions and on the early stages of ageing in the alloys. The indirect observations in this work, together with the results of previous work, provide useful information on the structure in the early stages and allow some interpretation of the changes taking place. The indirect measurements may be roughly divided into two classes; those that depend on the electronic structure and the bonding in the alloys and those which depend on the local atomic configurations. These are necessarily related and provide corroborative evidence for a decomposition model.

6.1. Pre-precipitation phenomena

Bagyriatskii and Tiapkin [32,33] carried out a number of X-ray studies on alloys containing 14 and 17 At% Al. They observed ordered γ' zones in the as quenched condition, whose size (from X-ray line broadening) depended on the solution treatment temperature. At very short ageing times satellite reflections in [100] directions were observed, attributed to sinusoidal composition fluctuations; the wavelength appeared independent of time and temperature.

Guy et al [34] observed a peak in the diffuse X-ray scattering curve of a Ni-8.2 at% Al. solid solution alloy which they attributed to short

range order. Cold work reduced the height of this peak and it reappeared on heating. This suggests that even in alloys which are stable solid solutions there is pronounced short range order. Similar work on an 11.3 at% Al alloy showed two peaks in the diffuse scattering curve in the 'as quenched' condition; one peak could be removed by cold work. After long ageing times the double peak became very sharp and it was therefore suggested that the diffuse double peaks observed after treatments for shorter ageing times were due to the formation of small particles of ordered or newly ordered atomic arrangement. Resistivity measurements were also made showing an increase in resistivity at short ageing times, described by many workers as the K effect. Williams[3] noted a similar resistivity change in the stable solid solution as well as in supersaturated alloys. Hornbogen and Kreye [35] made similar observations to Guy et Al. on a 13.1% Al. alloy and also noted a small resistivity increase in a solid solution alloy on isothermal ageing.

Ardell and Nicholson [10] noted the presence of weak superlattice reflections in the electron diffraction patterns of their quenched 14.5% Al. alloy which they associated with decomposition to small particles of γ' during the quench. Superlattice reflections were also observed, in some instances, in the present work after quenching from 1100°C.

Das and Azarroff [27] studied the X-ray K absorption spectra of the solid solution Ni-Al alloys and of the compounds formed in this system. They point out that the collective electron theory of Stoner and Mott states that the addition of aluminium to nickel should result in a filling of the 3-d band of the alloy with a resultant decline in the magnetic moment of the Ni atoms. Crangle and Martin [31] have measured this change and conclude that the number of electrons transfered at saturation is about two per aluminium atom. This filling of the Ni 3-d band should lead to a decline in the first absorption maximum of the K absorption edge and this was observed by Das and Azarroff in a solid solution alloy containing 5.51 at% of aluminium.

When the aluminium content was increased to 8.35 at%, a further decline of the maximum was not observed and in fact the curve rose, a feature confirmed by a Ni 11.9% Al. alloy. The immediate conclusion that was drawn was that the number of states having p-type symmetry near nickel atoms had increased over that in pure nickel. However they also point out that the overlapping of Al p orbitals leading to local deviation from the rigid band model as described by Friedel [36] could give rise to similar effects.

Das and Azarroff interpret the electrical anomaly or K-effect as a transformation from the classical metallic bond to one more nearly covalent in character and more conducive to atomic ordering.

They confirm this interpretation by considering the absorption structures of the intermetallic compounds: In Ni_3Al a prominent rise in the first absorption edge was observed, suggested as being due to hybridisation with an overlap of Al orbitals having p-type symmetry, a similar effect to that postulated for the solid solution.

During their work Das and Azarroff noted anomalous behaviour in a Ni-4% Al alloy; this alloy was brittle and showed an anomalous increase in the lattice constant of the solid solution, and the X-ray curve had a close resemblance to that of Ni_3Al. They interpret these phenomena as a very strong ordering with Al atoms having Ni atoms as first and second nearest neighbours. Similar anomalies in a 4% alloy have been reported by Noskova and Pavlov [37].

The conclusions that may be drawn from this work are that the electronic structures of Ni-Al alloys even at low concentrations of Al are markedly different from those of pure nickel and also depend themselves very much on the aluminium content. These electronic structures are fundamental in determining the grouping of atoms in these alloys.

Ben-Israel and Fine [11], from Curie temperature measurements (measuring magnetization as a function of temperature) and electron microscopy showed that solution treated 10 and 8.8 at% Ti alloys were non-homogenous, indicating some decomposition during the quench. This, and the changes in Curie temperature with ageing, they attributed to spinodal

decomposition. Their results indicated discontinuities corresponding to certain titanium compositions which were attributed to the development of certain preferred compositions.

In the present work similar discontinuities were not resolved nor were 'veins' observed in the electron micrographs as reported by Sass and Cohen [74]. The appearance of veins may have been a result of the foil preparation technique or a contrast effect and may well not correspond with microstructural features. The composition spreads observed in the present work were not resolved by the Fine and Ben-Israel technique.

There is little literature on the pre-precipitation behaviour of Ni-Al-Ti alloys; Detert and Pohl [9] observed a maximum in resistivity and coercive force, on ageing at 600°C in a Ni 3.8 at% Al, 8.7 at% Ti alloy suggestive of the formation of small regions or short range order. At higher ageing temperatures anomalous behaviour was not observed, possibly because of the speed at which the transformation takes place.

The following features are established from the earlier investigations:

(i) Some decomposition occurs during the quenching of Ni-Al, Ni-Ti, and Ni-Ti-Al alloys.

(ii) Resistivity and coercive force maxima, small angle X-ray scattering and the X-ray analysis of the electronic structure all show evidence of local order in the solid solution.

(iii) There is evidence of alignment in Ni-Al and Ni-Ti alloys in the early stages which has been attributed to spinodal decomposition.

The structure of the quenched material:

In the present work the presence of superlattice reflections in the quenched material together with a range of Curie temperatures following quenching from 1100°C similarly suggest that decomposition began during the quench. The Curie temperatures obtained after quenching from 875°C however suggest that the decomposition has at least partly been suppressed.

The effectiveness of the 875°C quench suggests that there is a critical temperature below which the initial decomposition takes place at a rapid rate and it is considered that quenching from 875°C, whilst not giving an overall faster quenching rate, gives a very fast rate of cooling through this critical temperature range. The effect may however be due to the lower concentration of vacancies associated with the lower quenching temperature. It is assumed that the structure of material quenched from 875°C is very close to that of a homogenous supersaturated solid solution.

The decomposition of this supersaturated solution will now be considered in detail.

6.2. Models for the phase transformation.

The indirect evidence described above strongly implies the existence of inhomogeneity on an atomic scale in solid solution alloys of aluminium and titanium in nickel, even when the solid solution represents the equilibrium form of the alloy. In presenting a model for the decomposition the following phenomena must be accounted for:

(i) The changes in structure observed on the ageing of solid solutions in the single phase γ region.

(ii) The short range order defined by small angle X-ray scattering in the early stages of the ageing of supersaturated solid solutions. (The structure is described as local regions of high order similar to that exhibited by γ'; the X-ray absorption results and the presence of superlattice reflections in the early stages of ageing confirm this interpretation).

(iii) The sinusoidal composition variations in (100) directions described by Bagariatskii and Tiapkin and others.

(iv) The absence of an aligned structure when γ' particles are first observed in the electron microscope.

(v) The wide ranges of composition shown by the Curie temperature measurements in the present work.

(vi) The smooth transition from the wide ranges in Curie temperature to very narrow ranges as the ageing proceeds.

The possibility of classical nucleation of γ'.

A number of the pre-precipitation phenomena described above may be interpreted as evidence for the formation of very small particles of γ' in the matrix. It may be possible for these to exist and not be observed clearly in the electron microscope because of the visibility criteria dicussed in the work of Ashby and Brown.

γ' particles have a low interfacial energy (see coarsening section); Christian describes the composition profile associated with the classical nucleation and growth of the particles in terms of fig. 6.2.1 . When the interface has a low energy it is highly mobile and therefore the composition C_γ in the region adjacent to the particle cannot be far from the equilibrium concentration for the particular alloy composition.

On this model as precipitation proceeds C_γ remains constant (ignoring the effect of particle size on solubility) and C_m approaches C_γ . Describing this in terms of the Curie temperatures this would mean that immediately precipitation occurred the Curie temperature range would be that characteristic of a range of compositions from C_m to C_γ . On further ageing

the higher Curie temperature of the range would remain constant and the range would decrease due to the change in C_m as solute depletion takes place.

Consideration of the Curie temperature results on ageing at 400°C shows that the reverse situation is true, i.e. the solute-rich Curie temperature remains essentially constant whilst the nickel-rich Curie temperature steadily rises. These changes cannot be explained on a simple classical model. Precipitation at higher temperatures results in narrow Curie temperature ranges indicative of the matrix composition. It may be concluded that the composition ranges observed are not due to composition fluctuations in the neighbourhood of particles but represent a true fluctuation in the solid solution. The composition fluctuations which will be present when true precipitates form are therefore considered to be so small in extent that they are not resolved by the apparatus.

A further feature is that on a classical model a large volume of the matrix would be devoid of precipitate and therefore a large drop in permeability would be expected at a value of Curie temperature corresponding to the matrix composition. The actual curve shapes suggest more gradual changes in the early stages. The absence of an incubation time prior to decomposition even at low temperatures is further evidence for a decomposition process that cannot be described in a simple classical manner.

A modified classical nucleation model

The model described above is satisfactory for many classical growth processes; however in the present work the interfacial energy between γ and γ' is very low and thus very small nuclei will be stable. The consequence of this is, if the Gibbs-Thompson equation is considered, the solute content in contact with very small nuclei will be considerably higher than the equilibrium matrix solute content given by the phase diagram.

Fig. (6.2.2) shows the matrix content in equilibrium as a function of particle size for alloy A at 400 and 600°C (using data from the coarsening section). It may be seen that particles of diameter less than 20 Å have matrix solute contents, and hence Curie temperatures, differing considerably from the equilibrium values. It can also be seen from these curves that the smallest nucleus that can form is about 5 Å at 400°C and 10 Å at 600°C as the solute content in contact with such a nucleus will correspond to that of the supersaturated solid solution.

If now the classical model is compared with the Curie temperature ranges obtained after ageing at 400°C it may be seen that the change in the solute poor Curie temperature could be explained on the basis of an increasing particle size with time; other features of the experimental results must now be considered to see if they fit in with the theory.

The rapid decomposition in one minute's ageing at the higher ageing temperatures (500°C and

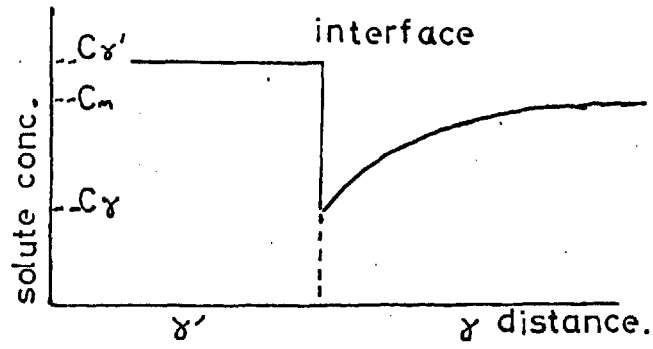

Fig.6.2.1 Composition profile at precipitate/matrix interface.

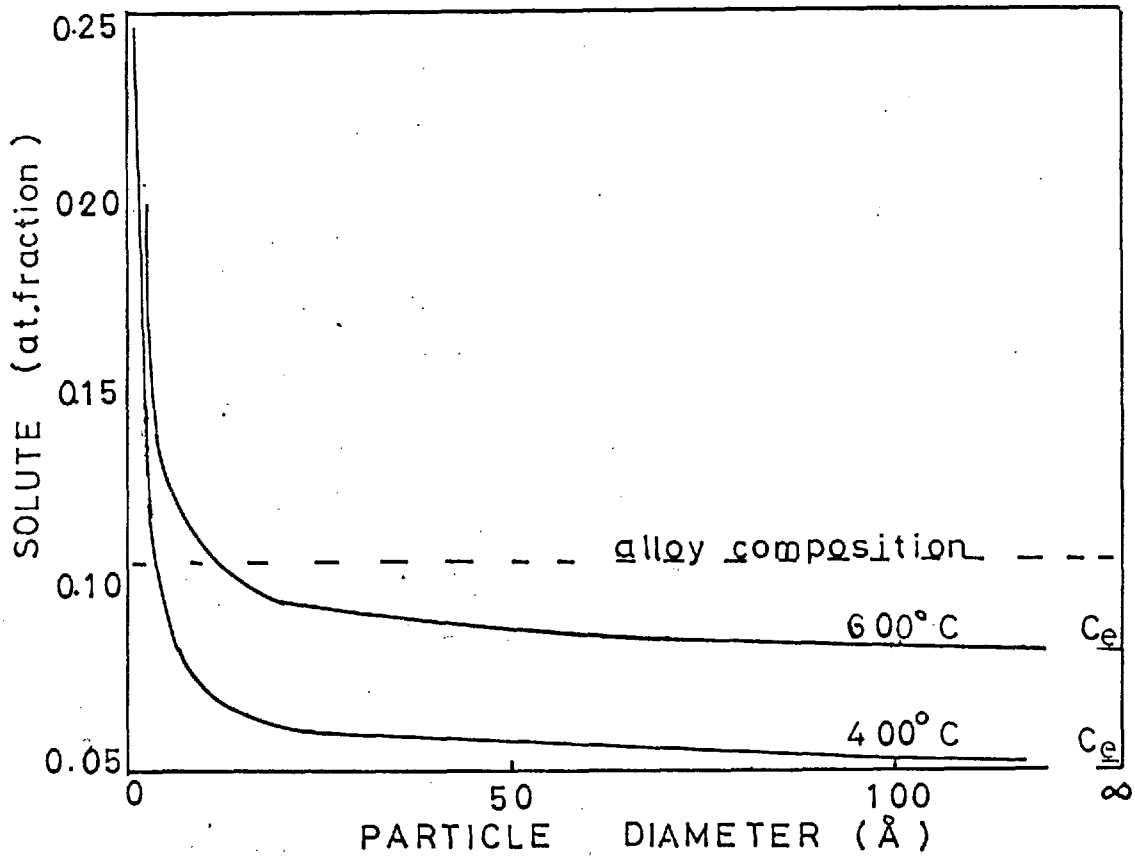

Fig.6.2.2.Equilibrium matrix solute content versus particle size.

above), as compared with the slower decomposition of the 400°C specimens, could be explained on the basis of C-curve type kinetics, the higher ageing temperatures being close to the nose of a rather blunt C-curve. Similarly the observed increasing transformation rate with time at 500°C could be explained on the basis of a sigmoidal kinetic curve.

The absence of alignment in the early stages of ageing is clearly the result of a random nucleation process, the alignment occurring at longer ageing times as described earlier. The observation of widely spaced dislocation pairs in the early stages implies a low degree of order in the particles, but this is not unreasonable as small particles will tend to adjust their composition to minimise the surface energy effects.

The above features would seem to fit in with a classical model of precipitation of small particles with the modification of a lower degree of order and a more diffuse interface. A number of difficulties however remain with this model:

On this model the Curie temperature ranges observed are interpreted in terms of the concentration gradients around the small particles and the diffusion distances involved are small and proportional to the particle size. Although there will be a large volume of material having such composition gradients because of the large number of small particles, it is unlikely that the gradients would be resolved by the technique as such gradients

are not resolved for somewhat larger particles at higher temperatures. (Assuming that the volume of γ' remains constant then the fraction of the specimen volume over which the composition varies will be similar at all particle sizes as the diffusion distance is proportional to the particle size; the magnitude of the composition differences will decrease with particle size but would still be detected if the technique allowed). Another likely possibility is that, over the very small distances having composition variations, the electron band structure will average out over a number of atoms and an average Curie temperature should be obtained.

Whilst the comments above are not necessarily quantitatively correct there is a more damaging effect on the model if the solute-rich Curie temperatures at 400°C are considered; these suggest that there are regions of the matrix which retain almost all their solute whilst the process of nucleation and growth is occurring. Such a situation would occur on a classical model only if very few nuclei were formed; in such a case there would be a large change in permeability at a temperature corresponding to the solute content of the bulk of the matrix; this effect has not been observed.

Whilst the above comments do not entirely rule out some form of classical nucleation process there are sufficient anomalies for other modes of decomposition to be considered.

Spinodal decomposition.

The work of Gibbs showed that it is thermodynamically favourable for composition fluctuations to develop in certain solutions. This can occur when the composition of the solution lies in that part of the free energy/composition diagram where the second derivative of the free energy with respect to composition is negative. The boundary of the region in which this instability can occur is defined by the locus of the second derivative equated to zero and is called the spinodal.

Cahn [17] [41] extended the ideas of Gibbs to solid solutions by deriving an expression for the free energy associated with the composition gradients. He also introduced a term to account for the strain energy associated with the difference in molar volume of the regions of different composition. The effect of the strain contribution is to depress the spinodal to lower temperatures than those calculated from purely thermodynamic data. The decision as to whether a particular alloy lies within the spinodal requires a knowledge of the variation in free energy with composition at various temperatures. This information is not available for the present alloys and one can only speculate on the possibility with reference to the phase diagram.

The theory developed by Cahn shows that on quenching a supersaturated alloy a range of infinitesmal fluctuations of varying wavelengths is formed. On ageing there is a certain wavelength

favoured by the kinetics and this wave increases in amplitude at the expense of the other wavelengths. In a later paper Cahn [17] shows that for cubic elastically anisotropic materials where $2C_{44} > C_{11}-C_{12}$ the waves are parallel to [100] directions in the crystal. A further condition of the thermodynamics inside the spinodal is that uphill diffusion is favoured; this is a necessary condition for the development of the composition fluctuations. It should be noted that Cahn's theory, as considered so far, applies only to the early stages of the decomposition.

A spinodal decomposition sequence for the present alloys would be:

(a) Supersaturated solid solution with infinitesmal composition fluctuations.

(b) Growth of waves of a certain wavelength, dependent on temperature, in (100) directions in the crystal.

(c) Formation of discrete γ' particles at the solute rich parts of the waves when the kinetics and thermodynamics of the reaction are favourable.

Comparison of the model with the experimental results:

(i) Composition fluctuations:

(a) and (b) above would require the development of compositions both richer and poorer in solute than the supersaturated solid solution, the magnitude of these differences increasing with

time. The results of ageing at 400°C certainly show the gradual increase with time of the solute-poor composition peak but fail to show the existence of a solute-rich portion of the curve. There are several possible reasons for this:

(1) It may be a function of the experimental technique in that a fall in permeability due to solute-rich compositions will be superimposed on the rising part of the curve due to increased domain wall mobility with temperature. The fact that the temperature dependence of the electrical resistivity suggests lower Curie temperatures than the initial permeability method lends some weight to this idea.

(2) The decomposition may not in fact be spinodal.

(3) Another reaction superimposes itself on the spinodal decomposition; the strong tendency to order described by other workers and its possible effect on the Curie temperature may explain the results. Ben Israel and Fine [11] explained their results on nickel-titanium alloys in terms of spinodal decomposition with preferred compositions in the solute-rich waves. These preferred compositions were confirmed by peaks in the magnetization/temperature curves at certain temperatures.

(ii) Alignment of the particles:

The theory also requires the waves to develop parallel to (100) directions. Alignment in

(100) directions is observed at a later stage in the ageing and it was at first thought that this was evidence of a distribution of nucleation sites provided by spinodal decomposition. The work of Ardell and Nicholson [10], confirmed by observations in this work, shows that pronounced alignment is not present when γ' is first visible in the electron microscope. It has been shown that the alignment observed in the later stages is a function of an elastic interaction between the particles. The question remains as to whether γ' particles can be nucleated in an essentially random manner following spinodal decomposition in preferred directions.

Before modifying the decomposition model there are tests which may be applied to decide whether the decomposition follows spinodal form; in addition, precipitation just outside the spinodal must be considered.

Depression of the spinodal by strain.

Cahn gives an expression for the depression of the apex of the spinodal curve by strain energy:

$$\Delta T_c = \frac{\eta^2 E}{(1-\upsilon)k n_v}$$

where η is the linear expansion coefficient per unit composition change.

υ is Poisson's ratio.

k is Boltzmann's constant.

E is Young' modulus (in the 100 direction for this system).

N_v is the number of atoms per unit volume.

Calculation shows a depression of approximately 700°C for alloy A and 500°C for alloy B. To make any use of these figures knowledge of T_c is required. T_c may be approximated by estimating the maximum temperature at which the $\gamma + \gamma'$ two-phase region would exist in the absence of the formation of the liquid phase. This may be done very crudely by extrapolating the two-phase boundaries in the nickel-aluminium and nickel-titanium binary diagrams. A value of about 1400°C is obtained which would allow both the alloys to be just within the spinodal at the ageing temperatures used.

Cahn [17] has pointed out that at temperatures that are just within the spinodal region the rate of spinodal decomposition is too slow to compete with a nucleation and growth mechanism. The absence of any marked composition ranges on ageing at temperatures of 600°C and above may be due to this effect or it may be that the reaction is proceeding too fast at these temperatures to be observed.

Effect of imperfections:

Spinodal decomposition should occur everywhere within a sample and should be unaffected by imperfections. Nicholson uses the fact that grain boundary denuded zones are observed as an argument against spinodal decomposition in γ' hardened alloys. The present work shows that the

denuded zones only appear as the γ' particles coarsen, and precipitation in the early stages does appear to be unaffected by the presence of grain boundaries and other imperfections.

Whilst it is easy to see on Cahn's argument that infinitesmal fluctuations can arise unaffected by point defect concentrations, it is difficult to see how vacancy depletion in certain areas will not affect the subsequent growth of the spinodal waves. Possibly the short diffusion distances involved may be the answer to this problem.

Nucleation and growth processes close to and within the spinodal.

Hillert [42] shows that near the spinodal the critical radius of a nucleus becomes very large, its interface diffuse, and its composition non-uniform. In the limit the radius of a nucleus becomes infinite at the spinodal just as the critical wavelength for spinodal decomposition becomes infinite at the same point. The essential fact is that the idea of a classical nucleus with a sharp interface is not accurate as the spinodal is approached, and it becomes very difficult experimentally to separate the two mechanisms. An incubation time might however be expected for nucleation just outside the spinodal; however, it may be very short as very small composition variations are required even though a very large nucleus is required.

Such a model would require the appearance of compositions having Curie temperatures below those

of the supersaturated solid solution. The majority of the matrix would retain approximately its initial Curie temperature; this effect is not observed.

A modified model for the decomposition.

An important aspect of the indirect results of other workers which has not been considered so far in the discussion of the decomposition is the strong evidence for regions of high local order. If it is assumed that decomposition initially takes place by a spinodal mechanism then the possibility that ordering can take place simultaneously in the solute-rich waves of the decomposition must be considered.

The work of Das and Azarroff [27] shows that the tendency to form bonds characteristic of γ' increases with solute content in the single phase region; it is not unreasonable to suppose that this tendency increases as the composition approaches closer to that of γ'. The solute-rich portions of the waves will be able to lower their energy by the formation of a structure similar to γ'; the formation of such a structure will require uphill diffusion of more solute atoms and the composition variation along the wave will be consequently modified. This mechanism need not change the general shape of the nickel-rich parts of the curve and uphill diffusion is legitimate as it has been assumed that the alloy lies within the spinodal. To explain the failure to observe the solute-rich regions by Curie measurements it is not necessary to invoke

complete ordering of the solute-rich parts of the wave; all that is required to explain the observation is for the structure to become non-ferromagnetic and this could be either because of the effect of the ordering on the band structure or by the absorbtion of a sufficient quantity of solute.

As ageing proceeds the ordered regions will reach such a size (since these modified parts of the wave will thicken rather than increase in amplitude) that a classical growth process becomes favourable. The wave-like nature of the nickel-rich regions will disappear as down-hill diffusion takes over and the γ' particles rapidly grow. The model is shown schematically in fig.(6.2.3.) and whilst doubts must remain as to its feasibility it does explain the observed composition fluctuations shown by the Curie temperature measurements. The effect of imposing an ordering reaction on the spinodal wave is not known and may be such that the spinodal mechanism is completely destroyed, leaving the composition gradients to be explained by one of the earlier arguments. This model is only truly applicable to the results of ageing at 400°C and the early stages at 500°C; it has been assumed that the reaction proceeds too rapidly at the higher temperatures to be observed. It may be possible however that a nucleation and growth process will prevail at the higher temperatures as the alloys will be closer to the spinodal boundary.

The absence of pronounced alignment

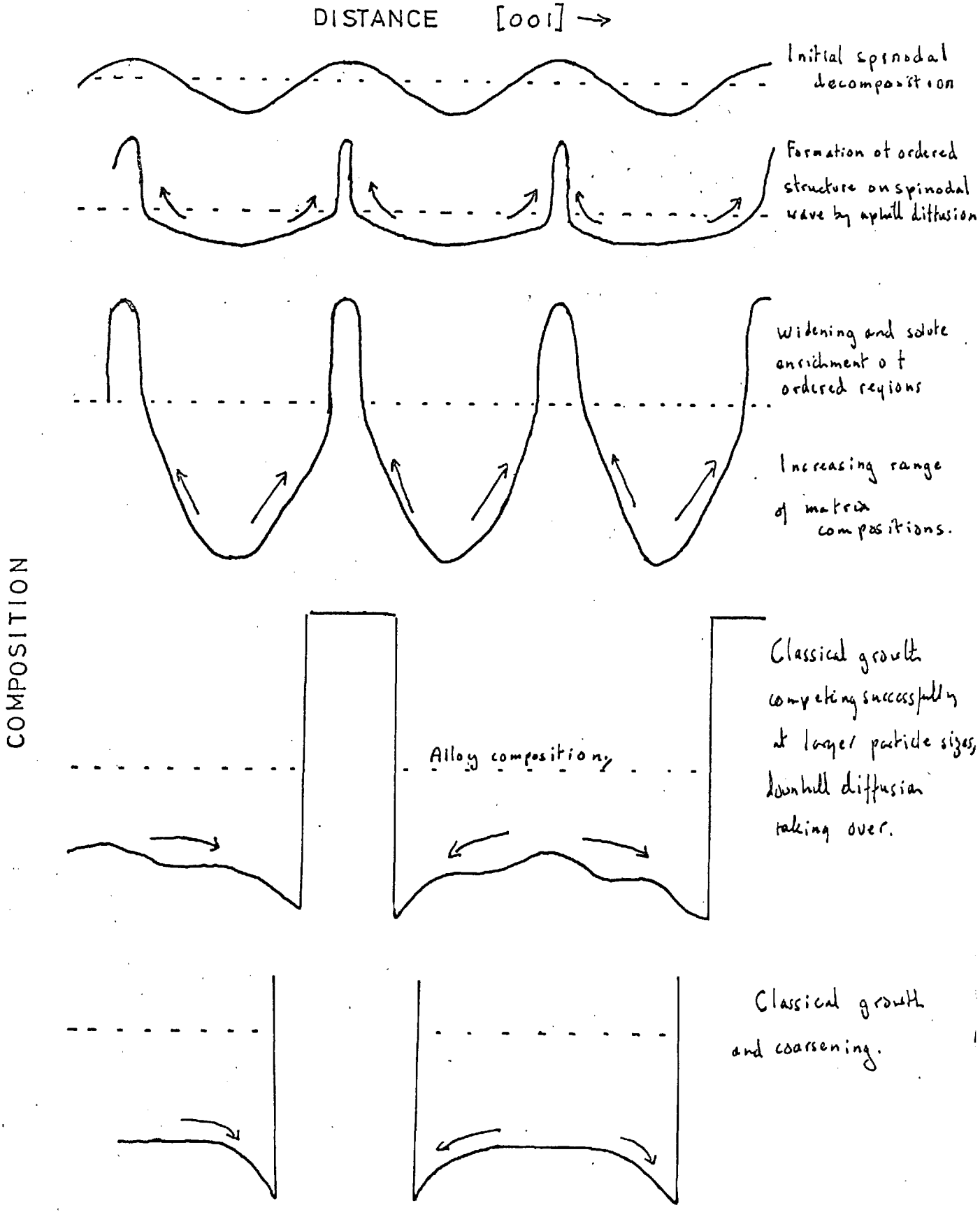

Fig 6.2.3. Schematic diagram of decomposition model

when the γ' particles are first seen remains to be explained; particles were only observed on ageing at temperatures of 600°C and above and therefore the absence of alignment may be because at these temperatures the decomposition process is nucleation and growth as suggested above. If however it is assumed that spinodal decomposition does occur at the higher temperatures the absence of alignment may be described in the following manner: If one of the ordered regions starts to grow classically its growth will be much faster than that of the spinodal wave (this arises from Cahn's analysis of the kinetics), down-hill diffusion will take place and a few γ' particles will grow at the expense of the locally ordered regions on the solute waves. This selected growth will be largely random and a preferred arrangement will not be observed. This description requires some of the ordered regions of the waves to reach a critical size for classical growth before other regions.

The degree of order in small particles.

The structure of lowest chemical free energy for the particles will, of course, be the fully ordered γ' structure. In view of the strain energy at the interface and the free energy associated with composition gradients at the interface a stable configuration may exist such that the reduction in free energy associated with the ordering is balanced against these two contributions to the interfacial energy. The degree of order will be a function of

the particle size and larger particles will be fully ordered. This variation in order has been determined indirectly by Gleiter and Hornbogen [43] and is important when considering the strength of alloys hardened by small particles. The existence of a diffuse interface would also account for the observation that the degree of order in small particles decreases away from the centres of the particles.

The later stages of the transformation.

The Curie temperature results at 500 and 600°C show an increase in transformation rate prior to the onset of the coarsening stage. The effect is most noticeable after the low temperature quench and may be explained in terms of the model in the following manner:

The spinodal decomposition, with the associated ordering reaction, takes place rapidly essentially unaided by the vacancy concentration; however at a later stage it is supposed that long range down-hill diffusion becomes favourable and this will be aided by the presence of point defects and by the ageing temperature. The 'plateau' may be associated with the transition from uphill to downhill diffusion and the reaction will not proceed very rapidly under these conditions because the concentration gradients will be small. The increase in transformation rate is due to the establishment of down-hill diffusion gradients and a rapid growth of the γ'. The time over which this change takes place is

expected and observed to be a function of temperature and the point defect concentration.

The models considered have the same qualitative result on the microstructure and only differ in the very early stages of ageing. The essential difference between the two models is that uphill diffusion is favoured for spinodal decomposition whereas downhill diffusion is favoured for classical nucleation and growth. It is difficult to separate the models experimentally although a number of experimental observations in this and previous work suggest the existence of composition gradients over greater distances than would result from a classical nucleation and growth process.

7. The relationship between mechanical properties and microstructure.

7.1. Solution treated material

The flow stress of the solution treated material is usually subtracted from the total flow stress when strengthening by particles is considered, as the solid solution contribution to the flow stress is difficult to assess directly in the presence of particles. Phillips [65] has recently suggested that the solid solution contribution is about 30% of the total flow stress in Ni 12.7 at % Al alloys, although he apparently ignores the effect of solute depletion during ageing.

The solution treated values obtained for the two alloys are very close, (alloy A 24 Kg/mm^2 and alloy B 22 Kg/mm^2). This is to be expected as they have similar amounts of solute in solution. Titanium has a slightly larger atomic diameter than Aluminium (both are larger than Nickel) and this would account for the slightly higher flow stress of alloy A.

The increased flow stress (30 Kg/mm^2) obtained on quenching from 1100°C is attributed to the appearance of regions of high local order in the solid solution rather than to any defect concentration effect. Although material showing local order may be described as a solid solution its strength relative to that of the solution treated material will be considered as part of the precipitation hardening discussion.

7.2. Alloys containing coherent ordered particles in the absence of strain fields in the matrix.

There are three possibilities for the behaviour of dislocations in these structures:

(i) The dislocations shear through the particles.

(ii) The dislocations bow between the particles leaving rings of dislocations around the particles.

(iii) The dislocations cross slip to avoid the particles.

Peak hardening is usually associated with the first mechanism.

Cutting of the particles by dislocations

Kelly and Nicholson [49] related the hardening to the work done in creating an antiphase boundary in the cut particles and that done in forming an additional area of particle matrix interface. They point out that for precipitates having high values of the antiphase boundary energy (such as γ') this will be a much larger factor than the interface contribution. On this basis they derived the relation:

$$\Delta\tau = 0.89\,\gamma f^{\frac{1}{2}} b^{-1}$$

where $\Delta\tau$ is the yield stress increase due to the particles.

γ is the antiphase boundary energy.

f is the volume fraction of the precipitate.

b is the Burgers vector.

The derivation of this relation assumed that the dislocations were pure single dislocations of the matrix. Electron microscope observations show that in these alloys dislocations move in pairs during the stage during which the precipitate particles are cut, in a similar manner to those observed in fully ordered structures. The first dislocation creates an antiphase boundary in the particle and hence has a dragging force on it due to the energy of the antiphase boundary it is creating. The second dislocation recreates order as it passes through the particle and thus there is a tendency for the dislocation to be pulled through the particle. The resulting dislocation configuration is of pairs of dislocations, each having the perfect Burgers vector of the matrix, separated by a distance which is governed by the elastic repulsion of the dislocations and the energy of the antiphase boundary.

A further assumption of the Kelly and Nicholson derivation was that the cutting dislocation remained straight; thus the average separation of the precipitates along the dislocation line was equated to the interparticle spacing derived from a knowledge of the particle size and volume fraction. This assumption would be reasonable for very small particles but not for larger particles (and lower volume fractions). In this situation the leading dislocation will bow between particles before shearing them and in the process will interact with other particles lying in the slip plane in front of a line connecting the two initial particles.

Davies and Stoloff [50] considered that as the passage of the superlattice dislocation resulted in a complete recreation of order in the particle the net effect on the flow stress would be negligible. They related the strength of their Ni-14 at% Al alloy solely to the strength of the matrix and the energy of the new interface created. The latter mechanism is however totally inadequate to account for the yield stress observed, as the interfacial energy is low (c.20 ergs/cm^2) and the strain energy contribution from the misfit will only be effective at larger particle sizes.

Two schools have been active in analysing the propagation of the dislocations and two theoretical models have been proposed.

The Gleiter and Hornbogen Analysis:

Gleiter and Hornbogen [51] considered the following factors which they suggested could influence the shear stress increase over that of the solid solution in the absence of elastic strain fields around the particles:

1. Different elastic constants and different stacking fault energies of the precipitate and matrix.

2. The increase in interfacial area due to the cutting process.

3. Jogs formed during the interaction of dislocations with vacancies.

4. The antiphase boundary energy.

5. Possible variation of slip system within the particle.

They consider (as did Kelly and Nicholson) that, for particles of virtually perfect order, (4) is an order of magnitude greater than (2), (5) does not occur and the other factors give a very small contribution. Working with the following assumptions Gleiter and Hornbogen set up different equations to describe the shape of the dislocation pairs on the slip planes:

1) Spherical precipitates.

2) Random precipitate distribution.

3) Negligible elastic anisotropy.

4) Dislocation spacing in all cases allowing the application of linear elastic theory.

5) Antiphase boundary energy constant within the particles.

They considered as the factors controlling the dislocation shape:

1) The effect of the external shear stress on the dislocations.

2) The elastic repulsion between the dislocations.

3) The antiphase boundary energy.

Their results are shown as curves of maximum and minimum dislocation spacing under two conditions namely of zero applied stress and of $\Delta\tau$ max (the maximum shear stress sustained by the alloy).

Their expression for the increase in shear stress due to the ordered particles is derived after making the following further assumptions:

1) That the kinetics of the γ' precipitation follow an equation of the form

$$f_t = f_\infty \left(1 - (1 + bt)^{-\frac{1}{3}} \right)$$

where b is a constant.

2) That the ordering kinetics of the γ' particles can be described by a first-order rate equation:

$$\gamma = \gamma_\infty - \gamma_o e^{-kt}.$$

The equation that results is complex, but may be reduced in the case of very small particles to:

$$\Delta\tau = 0.28 \gamma^{\frac{3}{2}} f^{\frac{1}{2}} G_\gamma^{-\frac{1}{2}} b^{-2} r^{\frac{1}{2}}$$

Gleiter and Hornbogen applied their equation to a Ni-Cr-Al alloy [52] and their results suggest that the simplified equation above applies up to about peak hardness. The assumptions made regarding the precipitate distribution and the precipitation and ordering kinetics make it difficult to apply the theory widely to a large number of systems.

Castagné analysis:

After a simpler analysis, again assuming a random precipitate distribution and again taking into account the bowing of the leading dislocation,

Castagné obtains the result:

$$\Delta\tau = 1.4 \quad \gamma^{\frac{3}{2}} f^{\frac{1}{2}} G_\gamma^{-\frac{1}{2}} b^{-2} r^{\frac{1}{2}}$$

applicable only to the case where the particles are cut by the dislocations. The difference between this equation and that of Gleiter and Hornbogen is in the numerical constant and the power to which the volume fraction is raised. These differences are partly due to the model used for calculating the interparticle spacing along the dislocation line and these are reviewed in appendix II.

A change to equation (4) (appendix II) for calculating interparticle spacing gives for Castagné's model:

$$\Delta\tau = 1.31 \quad \gamma^{\frac{3}{2}} f^{\frac{1}{3}} G_\gamma^{-\frac{1}{2}} b^{-2} r^{\frac{1}{2}}$$

which is some 4.5 times greater than the value predicted by Gleiter and Hornbogen's model. Castagné's value is higher because he makes as one of his assumptions that the dislocations in the pairs do not interact. This ignores the assistance given to the leading dislocation by the elastic repulsion of the second dislocation.

7.3. The effect on the yield stress of misfitting precipitates in the matrix.

Nott and Nabarro [60] were the first to consider in detail the effect of coherency strain fields around a precipitate. They determined the shear stress in the matrix around a spherical particle and the resulting equation for the shear stress at a distance p away from the particle is $\frac{\varepsilon r^3}{p}$ where ε is is a function of the lattice parameter mismatch and the elastic constants (it approximates to $\frac{2}{3}\frac{\Delta a}{a}$).

They derive the average shear strain in the matrix with a density of N precipitates per unit volume as $8 \varepsilon r^3 N$. Putting N in terms of the volume fraction and assuming that the flow stress is equal to the average of the internal stresses gives

$$\Delta \tau = 2 G \varepsilon f$$

This theory assumes that some bowing of the dislocations occurs but that the precipitates are finally cut. In the case of very small particles where the dislocations remain essentially straight the situation is analogous to that of a solid solution; there is little effect on dislocation motion because the elastic strain in some places along the dislocation line will assist dislocation motion and in other places it will impede motion.

Gerold and Haberkorn [63] and Gleiter [61] have performed more detailed analyses than Mott and Nabarro. Gerold and Haberkorn calculate the

repelling force on a dislocation due to its elastic interaction with the particles and show curves of the relative maximum interaction forces as a function of the height of the slip plane above the centre of the particle. The calculations show that there is a greater interaction with edge dislocations than with screw dislocations. Under conditions where the particles are cut by the dislocations, they show that the critical resolved shear stress due to the interaction of edge dislocations with the precipitates is given by:

$$\Delta\tau = 3 G \varepsilon^{\frac{3}{2}} f^{\frac{1}{2}} b^{-\frac{1}{2}} r^{\frac{1}{2}}$$

where ε is the Mott-Nabarro distortion parameter ($\sim \frac{2}{3} \frac{\Delta a}{a}$).

Only the result of Gleiter's analysis has so far appeared in the literature and is:

$$\Delta\tau = \sqrt{\frac{2.4\, b\, \varepsilon^3 E^3}{\pi T (1+\upsilon)^3}}\; f^{\frac{5}{6}} r^{\frac{1}{2}}$$

where ε is the Mott-Nabarro distortion parameter
T is the line tension of the dislocation.
υ is Poisson's ratio.

by taking $\varepsilon = \frac{2}{3} \frac{\Delta a}{a}$, $\upsilon = 0.33$ and $T = 0.5 G b^2$

the expression simplifies to:

$$\Delta\tau = 6.8 \left(\frac{\Delta a}{a}\right)^{\frac{3}{2}} G\, b^{-\frac{1}{2}}\, f^{\frac{5}{6}}\, r^{\frac{1}{2}}$$

Gleiter points out that the expression is not directly applicable to ordered coherent precipitates nor does it apply when Orowan looping occurs. Gleiter's expression gives a value $\sim 4x$ greater than Gerold and Haberkorn's. In a later paper[61] Gleiter considers that hardening by coherent ordered particles is a combination of order hardening and hardening by coherency strain fields. The effect of the strain fields on the dislocation configurations must also be considered as the use of the Gleiter expression above gives a value about 5 times too great. (Gerold and Haberkorn's expression would give a value of the right order but is presumable superseded by Gleiter's result as all three have worked in collaboration on parts of the theory).

The effect of strain fields on dislocation configuration.

Gleiter comes to the same conclusion as Mott and Nabarro, that there is a negligible effect on the flow stress so long as the dislocations remain essentially straight. As the particle size increases, depending on the position of the slip plane relative to the particle, the strain field around the particle can influence the dislocation pair configuration in a number of ways:

Positive edge dislocations

If the slip plane cuts particles on their equator there is no net force on the dislocation line from the strain fields as the positively strained

regions above the dislocation line are repelled by the particle whereas the regions below the line are attracted towards the particle. See fig.(7.3.1)a taken from the work of Gerold and Haberkorn.

If the slip plane cuts particles below their equatorial plane then there will be a resultant repulsion of the dislocation by the precipitate strain field; similarly for a slip plane cutting the particles above the equatorial plane there will be a resultant attraction for the dislocations moving on that plane. The force dK exerted by the particle on a segment of edge dislocation dl is given by the equation:

$$dK = 6G \frac{\varepsilon r^3 y z}{(x^2+y^2+z^2)^{\frac{5}{2}}} dl. \quad 6.$$

where ε is the Mott Nabbarro distortion parameter and x,y,z are the coordinates of the dislocation segment with respect to the centre of the particle.

Figs. (7.3.1) b and c show the effect of the strain fields on the dislocation pair configurations in the two cases. It may be seen from fig. (7.3.1.b) that a segment of dislocation that bows through between the particles, is then assisted in separating further from the other dislocation in the pair by the precipitate strain field. Because of this increased separation, a larger applied stress is required before the pair can cut through the particles. Gleiter points out that the extent of the separation can become so large that the second dislocation has no effect on the first and

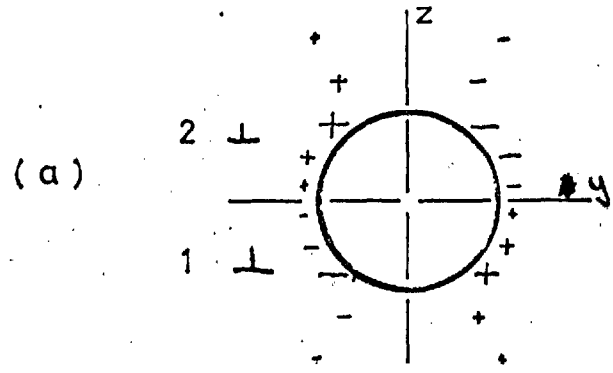

magnitude and direction of forces on a positive edge dislocation.

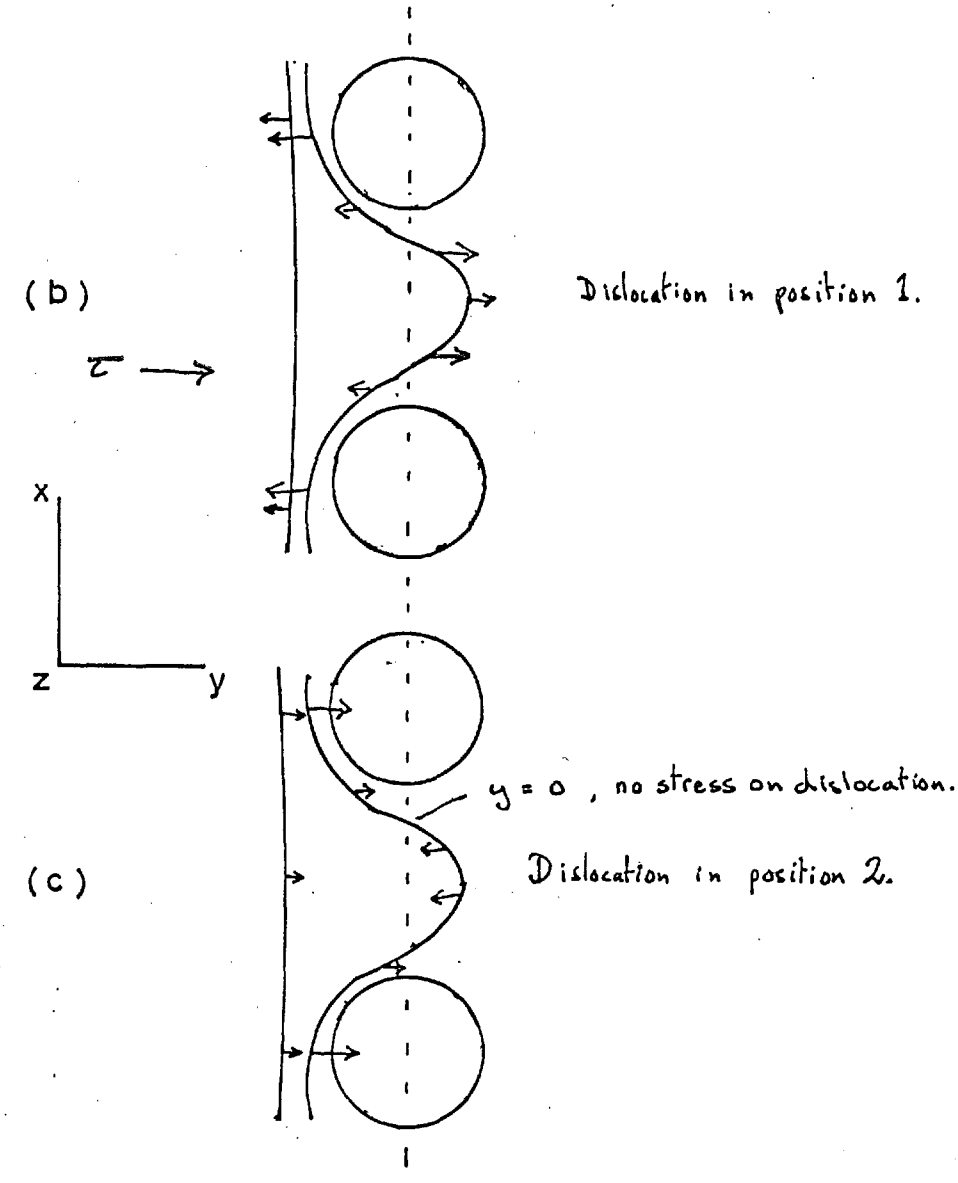

Fig. 7.3.1. Forces on edge dislocation pairs near misfitting particles.

the situation is that of a single dislocation cutting the particles. The magnitude of the effect increases with the mismatch and the particle size, and since it is shown that the strain fields enhance dislocation bowing an early transition to Orowan looping can occur.

The situation in fig. (7.3.1.c) results in a reduction in the dislocation pair spacing making it easier for the pair to pass through the particles and thus reducing the applied stress required. The net result of the two situations is an increase in the flow stress with particle size and lattice parameter mismatch. This increase is not as large as given by a simple consideration of the strain field effects because some of the dislocation pairs are assisted by the strain fields.

Gleiter points out that screw dislocations (which will always be repelled by the precipitate strain fields as they have radially symmetric strain fields) are able to cross slip assisted by the strain fields. Gleiter [62] analyses the cross slip mechanism in another paper. The pair separation is not influenced directly by the strains but rather indirectly by their effect in aiding cross slip. The cross slipping of the screw dislocations may raise the work hardening rate by increasing the likelihood of dislocation interactions.

Other experimental work in the literature

There are two other sets of experimental results in the literature that attempt to bring in the strengthening effect of the elastic strain fields. Fine [64] replotted the results of Mihilasin and Dekker [7] for a series of Ni-Al-Ti alloys of similar volume fraction. The results show an increase of the hardness at peak ageing with an increase in the lattice parameter mismatch.

Fine's curve may be criticised on two counts: firstly the misfit values were in one case incorrectly calculated by Mihalisin and Dekker and, secondly the hardness values themselves are functions of both the yield stress and the work hardening rate. It is possible that the latter parameters will vary somewhat differently with lattice parameter misfit.

Phillips [65] has recently attempted to analyse the various factors controlling the flow stress in his Ni 12.7 Al alloy. By considering the temperature dependence of the flow stress he calculates the following contributions to the observed flow stress:

Solid solution strengthening	28-36%
Dislocations	10-11%
Interface mismatch	12-18%
Modulus differences Antiphase boundary energy	38-47%

The last three factors are those included in the $\Delta\tau$ expressions of the hardening theories. Phillips' results suggest an elastic strain contribution of some 25% to $\Delta\tau$; the mismatch of his alloy was about 0.6% when aged at 700°C.

Dynamic Dislocation approach

An entirely different approach to hardening by coherent precipitates has been adopted by Copley and Kear [66] who attempt to take account of the dislocation motion by the use of dynamic dislocation theory. Their theory assumes that the dislocation pairs remain essentially straight. This assumption may well be reasonable for superalloys with a very high volume fraction but for the alloys in the present work the change in dislocation configuration with particle size must be considered. The approach is physically realistic but the present development of the theory is inadequate to account for the yielding behaviour of the alloys under consideration. Its use to analyse the temperature dependence of the flow stress may be more fruitful.

Transition to Orowan looping.

This transition corresponds to overageing in γ' hardened alloys and will be only briefly considered. At a critical value of interparticle spacing the stress to force a dislocation through the precipitates will be equal to that required to bow the dislocations round the particles in the

Orowan fashion. The stress required for the latter process is given by:

$$\Delta\tau = \frac{Gb}{4\pi} \frac{2}{(1-2\nu)} \ln\left(\frac{l-2r}{2b}\right)$$

Essentially the stress is inversely proportional to the particle radius. Gleiter and Hornbogen's analysis shows that a loss of strength can occur whilst the dislocations are still cutting the particles; in fact they show that dislocations will always cut the particles in the absence of coherency strain fields in the case of their Ni-Cr-Al alloys. Gleiter has shown, as described earlier, that the strain fields can assist the onset of Orowan looping and the cross slipping of screw dislocations.

In addition to the effect on the yield stress the creation of Orowan loops gives a rapid work hardening rate at low strains because the effective size of the particles is increased by the presence of the loops. The loops can however contract under their own line tension and it is possible for them to lie wholly within the particle, the stable radius being determined by the line tension of the dislocation and the area of the antiphase boundary formed. The effect will be to mitigate to some extent the rise in work hardening rate.

7.4. Application of theory to the present work experimental results:

It is assumed here that the contributions to the flow stress arising from modulus differences and from the increase in the particle matrix interface when the particles are cut have only a small effect (actually about 10%) on the flow stress. This assumption has been made by most workers in the field of γ' hardened materials.

Before it is possible to compare the results with the theories the following features of the present alloys must be considered:

(i) The effect of particle alignment and distribution.

(ii) The effect of particle shape.

(iii) The degree of order in the particles.

(iv) The antiphase boundary energy.

(i) The effect of particle alignment and distribution.

The strengthening theories are based upon an assumed model of either a regular distribution of particles throughout the volume or a truly random distribution. Consideration of the micrographs of material aged for long lengths of time shows that the particles are aligned in rows in (100) directions and are closely spaced along these rows. At very long ageing times the rows form into 'rafts' of particles. As the particles are very close even at intermediate ageing times a reasonable

approximation would be to consider the rows of cubic particles as rods, or at the later stages of ageing, plates of γ' in the matrix.

In the early stages of ageing the alignment is less pronounced although it does become evident before overageing occurs; however the particles are not closely spaced along the aligned rows until after peak hardness. The stages prior to peak hardness are those important for the application of the hardening theories and therefore it is in these stages that some assumption of the particle distribution must be made. The slip system cuts the aligned rows of particles at large angles and therefore the effect of the alignment is not to provide small regions of closely spaced particles on the slip plane but rather to increase the effective interparticle spacing in the slip direction. This follows from the fact that if the particles are closely spaced in rows then for a given volume fraction the rows will be spaced more widely apart. It is the distance between the rows that the dislocations effectively "see" as the spacing of obstacles in the slip plane.

On a simple model the increase in the mean interparticle spacing would decrease the flow stress from that predicted by a theoretical random model due to the added help given by the line tension of a dislocation bowed to a larger radius. In the case of paired dislocations however the increase will allow the leading dislocation to bow further under the applied stress; this reduces slightly the effect

of the second dislocation in helping the first through the obstacles and a small increase in the flow stress may result. The increased bowing of the dislocations, however, may also assist the transition to the Orowan mechanism and promote overageing.

At a later stage in the ageing the closely aligned particles may possibly hinder the cross slip of screw dislocations by presenting an effectively larger obstacle to be overcome by cross slip. If the cross slip is hindered, then the screw dislocations would have to bow by the Orowan mechanism. Foreman [76] has shown that screw dislocations bow less easily than edges and it is possible that alignment could resist to some extent the loss in strength on overageing of the alloys.

(ii) The effect of the particle shape:

The particles, when clearly defined in the electron microscope, are cubic and therefore corrections are required to the equations for the interparticle spacing which were derived for spherical particles. There is the possibility of a spherical particle shape in the early stages of ageing and it will be assumed that such a shape exists prior to peak hardness; the effect of particle shape will in any case be small compared with the other uncertainties in the interparticle spacing.

(iii) The degree of order in the particles:

The model proposed for the decomposition implies that the particles formed in the early stages of ageing do not exhibit complete order nor are the particle matrix interfaces clearly defined. Gleiter and Hornbogen [43] and Castagné [67] have derived values of the degree of order and the size of the small particles by counting the number of dislocation pairs along a pile-up required to cut the particles completely and by measuring the separation of the pairs along the pile-ups.

Gleiter and Hornbogen show that the degree of order is at a minimum at the particle boundaries and increases to a maximum at the centre. This corresponds well with the models proposed in this work for the formation of the particles. Their results show that the average ordering parameter of the particles reaches 0.9 at a particle size of about 150 Å and that the antiphase boundary energy follows a function of the form $\gamma = \gamma_\infty - \gamma_0 e^{-Kt}$ where $\gamma_0 = 0.4\gamma_\infty$ and K is a temperature dependent constant. A better way of displaying the Gleiter and Hornbogen result is to plot the antiphase boundary energy as a function of the particle size rather than the ageing time since the results may then be used for different ageing temperatures. A plot of the degree of order versus the particle size derived from Gleiter and Hornbogen is shown in fig. (7.4.1).

In interpreting the results of the present work the relation between degree of order and particle

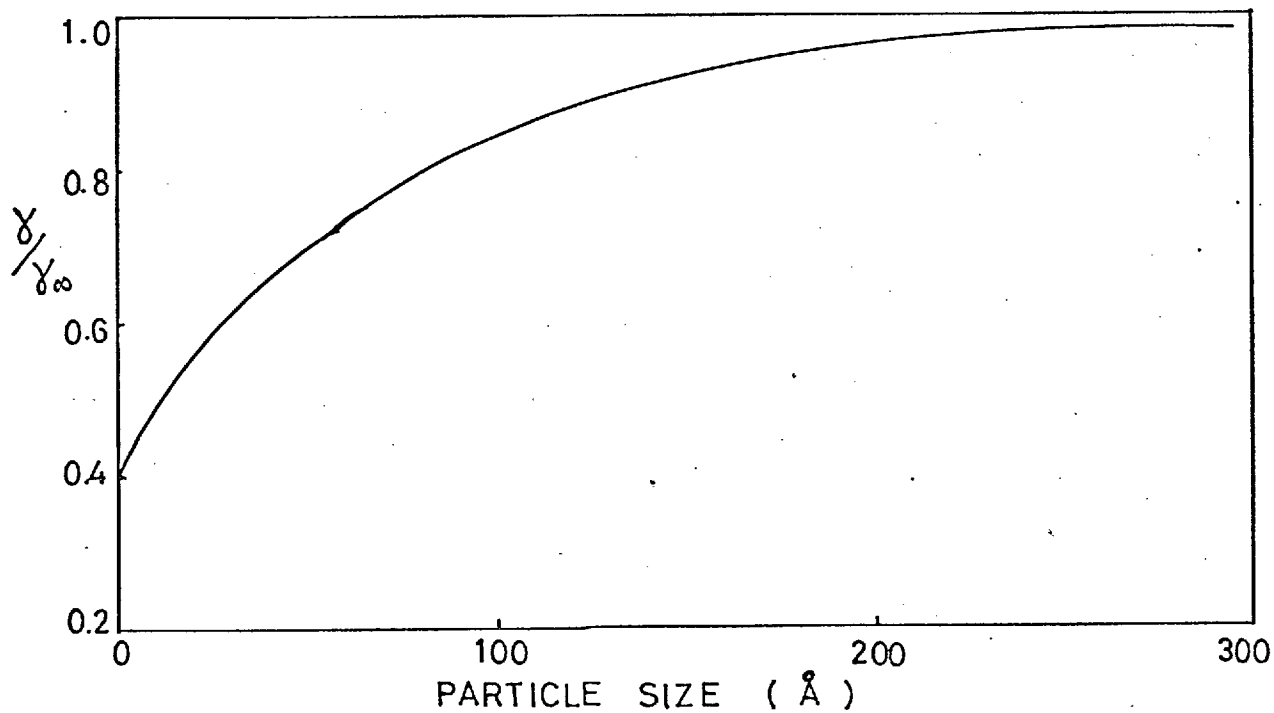

Fig.7.4.1. Variation in antiphase boundary energy with particle size.

(Re-plotted from Gleiter and Hornbogen)

size will be assumed from fig. (7.4.1) and it will also be assumed that the $t^{\frac{1}{3}}$ law for the coarsening of the particles holds down to small particle sizes.

(iv) The antiphase boundary energy.

A satisfactory value for the antiphase boundary energy γ is essential to allow any quantitative application of the theory; values in the literature vary from 150 to 250 erg/cm^2 Gleiter and Hornbogen assumed Williams [3] value of γ for Ni_3Al (164 erg/cm^2), but Williams did not give details of his quasichemical calculation. Flinn [68] derived a relation for the antiphase boundary energy on a quasichemical model:

$$\gamma_\infty = \frac{2v}{a^2}\,\frac{h}{\sqrt{N}}$$

where a is the lattice parameter, $N = h^2 + k^2 + l^2$, and v is the heat of formation of γ'. Assuming that $v = kT$ where T is the disordering temperature and if it is assumed further that γ' remains ordered up to the melting point (1670°K) then $\gamma = 218$ ergs/cm^2 for a (111) antiphase boundary.

Marcinkowski and Brown [69] using a more comprehensive quasichemical theory derived the relation $\frac{1.41\ kTc}{a^2}$ for the (111) antiphase boundary, giving $\gamma = 265$ ergs/cm^2. Recent work [71] suggests that the order-disorder transformation temperature is somewhat below the melting point and taking the lower end of the temperature range given, a value of 220 ergs/cm^2 is obtained.

The γ' precipitated in the alloys in this investigation contains titanium in solution, the titanium atoms substituting for the aluminium in the ordered structure. Guard and Westbrook [70] showed that a 10 at% addition of titanium to stoichiometric Ni_3Al increased the hardness by about 50%, which they attributed, at least in part, to a solid solution strengthening effect. The effect of alloying on the antiphase boundary energy has not been considered in this paper but the results for a number of different alloying elements substituted for aluminium showed a marked increase in hardening only when a large increase in the lattice parameter was observed. It may tentatively be concluded that the strength of alloyed γ' is due more to the solid solution strengthening than to a change in the antiphase boundary energy. The lack of knowledge on the variation of the antiphase boundary energy on alloying does put a limitation on the interpretation of the differing strengths of alloys A,B and the Ni 12.7 Al alloy solely in terms of the effect of the coherency strains.

Quantitative analysis of the results.

Having reviewed the current theories of hardening by γ' particles and made some comment on the possible modifications to the theory that might be required for the present alloys, it should now be possible to interpret the results on the basis of these theories.

The form of the complete Gleiter-Hornbogen curves for volume fractions corresponding to the present alloys is shown, together with values calculated from the present work, in figs. (7.4.2) and (7.4.3). The assumptionsmade in the derivation of these curves are given in table 7.4. The Gleiter-Hornbogen curves predict a loss in strength for particle sizes over $\sim$ 110 Å but for the present alloys a misfit contribution proportional to $r^{\frac{1}{2}}$ must be added and the results show good agreement with such an addition.

The Ni 12.7 Al alloy does not show an increase in strength over that predicted by the Gleiter-Hornbogen theory although it has an 0.6% mismatch; this may be explained by the increased effective interparticle spacing due to the alignment of the particles (a similar effect must be present for alloys A and B but cannot be estimated).

The apparent higher strength of alloy B (which has a lower misfit than alloy A) at 700 and 750°C is due to the volume fraction difference between the two alloys at these ageing temperatures. All the

alloys show increasing strength with decreasing ageing temperature for a given particle size as a result of the higher volume fractions and misfit at the lower temperatures. For a given volume fraction and particle size the strength of the alloys increases with the misfit.

The resistance to overageing may be explained partly by the misfit stresses but it is also possible that the particles will go incoherent on deformation at the larger particle sizes. The loss of coherency will not necessarily increase the strength as the misfit contribution to the flow stress will have been lost; it will however result in a higher work hardening rate, due to the interaction of slip dislocations with interfacial dislocations. This would result in a higher work hardening rate which would be reflected in the 0.2% proof stress measurements. A loss in coherency would also explain the rise in work hardening rate observed prior to peak hardness. The possibility of Orowan looping occuring in the early stages of overageing is unlikely since for a 15% volume fraction of γ' the Orowan stress for 500 Å particles is at least 46 kg/mm^2 (using $\Delta\tau = \frac{Gb}{L}$) This was calculated using a close packed particle distribution model (equation 4 in appendix 2) and therefore a lower value would be found when the effective interparticle spacing of the aligned structure is considered. The effect of alignment would be unlikely to permit Orowan looping in preference to particle cutting in the particle size ranges where overageing is first observed.

A number of dislocation loops were, however, observed in the presence of average particle sizes of about 200 Å and above, prior to peak hardness, and if it is true that Orowan looping is not possible at these particle sizes, then these loops must have arisen by the cross slip of screw dislocations as described in the theoretical section. Stereomicroscopy would be required to decide whether the loops were rings of slip dislocation or whether they were formed by cross slip of screw dislocations; the latter would appear above or below the slip plane, whereas the slip dislocation loops would appear in the slip plane.

The results are in good agreement with the current theories of hardening by misfitting coherent particles showing a compromise between the strength of disordered misfitting particles and ordered non-misfitting particles. The effects described in the phase transformation section explain the hardening at very small particle sizes and these are included in the curves calculated from the Gleiter and Hornbogen theory; the loss in strength whilst the particles are still being cut is a consequence of this theory and is restricted to some extent by the particle size dependence of the misfit contribution. The work hardening behaviour of the alloys has also been accounted for.

The behaviour of the alloys after peak ageing is not unambiguously described, as it may be a function of a loss of coherency or possibly the onset of the Orowan mechanism; the micrographs show evidence of both effects and both may well occur, particularly at the larger particle sizes.

TABLE 7.4.

Assumptions made in the calculation of the Gleiter and Hornbogen curve :

The antiphase boundary energy = 220 ergs/cm^2.

The shear modulus G = E = 7.5×10^3.

The Burgers vector b = 2.5 Å

The volume fraction = atom fraction.

Particle diameter = cube edge length extrapolated to short ageing times by a $(t)^{\frac{1}{3}}$ law.

The degree of order in the particles follows the curve in fig.7.4.1.

The interparticle spacing is as given by equation 4 in appendix II.

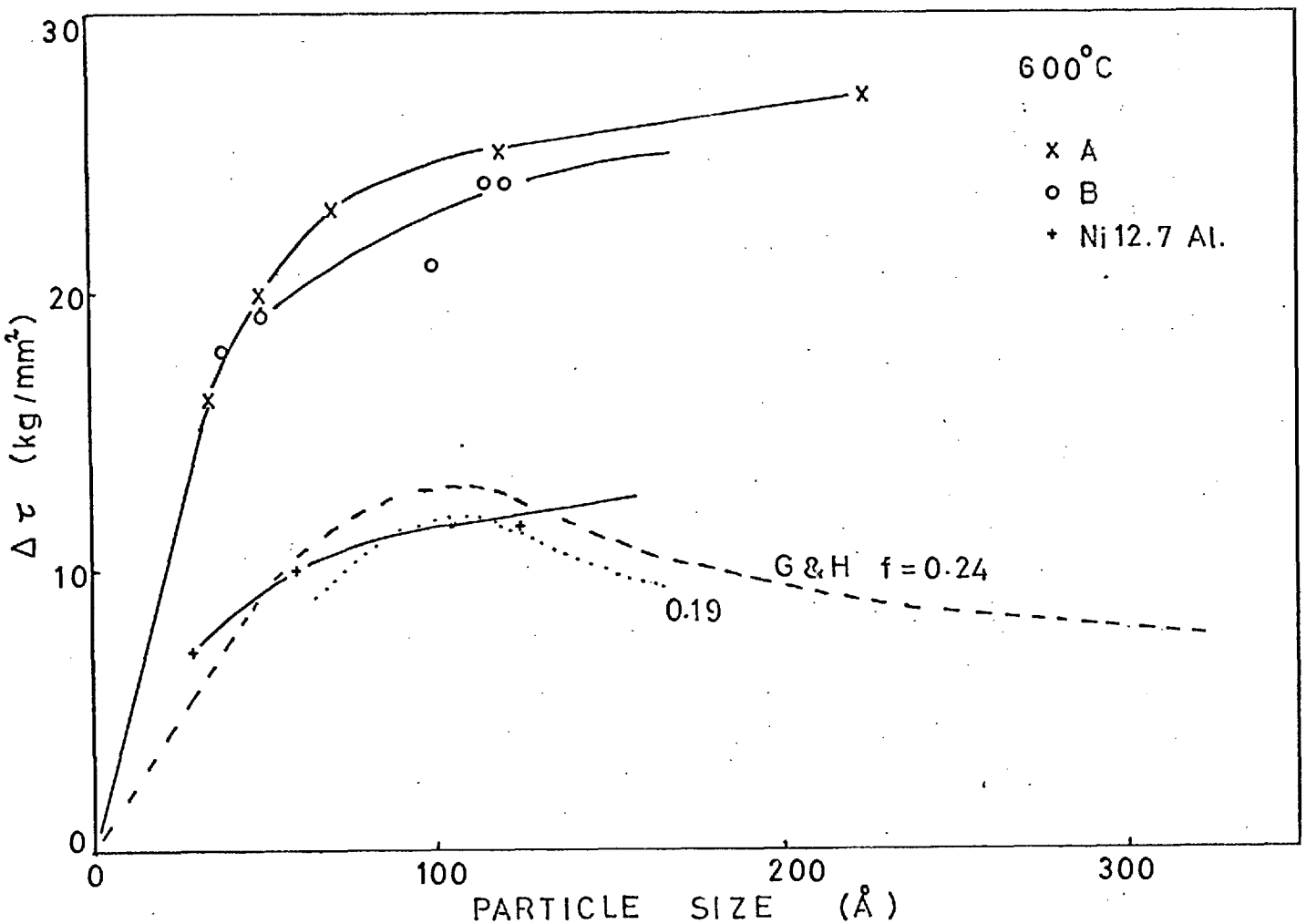

Fig.7.4.2. Comparison of experimental results with Gleiter and Hornbogen theory.

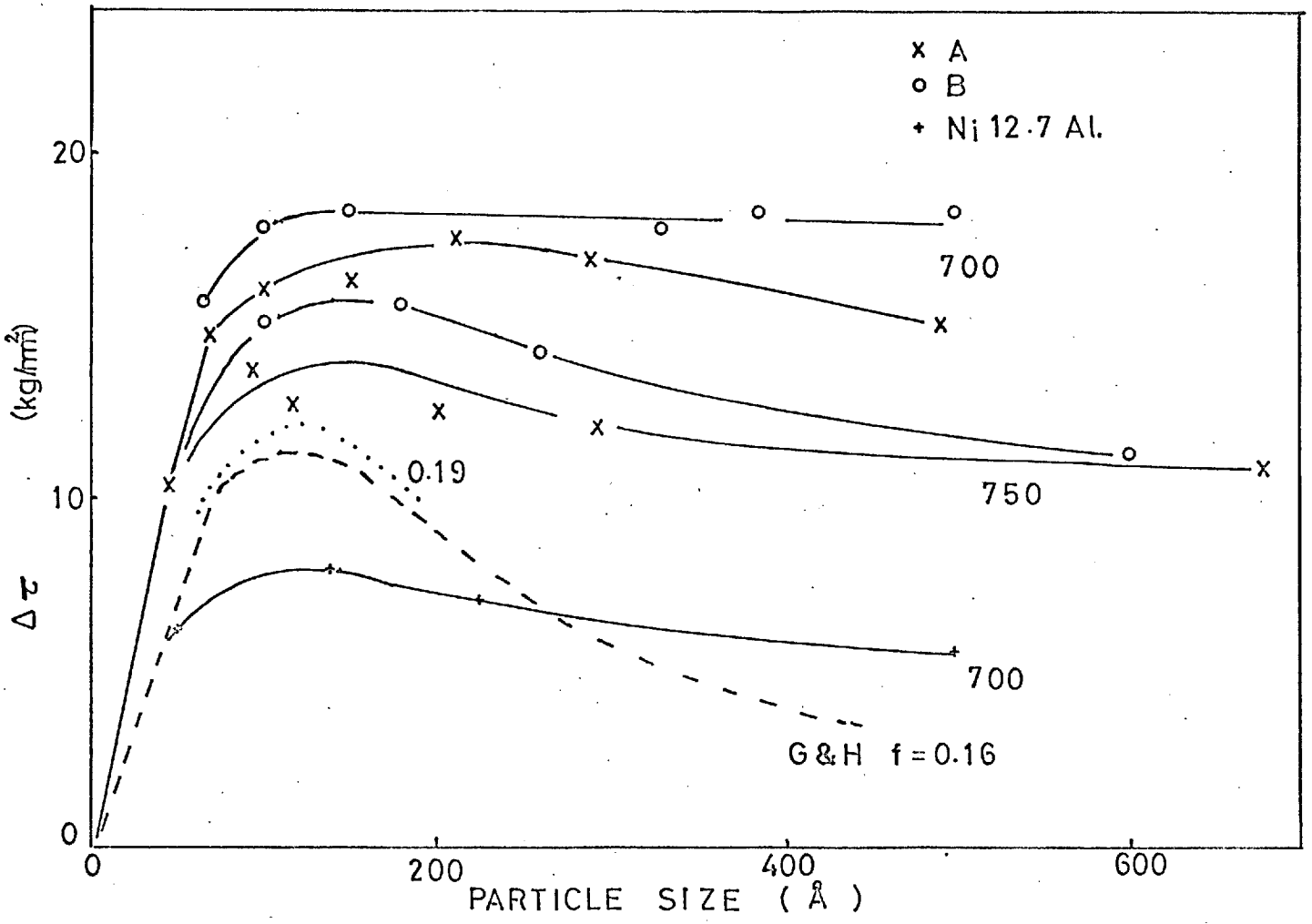

Fig.7.4.3.Comparison of experimental results with Gleiter and Hornbogen theory.

8.1. Conclusions.

The phase transformation:
supersaturated γ to γ + γ'.

1. There is a rapid initial decomposition, only retarded by a low temperature quenching technique, characterised by wide composition gradients and evidence of regions of high local order.

2. The initial stages of decomposition are still in some doubt; it is considered, however, that the best description is of spinodal decomposition with an ordering reaction on the solute-rich waves; this stage is followed by classical growth of the γ' precipitates.

3. At the higher ageing temperatures the decomposition is too rapid for it to be studied; the kinetics and thermodynamics are such that classical nucleation and growth may be preferred from the start of the decomposition.

4. The γ' particles do not exhibit complete order in the early stages of ageing.

5. The morphology of the particles is in agreement with the results of previous work; there is no loss in coherency of the particles up to the largest sizes observed, (i.e. 1500 Å).

6. Grain boundary denudation occurs as a result of the coarsening process and is absent in the early stages of ageing.

7. The alignment of the γ' particles in (100) directions appears to be a result of an elastic interaction during coarsening confirming the results of previous work. The spacing of the particles in the (100) directions appears to decrease as the lattice parameter mismatch increases.

8. The alloy with the higher mismatch appears to coarsen somewhat faster than the other alloy.

9. Independent values of the interfacial energy and the diffusion parameters have been determined from coarsening data:

	(ergs/cm^2)	Activation energy(k.cal/mole)
Alloy A.	23	72.5
Alloy B.	20	61.4

Mechanical properties:

10. The yield strengths have been interpreted in terms of current theories of hardening by coherent ordered particles and in terms of the observed microstructures and dislocation configurations.

11. An increase in lattice parameter misfit increases the strength of the alloys for a given microstructure.

12. Increasing work hardening rates, prior to peak hardness, have been interpreted in terms of a loss in coherency on deformation.

Other conclusions:

Dynamic elastic modulus measurements are sensitive to the changes taking place on ageing and have been interpreted in terms of the microstructural changes determined by other techniques.

8.2. Suggestions for further work:

1. The doubts remaining regarding the nature of the phase transformation may possibly be resolved using X-ray methods, particularly small angle scattering and the determination of absorbtion spectra. A refined and quantitative magnetic technique may enable the determination of the relative amounts of material with a given composition.

2. The alloys form the basis of a series of nickel based alloys used for high temperature service and having described the low temperature mechanical properties in terms of the dislocation arrangements, the determination of the dislocation structures after high temperature deformation should be made. These studies are particularly important in view of the observed increase in strength with temperature of the γ' itself.

3. The observation of the dislocation structures after the addition of an element such as Cobalt, which might lower the stacking fault energy and give rise to widely separated partial dislocations, would be interesting and informative. Cobalt-containing alloys might also have interesting magnetic properties.

ACKNOWLEDGEMENTS

The author wishes to thank Dr. D. R. F. West for his enthusiastic and careful supervision of the project and for much helpful advice, and Professor J. G. Ball for the provision of laboratory facilities.

Thanks are also due to Messrs. Henry Wiggins Ltd., of Hereford, who manufactured the alloys and to the Science Research Council for a research studentship during the period of the work.

The work of Mr. R. Ownsworth who made some of the measurements at 400°C as part of an undergraduate project is appreciated. Discussions with Miss J. M. Silcock of C.E.R.L. and Professor B. R. Coles and many colleagues and friends at Imperial College and elsewhere are gratefully acknowledged.

APPENDIX 1.

Young's Modulus Measurements at Elevated Temperatures.

A relatively simple technique was required that would allow the measurement of moduli at elevated temperature in order that changes taking place during ageing could be observed. In view of the fact that only small changes were anticipated the apparatus was required to have a high accuracy. The apparatus described is similar in many respects to that described by Lytton et al. (75). The problem was readily separated into two i.e. the accurate measurement of the modulus and the application of the technique to high temperatures.

Young's modulus is related to the vibrational frequency of prismatic bars by the formula $F_n = \frac{\pi k}{l^2}\sqrt{\frac{E}{\rho}}\,(\beta_n)^2$

where F_n is the resonant frequency
l is the length of the prism
k is the radius of gyration of a section of the prism about an axis normal to the prism axis and plane of motion.
E is Young's Modulus
ρ is the density of the material
β_n is a constant depending on the mode of vibration
(1.5056 for the fundamental mode with two nodes)

The only measurement that is required other than simple dimensional measurements is that of the resonant frequency of the prism. The

apparatus used was intended to measure this to a similar degree of accuracy to that with which dimensional measurements could be made. The main requirements of the apparatus were that it should induce resonance in the specimen, detect this resonance and measure the resonant frequency.

A schematic diagram of the apparatus is shown in Fig.(A.1.1.).

The main features are:

(i) Excitation of oscillations in the specimen:

A stable audio oscillator with an output of a few volts into 600 ohms was the prime mover. It was connected via an impedance matching transformer to the voice coil of a moving coil loudspeaker; a small hook was attached to the centre of the loudspeaker cone and one of the specimen suspension wires was attached to this hook.

(ii) Detection of the resonance.

The detection of the resonance is carried out by measuring the amplitude of the vibrations set up in the specimen. A barium titanate or Rochelle salt gramophone pickup provided a very sensitive detector; the output of the detector was connected to a vacuum tube voltmeter so that the amplitude of the signal could be measured.

(iii) Measurement of the resonant frequency:

A digital frequency counting device was employed to measure the frequency; it was checked against an internal crystal standard and was accurate to better than one part in 10,000.

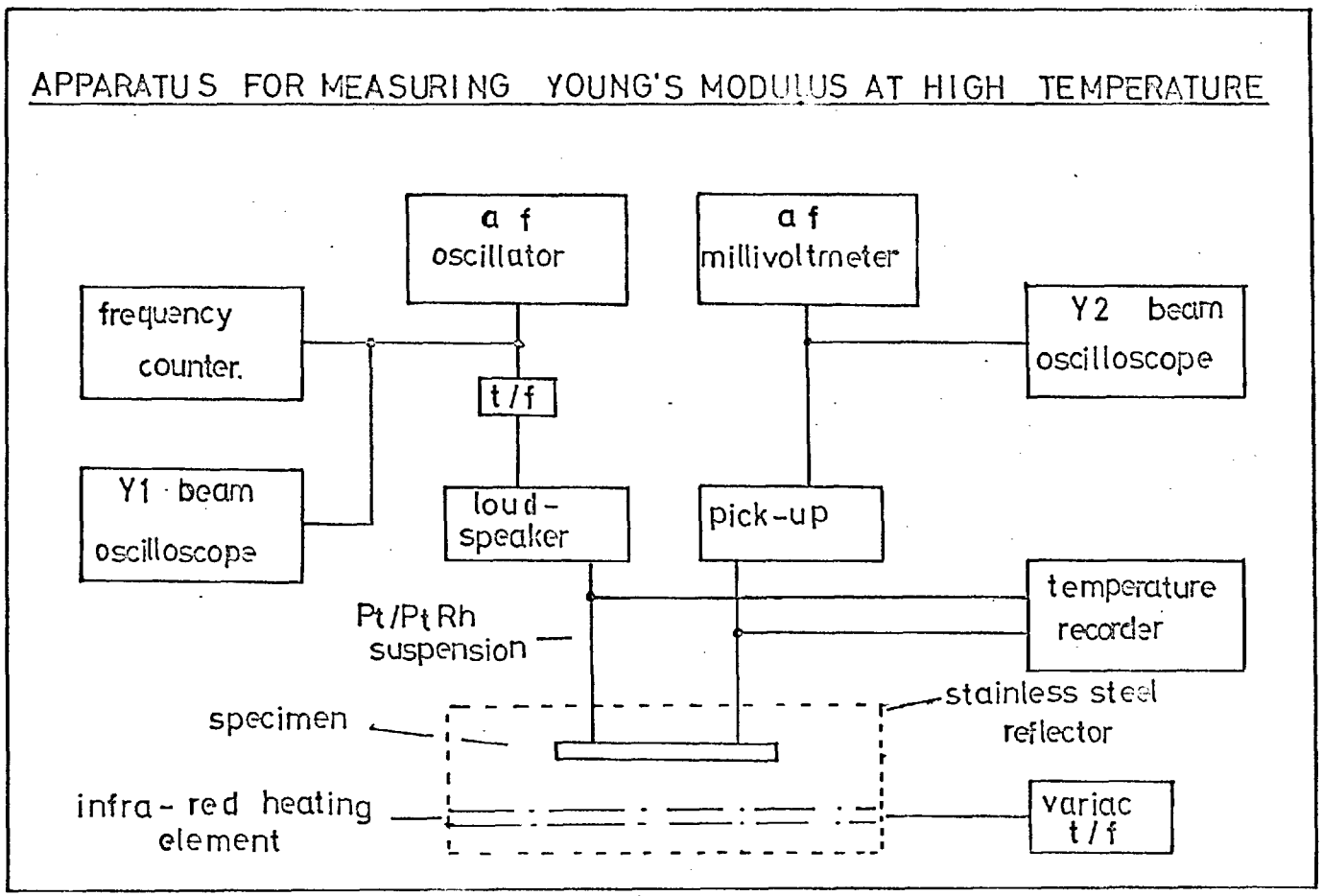

Fig.A.1.1. Schematic circuit diagram : Elastic modulus apparatus.

(iv) Obtaining of high specimen temperatures.

The specimen was raised to the testing temperature by means of a line-source image furnace (75). The specimen was placed at one focus of a highly polished elliptical stainless steel reflector with a quartz infra-red heating element at the other focus. Stainless steel oxidises at high temperature and therefore it was necessary to protect the reflector by housing the whole apparatus in a vacuum chamber. A typical performance curve from the furnace is shown in fig. A.1.2.

The specimen temperature was determined by suspending the specimen from platinum and platinum-15% rhodium wires respectively; the hot junction of the thermocouple is thus the specimen itself and an average value for the specimen temperature is obtained. Ordinary thermocouple devices in contact with the specimen could not conveniently be used due to the effect of these on the specimen vibrations; the device was however checked during blank runs on the furnace. The output from the thermocouple was recorded on a Honeywell recorder, thus allowing the performance of the furnace to be assessed over a prolonged length of time.

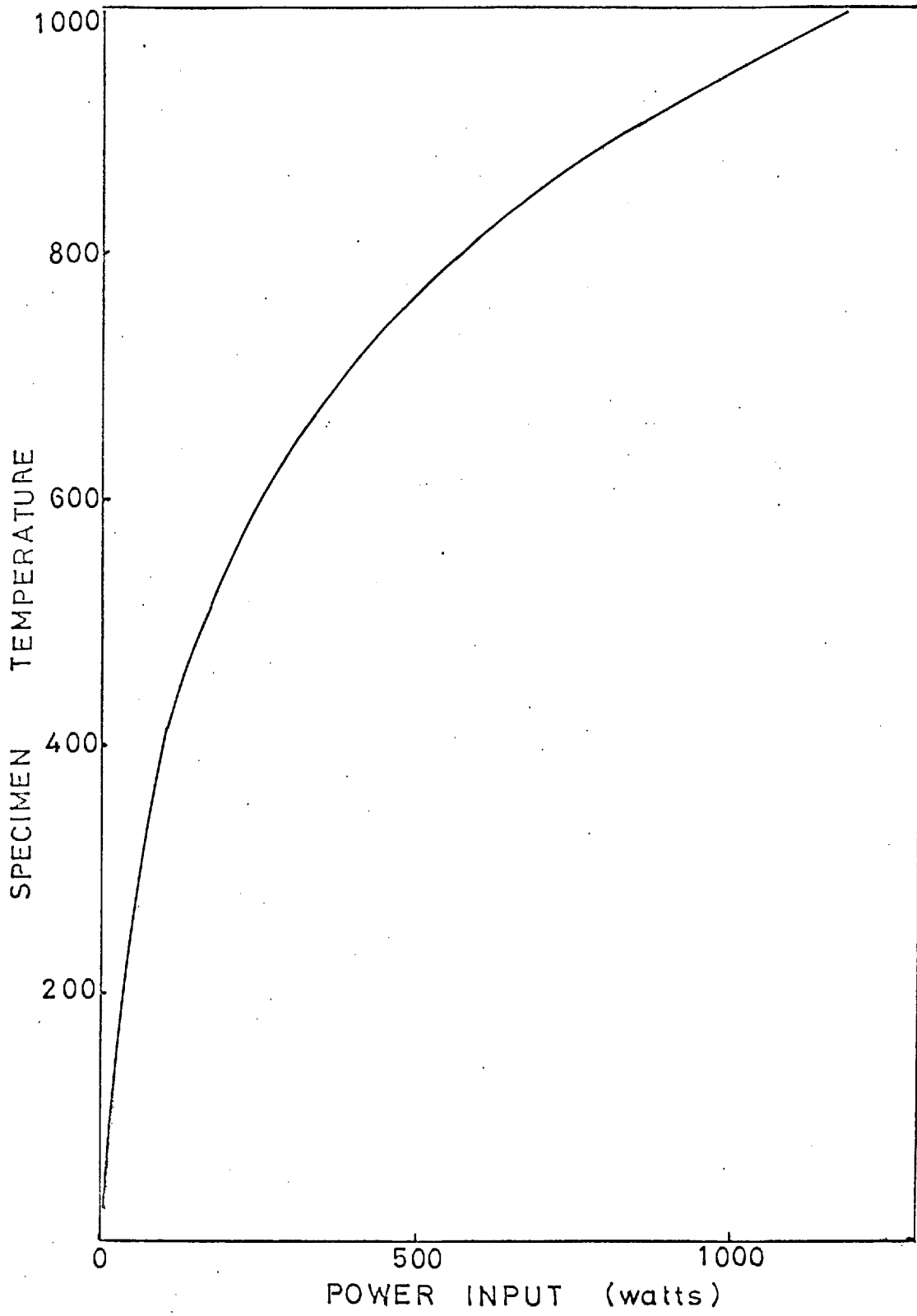

Fig.A.1.2 Furnace performance curve.

The accuracy of the measurements obtained may be ascertained by considering the accuracy of the various parameters in the formula for the resonant frequency.

(i) Applicability of the formula

The formula supposes that the diameter of the specimen is small compared with its length, and it ignores the effects of rotary inertia and shear. Corrections have been evaluated, and an absolute value of E 0.8% too low is expected in all cases with the specimens used; there is a minimal effect on the relative values.

(ii) Accuracy of measurement of the frequency

The frequency counter is able to measure frequency to $\pm$ 1 part in 10,000 and was not considered to add to the inaccuracies of the measurements; however, an uncertainty in the frequency measured exists because of the difficulty in locating the exact resonant point of the specimen. Setting precisely at the resonant point depends on the damping capacity of the specimen itself and on the restraint placed on the resonant system by the supporting wires. The restraint may also result in a slight shift of the resonant frequency due to the specimen support wires being also part of the resonant system. A maximum error of the order of 0.5% in the resonant frequency is considered reasonable and is borne out by the reproducibility of the experimental results.

(iii) Determination of the specimen dimensions and mass

Mass: Measured to better than $\pm$0.01%
Length: .. . . $\pm$0.02%
Diameter: .. . . $\pm$0.1%

These give rise to an error when comparing different specimens of 0.3% in the modulus.

(iv) Effect of the change in dimensions at high temperatures

Corrections for the expansion of the length and diameter of the specimens require a knowledge of the linear expansion coefficient, which is not known for these alloys. The figure for pure nickel was used and it is simple to calculate that a difference of 25% from this value would only change the absolute value of the calculated modulus by 0.3%

(v) Temperature

Although not featured in the formula, it is of little use to obtain highly accurate modulus data if the temperatures at which these data are obtained are not known to reasonable accuracy. The Pt/Pt-Rh couple with the specimen as the hot junction was found from blank calibration results to indicate to within about 2°C. the average specimen temperature. It was however difficult to measure the thermal gradients, if any, in the specimen, and hence it is considered that there is an uncertainty in the absolute value of the specimen temperature of some 10°C. The relative values however appeared from the reproducibility of the results to be within 2°C.

Experimental Procedure

Specimens 10 cm. in length and 0.5 cm. in diameter were used. In the "as received" condition these were straight and of uniform diameter, and the ends were made as square as possible. The specimen was heat treated as required, lightly smoothed with silicon carbide paper to remove any traces of oxide, measured, and weighed as accurately as possible and then slung on the support wires. The points of support were at 2 cm from the ends of the 10 cm specimens.

The resonant frequency was measured at room temperature and then the voltage across the furnace was increased gradually to give a slow rate of heating. Measurements of frequency and temperature were taken simultaneously whilst the specimen was heating. As far as could be ascertained there was little thermal lag of the specimen; if the specimen was allowed to come to a constant temperature fairly rapidly there was little further change in resonant frequency during the period in which it might have been expected that the interior of the specimen would be attaining the temperature of the surface.

The heating rate was increased in the ageing temperature range so that as short a time as possible was spent at ageing temperatures lower than those of interest in any particular run. There was little problem in heating rapidly through the lower regions of the ageing range as the furnace was capable of heating rates of the order of 600°C per minute. The

furnace temperature was allowed to remain constant for considerable lengths of time at selected ageing temperatures in order to investigate the effect of ageing on the value of the modulus.

Results:

Typical curves of resonant frequency versus temperature are shown in fig. (A.1.3). They show the expected fall in frequency and, hence, of modulus as the temperature rises. It may also readily be seen why useful results at the ageing temperature were not obtained; on reducing the temperature to room temperature after holding at ageing temperatures there is a change in modulus similar to those in the room temperature measurements reported earlier. At higher temperatures the curves for solution treated and aged alloys merge and little change may be detected.

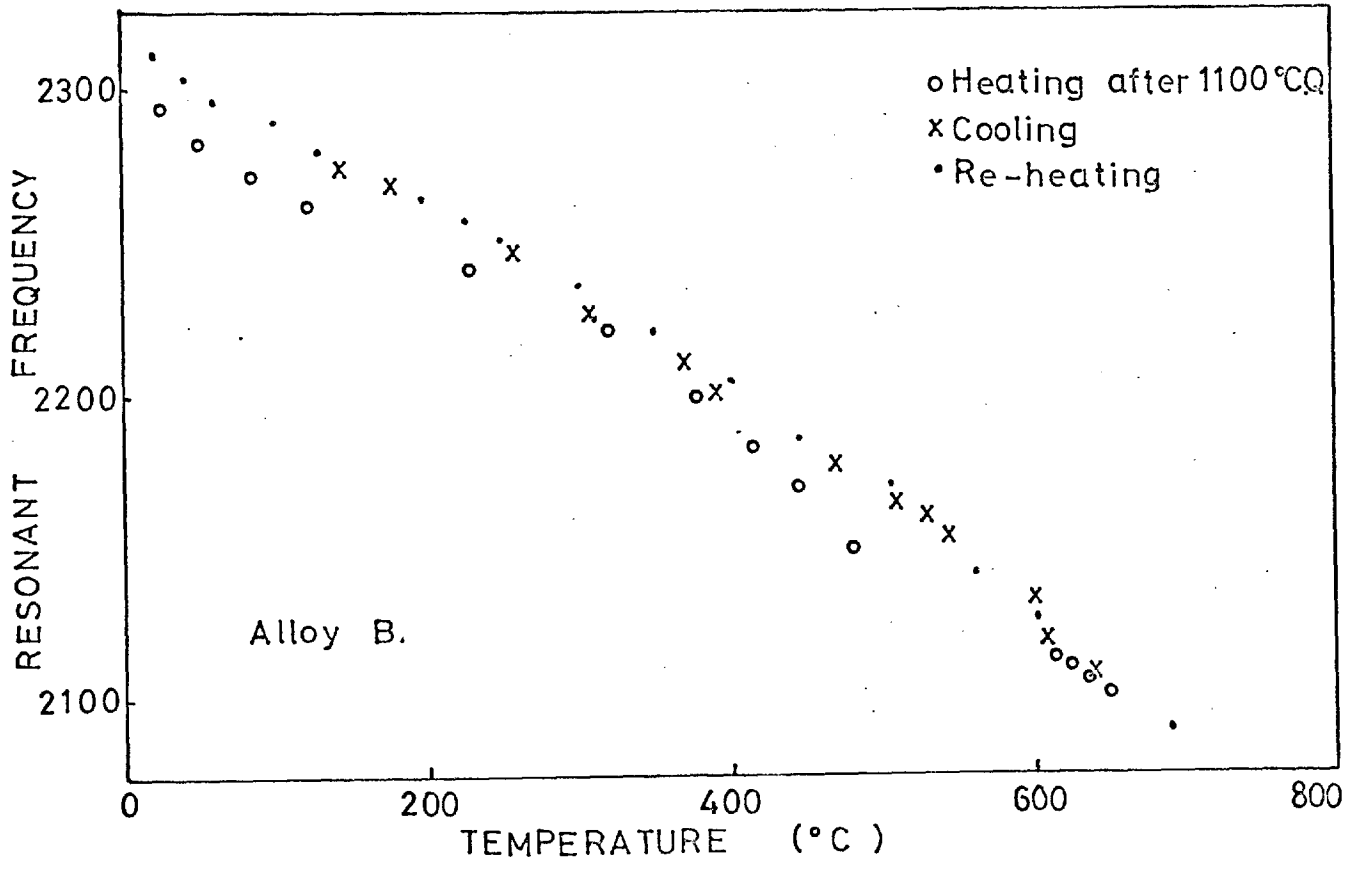

Fig.A.1.3.Typical experimental results:Resonant frequency versus temperature.

APPENDIX 11.

The effective interparticle spacing in a precipitation hardened alloy.

Several different functions for the mean interparticle spacing $\bar{\ell}$ on a slip plane have been used. Ashby [54] considered a planar approach in which the spacing is related to the area fraction of particles in a plane; if it is assumed that the particles are distributed on a simple cubic array in space then the expression

$$\bar{\ell} = \left[\frac{8}{3}\right] r f^{-\frac{1}{2}} \quad - \quad 1$$

results. Alternatively, a close packing of particles may be assumed which gives:

$$\bar{\ell} = \left[\frac{2\pi}{3}\right] r f^{-\frac{1}{2}} \quad - \quad 2$$

Ashby considers that neither of these gives the average spacing for a truly random distribution of particles. He shows that the separation can be evaluated as the radius of the smallest circle, in a plane, in which the probability of finding the second particle is unity; this gives:

$$\bar{\ell} = \left[\frac{\pi}{2}\right] r f^{-\frac{1}{2}} \quad - \quad 3$$

This same equation was derived by Westmacott et al. [55] using a more complex method.

Marcinkowski and Wriedt [56] attempted to justify equation 2 by saying that it is physically

more realistic to consider the planar separation of particles as the dislocations themselves move on planes. Ansell and Hirschorn [57] pointed out that the assumptions of particle distributions used in deriving equations 1 and 2 are too limiting for randomly dispersed particles. They consider that the only reliable means of obtaining $\bar{\ell}$ is by direct measurement. They show however that obtaining $\bar{\ell}$ by considering the mean spacing in a volume gives the closest approximation to the true value and they confirm this by experimental observation. The volumetric approach gives:

$$= \left(\frac{4\pi}{3}\right)^{\frac{1}{3}} r\, f^{-\frac{1}{3}} \quad - \quad 4$$

Using Ansell and Hirschorn's experimental results the models may be compared:

Experimental	405 Å
Equation 1	630 A
2	564 A
3	282 A
4	450 A

It would seem that equation 4 gives the closest approach to the experimental value.

Kocks [58] and Foreman and Makin [59] have discussed the effective interparticle spacing in terms of the nature of the dislocation movement through the obstacles. Kocks discusses all the models and comes to the conclusion that the value given by equation 2 is the most physically realistic. A more sophisticated calculation by Kocks suggests

that the value given by equation 2 should be increased by about 20%. Foreman and Meakin analysed the progress of a dislocation through a random distribution of obstacles using a computer model. They show that the effect of a random particle distribution is to reduce the critical shear stress (i.e. an effective increase in $\bar{l}$ is required for use in the simple equation for the flow stress) compared with a model which assumes a certain particle distribution. The widely spaced particles in the distribution can assist the dislocation motion elsewhere by an 'unzipping' process aided by the line tension. Foreman and Makin's results suggest that the value of $\bar{l}$ given by equation 2 should be increased by 23%.

The above models would seem to conflict with the experimental result of Ansell and Hirschorn and, if the experiment is to be believed, then the effective interparticle spacing will be that given by equation 4 increased by about 20% on the above arguments. The various ideas serve to show that theoretical values of the flow stress may be varied considerably by the choice of model for the particle spacing.

The mean interparticle spacing will be taken as $\bar{l} = 1.2 \left(\frac{4\pi}{3}\right)^{\frac{1}{3}} r f^{-\frac{1}{3}}$, Gleiter and Hornbogen's analysis takes into account the effective spacing along a dislocation line assuming this model.

REFERENCES

1. A. Taylor and R. W. Floyd. J.I.M. 1952, 81, 25.
2. J. Manenc. Rev. Met. 1957, 54, 867.
3. R. O. Williams. Trans. A.I.M.E. 1959, 215, 1026.
4. J. Manenc. Acta Met. 1959, 7, 124.
5. C. Buckle, B. Genty and J. Manenc. Rev. Met. 1959, 56, 247.
6. V. A. Phillips. Acta Met. 1966, 14, 1533.
7. J. R. Mihalisin and R. F. Decker. Trans. A.I.M.E. 1960, 218, 507.
8. C. Buckle and J. Manenc. Compt. Rend. 1957, 244, 1643.
9. K. Detert and H. Pohl. Z. Metallk. 1964, 55, 36.
10. A. J. Ardell and R. B. Nicholson. Acta Met. 1966, 14, 1295.
11. D. H. Ben-Israel and M. E. Fine. Acta Met. 1963, 11, 1051.
12. M. M. Dawance, D. H. Ben-Israel and M. E. Fine. Acta Met. 1964, 12, 705.
13. E. Hornbogen and A. Chakrabarty. Z. Metallk. 1966, 57, 28.
14. M. Jurkowitz and M. Fine. from M. E. Fine Phase transformations in condensed systems. 1964.
15. M. F. Ashby and L. M. Brown. Phil. Mag. 1963, 8, 1083, and Phil. Mag. 1963, 8, 1649.

16. F. R. N. Nabarro. Proc. Phys. Soc. 1940, 52, 90.

17. J. W. Cahn. Acta Met. 1962, 10, 179.

18. J. D. Eshelby. Acta Met. 1966, 14, 1305.

19. C. Wagner. Z. Elektrochem. 1961, 65, 581.

20. A. J. Ardell and R. B. Nicholson. J. Phys. Chem. Solids. 1966, 27, 1793.

21. R. A. Oriani. Acta Met. 1964, 12, 1399.

22. R. A. Swalin and A. Martin. Trans A.I.M.E. 1956, 206, 567.

23. A. J. Ardell. Acta Met. 1967, 15, 1772.

24. R. M. Bozorth. Ferromagnetism 1951, p.714.

25. .. .. p.763.

26. .. .. p. 37.

27. B. N. Das and L. V. Azaroff. Acta Met. 1965, 13, 827.

28. V. Marian. Ann. Phys. 1937, 7, 459.

29. A. Taylor and R. W. Floyd. J.I.M. 1951, 80, 577.

30. E. R. Stover and J. Wulff. Trans. A.I.M.E. 1959, 215, 127.

31. J. Cranghe and M. J. Martin. Phil. Mag. 1959, 4, 1006.

32. Y. Bagariatskii and Y. Tiapkin. Soviet Physics (Crystallography) 1957, 2, 414.

33. Y. Bagariatskii and Y. Tiapkin. Soviet Physics (Crystallography) 1960, 5, 513.

34. E. A. Starke, V. Gerold, and A. G. Guy. Acta Met. 1965, 13, 957.

35. E. Hornbogen and H. Kreye. Z. Metallk. 1966, 57, 122.

36. J. Friedel. Phil. Mag. 1952, 43, 153.

37. N. I. Noskova and V. A. Pavlov. Phys. Met. Metallog. 1960, 7, 75.

38. H. Brooks. Metal Interfaces. A.S.M. 1952, 20.

39. L. M. Brown. Unpublished work.

40. J. W. Christian. The Theory of Transformations in Metals and Alloys. 1965, p.442.

41. J. W. Cahn. Acta Met. 1961, 9, 795.

42. M. Hillert. Acta Met. 1961, 9, 525.

43. H. Gleiter and E. Hornbogen. Z. Metallk. 1967, 58, 157.

44. M. E. Fine and C. Chiou. Trans. A.I.M.E. 1958, 213, 553.

45. C. Chiou, H. Herman and M. E. Fine. Trans. A.I.M.E. 1960, 218, 299.

46. H. Herman and M. E. Fine. T.A.I.M.E. 1960, 218, 44.

47. J. B. Cohen and M. E. Fine in "Metallic Solid Solutions". Ed. Friedel & Guinier, 1963.

48. M. S. Wechsler and R. H. Kernohan. Acta Met. 7, 599, 1959, and J. Phys. Chem. Solids, 1961, 18, 175.

49. A. Kelly and R. B. Nicholson. Prog. in Mats. Sci. 1963 10.

50. R. G. Davies and N. F. Stolloff. Trans. A.I.M.E. 1965, 233, 714.

51. H. Gleiter and E. Hornbogen. Phys. Stat. Sol. 1965, 12, 235.

52. H. Gleiter and E. Hornbogen. Phys. Stat. Sol. 1965, 12, 251.

53. J. L. Castagne. J. de Physique 1966, 27C3, 233.

54. M. F. Ashby. Z. Metallk. 1964, 55, 5.

55. K. Westmacott, C. Fountain and R. Stirton. Acta Met. 1966, 14, 1628.

56. M. J. Marcinkowski and D. F. Wriedt. Acta Met. 1965, 13, 573.

57. G. S. Ansell and J. S. Hirschorn. Acta Met. 1965, 13, 572, 574.

58. U. F. Kocks. Acta Met. 1966, 14, 1629.

59. A. J. Foreman and M. J. Meakin. Phil. Mag. 1966, 14, 911.

60. N. F. Mott and F. R. Nabarro. Proc. Phys. Soc. 1940, 52, 86.

61. H. Gleiter. Z. Metallk. 1967, 58, 306.

62. H. Gleiter. Z. Metallk. 1967, 58, 101.

63. V. Gerold and H. Haberkorn. Phys. Stat. Sol. 1966, 16, 675.

64. M. E. Fine. N. P. L. Symposium on the relation of properties to microstructure 1963.

65. V. A. Phillips. Phil. Mag. 1967, 13, 103.

66. S. M. Copley and B. H. Kear. Trand. A.I.M.E. 1967.

67. J. L. Castagne. Compt. Rend. 1966, 263C, 1465.

68. P. A. Flinn. Trans. A.I.M.E. 1960, 218, 145.

69. M. J. Marcinkowski, N. Brown and R. M. Fisher. Acta Met. 1961, 9, 129.

70. R. W. Guard and J. H. Westbrook. Trans.A.I.M.E. 1959, 215, 807.

71. C. L. Corey and B. Lisowsky. Trans.A.I.M.E. 1967, 239, 239.

72. B. R. Coles. Private communication.

73. D. E. Peacock. Ph.D. Thesis Imperial College 1963.

74. S. Sass and J. B. Cohen. Manchester Electron Microscopy Conference 1966.

75. J. L. Lytton, J. A. Hren, K. T. Kamber and O. D. Sherby. Brit. J. A. P. 1964, 15, 1573.

76. A. J. Foreman. Phil. Mag. 15 1967 1012